THE UNIVERSITY OF CHICAGO

HEMODYNAMIC REGULATION OF ENDOTHELIAL METABOLISM AND EPIGENOME

A DISSERTATION SUBMITTED TO

THE FACULTY OF THE DIVISION OF THE BIOLOGICAL SCIENCES

AND THE PRITZKER SCHOOL OF MEDICINE

IN CANDIDACY FOR THE DEGREE OF

DOCTOR OF PHILOSOPHY

COMMITTEE ON MOLECULAR METABOLISM AND NUTRITION

BY

JIN LI

CHICAGO, ILLINOIS

JUNE 2023

TABLE OF CONTENTS

LIST OF FIGURES

LIST OF TABLES

ACKNOWLEDGEMENTS

I would like to express my deepest appreciation to my PhD advisor Dr. Yun Fang for his mentorship and belief in me. He saw my potential when I did not realize it myself. He has continued to spark my research interests by updating me with the advances in the field and is always willing to share his scientific insights and listen to mine. He encouraged me to explore the research direction, test hypotheses, and take challenges to become an independent scientist. Knowing my interest in employing both computational and experimental approaches to address research questions, Yun gave me the most incredible support to equip those skills. He also offered me many great opportunities to collaborate and learn from others and motivated me to pursue my PhD studies and career development goals. I truly appreciate the efforts and time Yun has spent training me.

I would also like to thank all the current and former members of the Fang Lab. Dr. David Wu has been a second mentor to me. He challenged me intellectually, generously shared his strong knowledge of basic science and medicine, and offered advice to motivate me to become a problem-solver. I would like to express my gratitude to Dr. Ru-Ting Huang, Dr. Tzu-pin Shentu, Dr. Chih-Fan Yeh, Dr. Jiayu Zhu, Dr. Zhengjie Zhou, Dr. Matthew Krause, Dr. Devin Harrison, Dr. Myung-Jin Oh, and Kaitlyn Sun and Dr. Angelo Meliton from Dr. Mutlu's lab, for sharing their wisdom in doing research and giving expert assistance to my studies. I would also like to acknowledge Dr. Georgios Kellaris, Ha Ram Kim, Lauryn Carver, and Dr. Siyang Wang for their moral support for my thesis writing.

I would like to gratefully acknowledge my thesis committee, Drs. Matthew Brady, Anna Di Rienzo, and Alexander Muir, for their time, insightful guidance, and consistent support. I want to thank Dr. Di Rienzo for her constructive input on my super-enhancer studies to help me

pursue more rigorous work. I want to thank Dr. Brady, who is also the chair of my graduate program, for helping me find the optimal solution when I have been struggling to achieve my goals. He also cares if I am happy beyond my academic progress, for which I am truly grateful.

I would like to thank the following people for collaborating with me on my PhD work: Dr. Yan Li from the Bioinformatics Core and Dr. Ani Solanki from the Animal Resource Center at UChicago; Dr. Xiaoming Zhong, Dr. Olivia Gray, Dr. Débora R. Sobreira, Dr. Noboru Jo Sakabe, Dr. Marcelo Nobrega, Wenchao Liu, and Dr. Yingming Zhao from UChicago; Dr. Casey E. Romanoski from the University of Arizona; Dr. Mete Civelek from the University of Virginia; Ilakya Selvarajan and Dr. Minna Kaikkonen-Määttä from the University of Eastern Finland.

I would like to acknowledge the CMMN students for creating such a supportive cohort. Exploring science and life with you made my graduate life much more delightful.

I would like to thank my family and friends for their continued support and trust in me through my ups and downs. I am grateful to my dad, who taught me to embrace each adventure and never be afraid. I want to thank my mom for her unconditional love. This endeavor would not be possible without you.

ABSTRACT

Mechano-transduction mechanisms play a critical role in embryogenesis, tissue homeostasis, and disease pathologies. This is especially important in the vasculature, where local disturbed blood flow activates vascular endothelial cells at arterial curvatures and bifurcations prone to atherosclerosis, the leading cause of human mortality and morbidity worldwide. In contrast, unidirectional blood flow associated with higher time-average shear stress in straight parts of blood vessels promotes endothelial quiescence and barrier integrity. Endothelial cells transduce mechanical signals from hemodynamics through their metabolic pathways and epigenetic landscapes, which together dictate transcriptome remodeling. However, it remains unexplored how these processes are interconnected to achieve such high coordination, specifically how the individual *cis*-regulatory elements work synergistically on gene regulation, and how the glycolytic signal is translated into atherogenesis. Addressing these two questions will enhance our understanding of how endothelial cells integrate and orchestrate individual modules from different layers to achieve flow-induced functional phenotypes. My studies in Chapter Two found that mechano-sensitive super-enhancers collectively activate genes with prominent functions in mechano-transduction. It provides new molecular mechanism underlying systematic transcriptome reprogramming in response to hemodynamics. My studies in Chapter Three identified that disturbed flow upregulates endothelial lactate dehydrogenase A to drive atherogenic gene transcription and leads to atherosclerosis, and proposed a novel epigenetic model through histone lactylation. Collectively, these studies demonstrate the effective crosstalk between metabolism and epigenome in mediating endothelial mechano-transduction, and emphasize the sophisticated molecular coordination involved in driving cardiovascular pathophysiology.

CHAPTER ONE: GENERAL INTRODUCTION

1.1 Cardiovascular diseases

1.1.1 Incidence of cardiovascular diseases

Cardiovascular diseases (CVD), the dysfunction of the heart and blood vessels, have emerged as the leading cause of morbidities and mortalities globally and in the United States. According to the World Health Organization, 32% of the global deaths in 2019 were attributed to CVD, reaching 38% for deaths under the age of 70[1]. Within the United States, 697,000 people died from heart diseases in 2020, accounting for 20% of the annual death[2,3]. The incidence of CVD varies across races and is higher among males than females in most ethnic groups, suggesting a contributing role of sex and race in the formation of CVD[2]. Financially, the medications, healthcare services, and productivity loss due to heart diseases cost the United States $229 billion annually, an enormous burden to society[4]. Moreover, although the mortalities of CVD are declining, their incidence is still on the rise, leading to rapidly increasing medical costs and reduced quality of life for those affected[5]. Therefore, exploring therapeutic targets and developing effective interventions are needed to slow down this global prevalence and improve people's life.

1.1.2 Risk factors contributing to CVD

CVD are induced by both inherited (genetics) and acquired (environmental) risk factors. Genome-wide association studies for CVD started in 2007[6], and for coronary artery disease alone, more than 320 risk loci have been discovered ever since[7]. These genetic variants have been shown to affect CVD by regulating blood pressure, lipid metabolism, insulin levels, etc.,

but the pathophysiological pathways for most of these variants remain unknown. The importance and challenge of utilizing these GWAS datasets for CVD studies will be discussed in section 1.5.

On the other hand, environmental risk factors also have a substantial effect on the occurrence of CVD. These include high blood cholesterol and triglycerides levels, high blood pressure, smoking, diet, physical inactivity, aging, lack of sleep, and infection such as COVID-19. The contribution of these components has been comprehensively discussed elsewhere[3]. Here, I would like to focus on metabolic disorders and briefly summarize their pathological contributions.

1.1.3 Contribution of metabolic diseases to CVD

Two major metabolic disorders associated with CVD are obesity and type 2 diabetes (T2D). Obesity is a condition of excessive fat, which is determined by the body mass index (BMI): a BMI above 25 and 30 kg/m^2 is considered overweight and obese, respectively[8]. Type 2 diabetes is a disease characterized by high blood sugar levels, which occurs when the body has an impaired response to insulin. People who are overweight or obese are significantly more likely to develop T2D[9–11], and the physiological mechanisms underlying this transition include fat-induced pancreatic beta-cell dysfunctions and organ-wise insulin resistance[12].

Excessive body fat and glucose dysregulation strongly affect the risk of CVD onset, which is suggested to be through metabolic risk factors hypercholesterolemia, hypertriglyceridemia, hyperglycemia, hypertension, and inflammation[13]. Specifically, obesity increases low-density lipoprotein (LDL) cholesterol level in the blood, which migrates into the arterial wall for oxidation and initiate atherosclerosis, and will be discussed in section 1.1.4. Furthermore, triglycerides (TG) constituting triglyceride-rich lipoproteins, such as very low-density lipoprotein (VLDL), have been shown to indirectly contribute to atherosclerosis through a

lipolysis-induced proinflammatory effect on endothelial cells and macrophages[14–16]. T2D is characterized by high blood glucose, and obesity can also give rise to hyperglycemia through induced gluconeogenesis. Consequently, hyperglycemia increases the glycosylation of proteins and lipids that participate in atherosclerosis, induces oxidative stress in vascular cells with their subsequent inflammatory responses, as well as activates protein kinase C, thus increasing expression of transforming growth factor-β (TGF-β) for extracellular matrix production[17,18]. In addition, obesity is a major cause of hypertension through impairing kidney function[19]. As a result, the over-stretching blood vessels at each heartbeat due to hypertension can injure endothelium and damage vessel elasticity, promoting the formation of many CVD events[20,21].

Moreover, the obesity and T2D-induced nutritional overload in the adipose tissue also increases their production of proinflammatory adipokines such as leptin, tumor necrosis factor-alpha (TNF-α), interleukin-1 (IL-1) and interleukin-6 (IL-6), which can further lead to a systematic inflammation induction thus promoting CVD development[22]. Last but not least, insulin resistance has been shown to promote many types of CVD, mainly through the irresponsive adipose tissue releasing excess fatty acids into the circulation thus causing dyslipidemia[23,24]. In addition, insulin resistance also contributes to CVD through many of the abovementioned metabolic disorders (hyperglycemia, hypertension, etc.). Broadly, enormous studies indicate the vital contribution of metabolic syndromes to the onset and progression of CVD, suggesting a complex system crosstalk in this disease regulation and emphasizing the necessity of intervening in metabolic risk factors for CVD prevention and treatment.

1.1.4 Overview of sequential steps in plaque formation

My studies in Chapters Two and Three both focus on atherosclerotic CVD (ASCVD). Atherosclerosis, the hardening of blood vessels due to the buildup of lipid deposits, is the

primary cause of many CVD[25]. In general, atherosclerosis starts with endothelial dysfunction[26]: when the systematic risk factor circulating LDL enter the intima, it will be oxidized, causing endothelial cell activation. In addition to the systematic risk factor, local disturbed blood flow can also activate endothelium at given sites of the arteries, which leads to focal plaque development[27–29]. As a result, endothelial increased their expression of selectins, cytokines, chemoattractants, adhesion molecules, and inflammatory markers, which collectively capture, activate and arrest monocytes, causing them to adhere and transmigrate into the intima layer[26]. The recruited monocytes will be differentiated into macrophages and dendritic cells, both of which uptake and deposit the lipids and become foam cells[30]. At this point, the first grossly visible plaque is formed, called fatty streaks[31]. The persistent inflammation would induce macrophage apoptosis, causing them to release lipids and debris that drive the formation of the necrotic core[30]. Other immune cells also participate in plaque formation, including T and B lymphocytes, which can play a pro- or anti-inflammatory role to either aggravate or attenuate atherosclerosis, respectively[32]. The cytokines and growth factors released by endothelium also induce the proliferation and migration of smooth muscle cells, which produce a collagenous-proteoglycan matrix and form the fibrous cap together with the infiltrated immune cells[33]. At this stage, fibroatheroma is developed. As atherosclerosis progresses, calcification will occur as contents in the necrotic core serve as a nidus for calcium to deposit[34]. Thereafter, the necrotic core will be partially and even wholly calcified, making arteries stiff and contractility compromised, which gives rise to a higher risk for myocardial infarction[34].

Stable atherosclerosis plaques only obstruct the artery to restrict a sufficient supply of oxygen and nutrients to the surrounding tissues, but it becomes more destructive when the plaques rupture. Plaques with thinner fibrous caps (thickness < 65 um) and fewer smooth muscle

cells are more vulnerable and easier to break, causing thrombosis with the accumulation of platelets and immune cells[35]. On the other hand, thrombosis can still occur without the plaque rupture but as a consequence of erosion, which is often associated with endothelial cell death and desquamation, thus poor vessel integrity[36]. However, the pathobiology of erosion-induced thrombosis and fatal events is poorly characterized.

The early stage of atherosclerosis has no symptoms, but they will appear as the disease progresses or when patients are triggered by physical and emotional stress[37]. Depending on the location of the blocked artery, atherosclerosis may induce stroke, peripheral artery diseases, angina, and even myocardial infarction[37].

1.1.5 Current therapies to ASCVD

Treating ASCVD can be both easy and challenging. As for the easy part, most CVD occurrences can be reduced and even prevented by controlling the environmental risk factors[38–44]. For instance, a 5 to 10 percent of body weight loss is sufficient to reduce CVD risk[45,46]. Nevertheless, keeping a stringently healthy lifestyle for a whole lifetime can be essentially difficult. Furthermore, since early ASCVD are asymptotic, attention will mostly be gained only when they become severe, which is when medicines or even surgeries are needed. As the complex pathology of ASCVD, finding effective therapeutics for all affected individuals can be challenging, which is the difficult aspect of treating ASCVD.

So far, the most effective ASCVD treatment strategy is to lower the LDL cholesterol level. An early and intensive atherosclerosis intervention is effective in reducing the occurrence of major adverse CVD events[47]. Maintaining a very low LDL cholesterol (< 40 mg/dL) in a lifetime has been recommended to delay the onset of ASCVD[48], but achieving it is very challenging. Multiple drugs have been developed to reach this goal, among which the two most

well-known and widely used ones are statins and inhibitors of proprotein convertase subtilisin/kexin type 9 (PCSK9). Statins suppress the endogenous cholesterol synthesis pathway by inhibiting β-hydroxy β-methylglutaryl-coenzyme A (HMG-CoA) reductase, and antibodies/small interfering RNA targeting PCSK9 prevent them from degrading the LDL receptors. Statins and PCSK9 inhibitors have been shown to decrease major coronary events in a long-term run[49–53]. Another lipid-lowering strategy is suppressing angiopoietin-like protein 3 (ANGPTL3), which consequently activates the activity of both lipoprotein lipase and endothelial lipase to reduce hypertriglyceridemia and hypercholesterolemia[54]. However, the effectiveness of these cholesterol-lowering therapies in reducing CVD mortality and prolonging lifetime has been seriously doubted after an increasing number of clinical trials have been performed[55,56], thus identifying new targets beyond lipids are called on for treating ASCVD.

As atherosclerosis is defined as a chronic inflammatory disease, anti-inflammatory strategies have also been attempted to reduce its progression. Among them, targeting the inflammasome leucine-rich repeat–containing receptor (NLR) family pyrin domain-containing 3 (NLRP3) and its downstream target Interleukin 1β (IL-1β) have been proposed to provide positive outcomes[57,58].

Besides, drugs targeting hyperglycemia have also been demonstrated to be beneficial in reducing ASCVD preclinically or clinically. These include metformin, an anti-diabetes drug that has been shown to promote endothelial NO production and suppress macrophage inflammation in atherosclerosis[59,60]. Preclinical data have also suggested that inhibitors of sodium glucose cotransporter 2 (SGLT-2), which can reduce urinary glucose reabsorption from the proximal tubule, ameliorated the progression of ASCVD[61–63]. Although diabetes is often seen as the comorbidity of ASCVD, not all ASCVD conditions are associated with hyperglycemia.

Therefore, these glucose-lowering drugs may bring more benefits only to specific groups of ASCVD patients, and their mechanism and effect in those with normoglycemia need to be further characterized.

In addition to medicines, procedures and surgeries have also been used to treat ASCVD patients with severe conditions. These include coronary artery bypass graft, percutaneous coronary intervention, endarterectomy, and weight-loss surgery for obese patients, and their anti-ASCVD effects have been extensively discussed elsewhere[64–71]. As these surgeries are all invasive, they will mainly be performed in very advanced ASCVD and are not considered as practical approaches to intervene in the disease at its early stage.

Collectively, current medicine treatments for ASCVD primarily focus on reducing hypercholesterolemia, inflammasome, and hyperglycemia, which only result in marginal gains in health or lifespan. It is recommended that new drug targets with higher efficacy and precision should be discovered for ASCVD treatment[47], which is also the overall goal of my doctoral thesis work.

To improve the possibility of finding an effective drug target, fully leveraging the information obtained from genetic studies is essential. Statistics show that candidate drugs with human genetics evidence are more likely to be successful in Phase II and III clinical trials[72], emphasizing the importance of employing Mendelian and GWAS data for drug discovery. One example is that PCSK9 was uncovered as a target from multiple GWAS[73–75]. Notably, the majority of the discovered GWAS coronary artery disease loci are not associated with lipid-relevant genes, addressing the vital contribution of additional mechanisms in ASCVD development[76]. Nevertheless, challenges remain in identifying the causal genes and

understanding the mechanism linking these variants to disease pathology[77], which requires more mechanistic investigations.

To achieve treatment with greater precision, we should also consider the contribution from local risk factors such as hemodynamics in ASCVD development and fix the focal point exclusively. Such investigations will be further discussed in my studies from Chapters Two and Three. In addition, targeted delivery systems such as modified polyelectrolyte complex micelles would significantly prevent the unfavorable side tissue effects resulting from systemic administration[78].

1.2 Endothelial cells in tissue homeostasis and disease progression

Endothelial cells are originated from mesodermal progenitors during development and go through vasculogenesis to form the circulatory system in support of the development of other organs. Lining the interior layer of blood vessels and lymphatic vessels, endothelial cells come into direct contact with the blood or lymphatic fluid and interact actively with them to pass on signals to surrounding tissues. In this section, I will focus on the endothelial cells from blood vessels and summarize their functions in maintaining homeostasis and disease progression.

Firstly, the endothelium is responsible for transporting and exchanging oxygen and nutrients from the blood to all tissues, which sustains the energy supply to the body. Secondly, it also maintains the vascular tones by releasing NO and endothelin-1 (EDN1) which act on smooth muscle cells to induce vessel dilation or constriction, respectively. Thirdly, endothelial cells also form a barrier to adjust vascular permeability by connecting with each other through adherens and tight junctions and assistance from glycocalyx, basement membrane, and mural cells[79]. The endothelial barrier in arteries and veins is relatively tight, whereas, in capillaries, it can be either

continuous, fenestrated, or discontinuous to meet different exchange demands of solutes, hormones and macromolecules in specific tissues[79]. Failure in maintaining vascular integrity can lead to infection of pathogens, entry of low-density lipoprotein (LDL), edema, impaired gas exchange, thus hypoxia and hypercapnia[80–82]. Fourthly, endothelium produces anticoagulant and antithrombotic signals to ensure regular flow of blood cells during homeostasis and shifts to procoagulant and prothrombotic pathways at areas of the damaged vessel for healing [83]. As expected, failure of endothelium in adjusting the coagulation balance would lead to thrombosis or blood loss. Furthermore, migration is also one major function of endothelial cells to support vasculogenesis, wound repair, and angiogenesis in multiple physiological and pathological processes[84]. Lastly, endothelial cells are also involved in both acute and chronic inflammation, as they respond to inflammatory stimuli and recruit immune cells to sites of injury by producing cytokines, chemokines, growth factors, and presenting adhesion molecules[85]. One consequence of these inflammation activations is increased leukocyte adhesion and transmigration into the vessel wall, which initiates atherosclerosis-associated cardiovascular diseases.

In summary, due to the universal distribution in all organs throughout the body, endothelial cells share many general functions and act in specified roles based on their location. Endothelium modulates vascular homeostasis by maintaining the balance of vascular tones, growth, fluidity, and inflammation; their activation and dysfunction are implicated in many pathological processes.

1.3 Mechano-transduction in vascular diseases

Mechanical forces are instrumental to vascular development and disease progression[86]. Generally, mechanical forces in the vasculature can be divided based on the tissue bed or the

type of force, such as hemodynamic, stretch, stiffness, and hydrostatic pressures[87]. Endothelial cells line the innermost layer of arterial, venous, and lymphatic vascular trees and are accordingly subject to different mechanical signals. As endothelial cells contract, migrate, signal inflammation, and possibly transdifferentiate into other cell types, they usually do so as a response to changes in mechanical cues and coordinate their intracellular processes to meet this plasticity need[88]. This underscores the significant role of cellular metabolism and epigenome in accommodating such phenotypic changes. As my thesis studies focus on artery-related diseases, I will mainly summarize the mechano-transduction in large vessels in this section.

The mechanical forces in large vessels like the aorta are mainly from blood flow and stiffness. Macrovascular flow (vessels > 10 μm in diameter) is complex, varying in both space and time as vessel boundary conditions continuously change and heart pump strength is modulated dynamically by both neural and volumetric fluid inputs in a beat-to-beat fashion[89]. Endothelial cells are subjected to shear stress from 10 to 50 dyne/cm^2 in large arteries [90]. Generally, arterial flow can be classified into two classes: "atheroprotective" and "atheroprone"[91]. Atheroprotective flow is unidirectional ("unidirectional flow", UF), whereas atheroprone flow has no time-averaged direction but is instead chaotic and reminiscent of eddy currents or vortexes ("disturbed flow", DF).

Aortic hemodynamics have been the most studied in the context of development [92–94] and atherosclerosis, as arterial branch points and vessel curvature result in disturbed flow, leading to coronary artery disease, aortic atherosclerosis, and carotid artery disease [95,96]. Aortic and carotid hemodynamics have been modeled based on magnetic resonance imaging studies of flow, which are used in clinical practice [97], making *in vitro* study of flow-related changes in endothelial cell biology possible [98–102]. In general, unidirectional flow results in the elaboration of nitric oxide

and barrier protection and is protective against inflammation and thrombosis, whereas disturbed flow results in vessel constriction, permeable barriers, thrombotic pathways, and inflammatory signaling – hallmarks in the development of atherosclerosis. Although not discussed in detail here, vascular endothelial cells are also subjected to significant circumferential cyclic stretch [103]. For instance, heart propulsions result in the cyclic stretch in arterial endothelium, and spontaneous respiration (or mechanical ventilation in critically ill patients) causes mechanical stretch of lung microvascular endothelium[104].

Microenvironmental stiffness also plays a fundamental role in cell differentiation. Endothelial cells produce fold-changes in actin with increasing substrate stiffness [105] and affect, for instance, leukocyte transmigration in *in vitro* studies [106]. Like flow, mechano-transduction by stiffness sensors causes nuclear translocation of transcription factors[107,108].

Matrix stiffness and disturbed flow work in tandem, amplifying disease processes. Stiffer vessels could lead to increased flow and/or reduced pulsatility, which is particularly harmful to endothelial cells in the brain vascular bed. Vascular stiffening is by itself sufficient to explain primary hypertension [109]. In systemic arterial circulation, increased vascular stiffness is associated with and precedes systemic hypertension [109,110], a predictor of cardiovascular morbidity [111,112] and mortality [113]. Vascular stiffening is also pathological in the pulmonary circulation and microvasculature. Increased macrovascular stiffness promotes microvascular damage [114–116] and, therefore, end-organ damage through the dysregulated transmission of hemodynamics from large vessels and stiffness-dependent control of RhoA GTPase activity, permeability, and inflammation [117–119]. Besides arterial hypertension, microvascular stiffness in the pulmonary circulation has been identified as an independent cause of mortality in pulmonary

hypertension [120–124]. The current standard of care antihypertensive treatment is thought to have an anti-stiffness component [125] and improve mortality [126].

In summary, due to their specific location, vascular endothelial cells are constantly subject to various dynamic mechanical forces mainly generated from blood flow, matrix stiffness, or cyclic stretch. Therefore, mechano-transduction is extensively involved in modulating endothelial plasticity and consequently vascular homeostasis and pathology. Two interconnected signaling systems, metabolism and epigenome, translate these mechanical cues into phenotypical changes, and will be discussed in the following sections.

1.4 Hemodynamic regulation of endothelial metabolism

Despite their sufficient access to oxygen, endothelial cells rely on glycolysis to generate 75-85% of ATP, whereas oxidation phosphorylation (OXPHOS) only contributes to a small portion of energy production[127,128], a phenotype similar to cancer cells and is referred to as the "Warburg effect"[129]. Mechanical forces, including shear stress, can further modulate the bioenergetic preference of endothelial cells[130,131], and this metabolic signaling has a profound impact on endothelial physiology. In my doctoral studies, I mainly focused on atherosclerosis-associated cardiovascular diseases, and therefore in this section, I will summarize the metabolic regulation from blood flow on arterial beds. I will divide these metabolic pathways/substrates into glycolysis, mitochondria, fatty acids, and amino acids.

1.4.1 Glycolysis

The hemodynamic regulation of endothelial glycolysis has been mainly reported through three transcription factors: Krüppel-like factor-2 (KLF2), hypoxia inducible factor-1α (HIF-1α), and Yes-associated protein (YAP) with PDZ-binding motif (TAZ).

KLF2 expression is significantly upregulated by high shear stress unidirectional flow and is anti-angiogenic, barrier protective, anti-inflammatory, and protective against atherosclerosis and acute lung injury [132–136]. KLF2 reduces endothelial glycolysis via suppressing the transcription of glycolytic enzymes hexokinase 2 (HK2) and 6-phosphofructo-2-kinase/fructose-2,6-biphosphatase-3 (PFKFB3) [137]. Notably, HK2 catalyzes the phosphorylation of glucose, the rate-limiting and first committed step in glycolysis. As expected, the HK2-mediated reaction is indispensable in glycolysis, and HK2 has been shown to be essential in lymphangiogenesis [138]. On the other hand, PFKFB3 is an allosteric activator of phosphofructokinase (PFK) in the second rate-limiting reaction of glycolysis. Thus, it is possible that PFKFB3 may preferentially supply non-essential glycolytic needs in endothelial cells, such as for pathological activation. Indeed, deletion or suppression of PFKFB3 led to an impaired endothelial proliferation in pathological angiogenesis [139,140], and reduced endothelial inflammation and leukocyte adhesion, which ameliorated pulmonary hypertension [141]. Furthermore, pharmacological inhibition of PFKFB3 in high-fat diet-fed $LDLR^{-/-}$ mice attenuated atherosclerosis progression and increased plaque stability, indicating the atherogenic function of this DF-induced enzyme [142]. The inhibition of KLF2 on PFKFB3 also indirectly shuttles the glycolysis pathway into hexosamine- and glucuronic acid biosynthesis pathways for hyaluronan production [143]. Hyaluronan is the major structural component of glycocalyx on the endothelial cell surface that senses shear stress[144–147], preserves vascular integrity [148,149], and suppresses leukocyte-endothelium adhesion [145,150]. Collectively, the UF-induced KLF2 mainly inhibits endothelial glycolysis to promote vascular homeostasis.

The HIF family of transcription factors is regulated by targeting for degradation via hydroxylation by prolyl hydroxylases (PHDs), which are sensitive to oxygen concentration [151,152]

and shear stress [153]. Disturbed flow activates HIF-1α to increase endothelial metabolism beyond its high baseline glycolysis [130,153]. Three mechanisms have been demonstrated related to DF-induced HIF-1α activation: (1) transcriptionally, HIF-1α is upregulated by nuclear factor NF-κB [130]; (2) post-translationally, HIF-1α protein is stabilized by deubiquitinating enzyme Cezanne [130], and also (3) post-translationally, HIF-1α is stabilized by reactive oxygen species (ROS) produced by NAD(P)H Oxidase-4 (NOX4) [153]. HIF-1α promotes endothelial glycolysis by upregulating a cohort of glycolytic genes, including lactate dehydrogenase A (LDHA), glucose transporter-1 (SLC2A1/GLUT1), HK2, PFKFB3, and probably additional glycolytic genes as the glycolysis and angiogenesis gene sets have a high degree of overlap [130,153]. Furthermore, DF-induced HIF-1α can shift the fate of pyruvate towards glycolysis away from the TCA cycle by enhancing the transcription of pyruvate dehydrogenase kinase-1 (PDK1) [153,154]. HIF-1α -driven glycolytic reprogramming is required for the DF-induced endothelial inflammation, excessive proliferation, and monocyte adhesion, leading to atherosclerosis formation [130,153,155]. The endothelial-specific knockout of HIF-1α suppressed DF-induced atherosclerosis in $Apoe^{-/-}$ mice [130]; similarly, knockdown of SLC2A1 reduced DF-induced HIF-1α expression and endothelial inflammation [153]. Interestingly, HIF-1α and KLF2 are counter-regulated: KLF2 has been shown to disrupt binding between HIF-1α and its chaperone HSP90 [156]. This suggests that two exclusionary metabolic poles may together define the metabolic state of aortic endothelial cells.

Other transcriptional co-activators that promote endothelial glycolysis are YAP and TAZ, which are involved in the Hippo pathway. YAP/TAZ plays a significant role in mechano-transduction and is also regulated by shear stress: disturbed flow increases while unidirectional flow reduces YAP/TAZ activity in endothelial cells [157,158]. One mechanism underlying the UF-suppressed YAP/TAZ activity is through the Gα13-mediated RhoA inhibition [157]. As a

metabolism regulator in multiple cell types, YAP/TAZ is activated when nutrient supply is sufficient and will in turn drive glycolysis, glutaminolysis, anapleurosis, and lipogenesis to promote cell growth and homeostasis [159]. Moreover, in endothelial cells, YAP/TAZ has been shown to regulate genes involved in both glycolytic and OXPHOS pathway [160], suggesting YAP/TAZ may stimulate endothelial metabolism to support both migration and growth. Nevertheless, fewer YAP/TAZ activity is associated with more endothelial quiescence: reduced YAP/TAZ downregulated pro-inflammatory genes, reduced monocytes adhesion and infiltration [157,158], and impaired DF-induced endothelial proliferation [158]. Furthermore, *in vivo* blockade of YAP/TAZ activity reduced the atherosclerotic plaque size in hyperlipidemic Apoe$^{-/-}$ mice [157,158], indicating the atherogenic role of DF-induced YAP/TAZ.

Whereas many studies collectively revealed that DF-induced endothelial glycolysis is detrimental to vascular health, research demonstrated the beneficial role of a DF-upregulated glycolytic regulator protein kinase AMP-activated (AMPK) in protecting against atherosclerosis [161]. Surprisingly, selectively deleting endothelial PRKAA1, the major catalytic subunit of AMPK in vascular cells, reduced endothelial glycolysis and proliferation while aggravating atherosclerosis in hyperlipidemic mice. In addition, inducing glucose usage by overexpressing SLC2A1 could rescue the impaired glycolysis in PRKAA1-deleted endothelial cells and reverse the severity of atherosclerosis. However, excessive glycolysis also triggers atherosclerosis, as overexpressing SLC2A1 in PRKAA1-intact endothelium led to increased plaque size in the partial carotid artery ligation mouse model [161]. The discrepancy between findings from this study and the widely recognized atheroprone effect of DF-induced glycolysis could be due to AMPK may induce other glycolysis-independent biological processes that protect against endothelial

activation. Nevertheless, these findings demonstrate the precise and complex operation of metabolic signaling in mechano-trasduction.

A primary product from glycolysis is lactate, and emerging studies have shown lactate can act as a metabolic fuel and signaling molecule rather than simply a waste[162]. Endothelial cells play an essential role in providing lactate to other cells: they not only deliver it from blood to the tissue sites by serving as a 'gatekeeper', but can also actively produce and release lactate to support their surrounding cells and tissues through an 'angiocrine' fashion[163–165]. In addition, within endothelial cells, lactate has been shown to act as a (1) pro-angiogenic molecule by stimulating the NF-κB pathway and stabilizing HIF-1α to promote VEGFR2 expression and VEGF production[166–168], and (2) as a barrier destructor by increasing VE-cadherin endocytosis[169]. However, whether lactate exerts a function in endothelial mechano-transduction is not understood.

Interestingly, inflamed sites have been recognized to be accumulated with a high concentration of lactate. In rheumatoid arthritis, lactate buildup has been shown to increase the expression of its transporter SLC5A12 on $CD4^+$ T cells, consequently leading to increased lactate uptake, which induces IL-17 production[170]. Blockade of SLC5A12 reduced the arthritis severity in mouse models, emphasizing that targeting the lactate axis could be promising therapeutics in chronic inflammation diseases[170]. In obese mice, lactate secreted from adipocytes fosters an inflammatory stage of adipose tissue macrophages, establishing a link between nutritional overload and chronic inflammation[171]. In atherosclerosis plaques, lactate concentration is almost 15 times higher than that in healthy tissues, and its level is positively correlated with plaque severity[172], indicating lactate is also associated with this pathological condition. Furthermore, as shown *in vitro*, the DF-induced endothelial glycolysis is accompanied

by elevated extracellular acidification rate (ECAR)[173], a surrogate measurement of lactate production, supporting the notion that lactate may participate in the blood flow-mediated mechano-transduction and possibly induce endothelial activation. This hypothesis was tested in my project in Chapter Two.

1.4.2 Mitochondria

As OXPHOS only generates 15-25% ATP in cultured endothelial cells, it indicates that instead of a major energy source, mitochondria in endothelial cells may play a more vital role as an organelle for signaling and metabolic intermediates production[174]. Indeed, endothelial mitochondria participate in maintaining Ca^{2+} homeostasis and regulating oxidative stress[175]. In this section, I will summarize how hemodynamics modulate endothelial mitochondria on their respiratory activity, dynamics, and signaling functions.

Studies from our lab and others have collectively shown that disturbed flow reduces, whereas unidirectional flow increases oxidative phosphorylation in cultured human aortic endothelial cells[153,176]. This is in accordance with *in vivo* data which demonstrated that increased vascular shear stress boosted mitochondrial health in rodents[176,177]. The UF-induced OXPHOS depends on elevated mitochondria biogenesis regulated by transcription factors KLF2/4[176,178], deacetylase sirtuin 1 (SIRT1)[177,179], and YAP/TEAD1 complex[180]. In addition, UF can reduce the cholesterol in the endothelial plasma membrane, which in turn activates OXPHOS[181].

Shear stress has also been shown to regulate mitochondria dynamics in endothelial cells. Mitochondria fusion and fission are essential for their proper cellular distribution, inheritance of mtDNA, energy production, and removal of their dysfunctional companions by mitophagy [182], and are highly responsive to environmental stress [183]. Compared to DF, high shear stress from UF promotes mitochondria fusion by upregulating mitochondria fusion protein optic atrophy

protein 1 (OPA1) and mitofusin 2 (MFN2), while downregulating mitochondria fission dynamin-related protein 1 (DRP1) and mitochondria fission 1 (FIS1) protein [184,185]. Lower mitochondria fission is associated with better endothelial health, as suppressing DRP1 in endothelial cells reduced TNFα -induced NF-κB activation, VCAM-1 expression, and leukocyte adhesion both *in vitro* and *in vivo* [186]. Consistently, in the diabetic Apoe$^{-/-}$ mouse, inhibiting DRP1 could improve endothelial function, reduce VCAM-1 and ICAM-1 expression, and attenuate the development of diabetic-induced atherosclerosis [187].

Endothelial mitochondria also contribute to intracellular calcium modulation: they are not only the second largest Ca^{2+} storage organelles in the cell, but their released ATP can also induce the extracellular Ca^{2+} entry [188] and ER-stored Ca^{2+} flux [189]. Intracellular calcium ion, or $[Ca^{2+}]_i$, acts as a critical second messenger in endothelial cells in regulating migration, proliferation, inflammation, vasodilation, and cell survival[190–195]. Shear stress can increase endothelial calcium influx [188,196–198], which has been shown to be required for shear stress-mediated eNOS activation, PECAM-1, and VEGFR-2 phosphorylation[188,197]. An irregular endothelial $[Ca^{2+}]_i$ could lead to a variety of pathological consequences, including impaired angiogenesis, barrier integrity, and vasodilation[191,195,199]. In brief, endothelial mitochondria can participate in shear stress-induced mechano-transduction through their calcium modulation capacity.

1.4.3 Fatty acids

Vascular endothelial cells are exposed to the circulated free fatty acids (FFA), which have been shown to regulate endothelial inflammation, NO production, and insulin signaling and contribute to disease formation, including atherosclerosis [200,201]. The endothelial metabolism of fatty acid, from uptake to oxidation and synthesis, can all be dynamically modulated by blood flows.

Proteomics in cultured human umbilical vein endothelial cells (HUVEC) detected high shear stress could induce proteins participating in lipid transport, oxidation, catabolism, and biosynthesis [202]. In comparison, atheroprone low shear stress reduced the membrane fraction of LDLR by accumulating them around the nuclei [202]. In another lipidomics study in endothelial cells, high shear stress has been found to elevate ether-containing lipids, which is responsible for attenuating the phorbol 12-myristate 13-acetate (PMA)-induced VCAM-1 expression [203].

Several mechano-sensitive signaling pathways all play a part in endothelial lipid metabolism. For instance, the UF-activated NOTCH1 signaling can promote fatty acid oxidation (FAO) through transcriptional activation of carnitine palmitoyltransferase 1A (CPT1A) [204,205]. On the contrary, DF has been indicated to induce endothelial fatty acid synthesis through sustained activation of sterol regulatory element binding transcription factor 1 (SREBP1), which enhances the transcription of HMG-CoA synthase and fatty acid synthase genes [206]. In concert, SREBP1 can also be increased by YAP/TAZ signaling to facilitate lipid accumulation [207]. Taken together, these studies demonstrate that UF tends to induce FAO while DF preferentially promotes lipid synthesis and accumulation in endothelial cells.

FAO has been shown to promote endothelial quiescence. It is essential for supplementing dNTP synthesis to maintain endothelial DNA replication and angiogenesis [208]. FAO also benefits redox homeostasis through NADPH regeneration, thus protecting cells from oxidative-stress exposure [204]. Suppressing CPT1A increased endothelial cell permeability *in vitro* and blood vessel leakage *in vivo* [209]. FAO also restrains endothelial-to-mesenchymal transition (EndMT) by maintaining the acetyl-CoA pool for the post-translational inhibition of the mesenchymal marker SMAD7 [210]. Mice with endothelial CPT2 deficiency had thicker heart valves and higher permeability in multiple vascular beds [210].

On the other hand, it has not been elucidated how DF-induced fatty acid synthesis modulates endothelial mechano-transduction. But in cardiomyocytes, fatty acids enhance HIF-1α hydroxylases by decreasing succinate concentration [211], a possible regulation in endothelial cells to protect against DF-induced glycolysis. On the contrary, in cancer cells, blocking monounsaturated fatty acids synthesis by inhibiting stearoyl-CoA-desaturase 1 (SCD1) reduced YAP/TAZ stabilization and nuclear localization [212], indicating fatty acid synthesis may also contribute to the hyperglycolysis in DF-exposed endothelium. In summary, FAO has been widely suggested to promote endothelial quiescence, while how fatty acid synthesis participates in mechano-transduction remains to be characterized.

1.4.4 Amino acids

As the most abundant amino acid in human plasma [213,214], glutamine serves as a primary carbon source for the TCA cycle in endothelial cells to support their proliferation [215,216]. The critical contribution of glutamine is that it serves as the precursor of asparagine, which is needed for protein synthesis in angiogenesis [216,217]. Besides its role as a building block, glutamine is also crucial in maintaining endothelial redox homeostasis by producing the antioxidant glutathione [218]. In addition, the glutamate generated by glutamine is subsequently converted to ornithine for synthesizing polyamine and nitric oxide (NO), a critical regulator of vasodilation and angiogenesis [219,220]. The glutamate production can be induced by stiffness through YAP/TAZ-dependent upregulation of glutaminase (GLS1), the first enzyme catabolizing glutamine to glutamate and ammonia [108]. However, whether other mechanical forces, including shear stress, also modulate glutamine metabolism has not been thoroughly investigated.

The other important amino acid that maintains vascular quiescence is L-arginine, which can be converted by eNOS to synthesize NO and citrulline in endothelial cells [221]. It has been

widely suggested that eNOS is a mechano-sensitive enzyme. Compared to DF, UF increases NO production by boosting functional eNOS through transcriptional activation [222–224], mRNA stabilization [224], and post-translationally phosphorylated at various serine residues [225,226]. Synergistically, the synthesis of L-arginine is also elevated by high shear stress through upregulating the transcription of argininosuccinate synthetase 1 (ASS1), which catalyzes the penultimate step to synthesize L-arginine [227,228]. As expected, interfering ASS1 impaired NO generation in bovine aortic endothelial cells [229]. Thus, the endothelial NO production pathway is promoted by unidirectional flow at several steps and levels in a synergistic manner.

Collectively, these studies demonstrate that in endothelial cells, multiple amino acids exert crucial regulating functions beyond serving as building blocks. And hemodynamics effectively controls the metabolism of these amino acids to support vascular growth and maintain the vascular tone.

1.5 Epigenetic regulation in endothelial cells

Epigenetics is referred to the study of stable gene transcription alteration without changing the DNA sequence[230]. Epigenetic changes include the addition and removal of methyl groups on DNA, and multiple post-translational modifications on histone octamers, which consequently regulate chromatin accessibility and the recruitment of transcription factors and cofactors[231]. Recent epigenetics studies uncovered that the non-coding human genome is enriched with *cis*-regulatory elements such as silencers, insulators, and enhancers, each with distinct histone modifications[232–234]. Emerging evidence revealed that enhancers orchestrate the majority of cell type-specific gene expression[235–237] and play critical roles in development, evolution, and diseases[238–243]. In endothelial cells, the enhancer landscape is globally remodeled

by CVD-relevant extracellular stimuli, including hemodynamics and proinflammatory treatments to impact their transcriptome[99,244,245].

Integrating epigenomics and human genetics studies has the potential to unveil the molecular underpinning of complex human diseases and discover new gene regulatory mechanisms[246,247]. More than 80% of disease-associated alleles identified by genome-wide association studies (GWAS) are in the non-coding genome with undefined functions[77,248,249]. Top-scoring disease-associated SNPs are frequently located within *cis*-regulatory elements, particularly enhancers explicitly active in distinct cell types[250]. GWAS have discovered hundreds of common genetic variants significantly associated with cardiovascular diseases (CVD)[77,251–254]. Most of the GWAS-identified CVD SNPs are also located in the non-coding genome, with their regulatory mechanism and functional relevance remaining largely unknown[77,249].

Notably, genetic predisposition to CVD is manifested largely through the endothelium, as the open chromatins of endothelial cells show high enrichment of GWAS SNPs associated with CVD[246], and genetic variants associated with endothelial transcription or epigenetic activity are enriched in CVD-relevant loci[255]. In support of this, Gupta *et al*. reported that the non-coding common variant at rs9349379, implicated in CVD by GWAS, is located in an endothelial enhancer region key to endothelin-1 expression in vascular endothelium[256]. Furthermore, previous work from our lab showed that rs17114036, a common non-coding polymorphism at 1p32.2 locus strongly associated with coronary artery disease (CAD) and ischemic stroke (IS), is located in a hemodynamics-sensitive enhancer. Unidirectional flow significantly increases the enhancer activity of rs17114036-containing region to promote the transcription of phospholipid phosphatase 3 (PLPP3, or PPAP2B), which maintains endothelial quiescence and monolayer integrity[257,258]. These studies collectively suggest a key role of endothelial *cis*-regulatory

elements, particularly enhancers, in integrating human genetics signaling to regulate vascular homeostasis and pathophysiology.

Recently, super-enhancers (SEs) have been used to describe groups of putative enhancers in close genomic proximity with a high degree of enrichment of transcriptional activators or chromatin marks (e.g., H3K27ac) as determined by ChIP-seq[259–261]. Several unique characteristics distinguish super-enhancers from the regular typical-enhancers (TEs): (1) their enrichment with the binding sites of key transcription factors of that cell type[259,260], (2) their tendency to regulate genes related to cell identity[259,260], (3) their enrichment with genetic variants associated with that cell-type relevant disease[259,260], and (4) they are dynamically regulated and implicated in development[262,263], disease progression and tissue damage[264–266]. In endothelial cells and other cell types, the super-enhancer architectures have been shown to be susceptible to pathological stimuli, such as proinflammatory exposures[244] and glucose levels[267], indicating their potential role in mediating the disease-related transcription dynamics. In cancer cells, transcriptional drugs preferentially affect the structure of super-enhancers rather than typical-enhancers to disrupt oncogene expression[268], highlighting the significance of utilizing SEs for effective therapeutics discovery. Therefore, super-enhancers are instrumental in identifying regulatory elements likely to control genes crucial to cell type specification and provide implications for disease perturbation. However, the typical- and super-enhancer landscape in endothelium under well-defined mechanical cues, such as hemodynamics, remains poorly understood[245,269].

Besides H3K27ac, acetylation at additional lysine sites and other histone modifications, like methylation and phosphorylation, have all been shown to be installed in endothelial cells to coordinate their dynamic transcriptome in different vascular systems and in response to vascular

diseases[270–274]. However, these studies in endothelial cells are still minimal, considering that many histone modifications have been discovered in the eukaryotic epigenome.

Furthermore, the epigenome and metabolism in a cell are tightly interconnected[275]. First of all, several metabolites act directly as the substrates for epigenetic modifications. For instance, the acetyl-CoA generated from glycolysis, fatty acid beta-oxidation, acetate and glutamine is used for histone acetylation[276]; the glycolytic product lactate can be adopted for histone lactylation[277]; the UDP-GlcNAc from hexosamine biosynthetic pathway is used for GlcNAcylation[278]; the methyl groups for H3 or H4 methylation at their lysine or arginine sites are donated from S-Adenosyl methionine (SAM) that produced by methionine[279]. Secondly, metabolite levels fine-tune the activity of multiple epigenetic enzymes (writers, readers, and erasers). For example, sirtuins rely on hydrolyzing NAD^+ to exert their deacetylase activity[280]; the function of DNA demethylase ten-eleven translocation (TETs) enzymes and histone demethylases is dependent on their cofactor α-ketoglutarate (α-KG), whereas inhibited by the TCA cycle intermediates 2-hydroxyglutarate (2-HG), succinate and fumarate[281,282]; the AMP-activated protein kinase (AMPK) phosphorylates histones by sensing the energy levels[283]. Thirdly, epigenetic modifications can in turn control the transcription of metabolic genes. For instance, histone deacetylation inhibits the expression of HIF-1α and MYC[284,285]. The timely communication between metabolism and epigenome is crucial for the cells to quickly and precisely coordinate their energy supply with other functional processes in response to extracellular cues such as hemodynamics. Future investigations on novel epigenetic mechanisms in endothelial cells would also be useful to uncover their specificity in different vascular beds and plasticity in response to pathological stimuli.

1.6 The contribution of my studies

Mechanical signals from hemodynamics are transduced through of endothelial cells' metabolic pathways and epigenetic landscapes to mediate their transcriptome, plasticity, and vascular pathophysiology. However, two critical questions remain to be addressed to understand better the highly organized coordination of endothelial mechano-transduction systems: (1) How do individual epigenetic elements work synergistically? (2) How are metabolism signals transduced to functional changes?

Relating to the first question, there is a significant knowledge gap regarding how endothelial cells integrate individual gene regulatory components to orchestrate the flow of biological information from DNA sequences and genetic variation in the 3D genome to the functional transcriptome. In Chapter Two, I utilized a combination of techniques, including H3K27ac ChIP-seq, ATAC-seq, Promoter Capture Hi-C, transcription factor ChIP-seq, transcriptomics, and human genetics studies to systemically identify the SNP-enriched cistome in vascular endothelial cells subjected to well-defined atherosclerosis-relevant flows. This work discovered and highlighted the regulatory function of mechano-sensitive super-enhancers enriched with CVD GWAS SNPs in governing the endothelial transcriptome. Furthermore, it provides a roadmap and public dataset for future investigations to identify causal variants/genes implicated by genetic studies, an ongoing challenge in the post-GWAS era.

The second question is how the disturbed flow-induced glycolysis in endothelial cells feeds their proinflammatory outputs to drive atherogenesis. In Chapter Three, I identified a novel atherogenic function of the key glycolytic enzyme LDHA, which acts as a master transcription regulator in endothelial cells by using its product lactate for histone lysine lactylation (Kla). I also established a mechanistic model whereby endothelial LDHA contributes to atherogenesis by installing histone Kla on a CAD GWAS gene JCAD to promote its transcription. The findings

from these studies promote our understanding of how mechanical cues can be efficiently translated into functional transcriptome outputs through metabolic products. These novel molecular mechanisms linking disturbed flow to focal plaque formation are of great importance and may provide a potential target for "local" atherosclerosis therapeutics.

CHAPTER TWO: INTEGRATION OF MULTI-LAYER OMICS TO IDENTIFY MECHANO-SENSITIVE SUPER-ENHANCERS IN VASCULAR ENDOTHELIAL CELLS

2.1 Introduction

Vascular homeostasis and pathology are tightly and dynamically regulated by mechanical forces generated by blood flow (hemodynamics). Blood flow characteristics have been established as major regulators of endothelial transcriptomes[131,257,286–288]. The mechano-sensitive transcriptome is dynamically controlled at epigenetic level through changes in transcription factor abundance and chromatin architecture[257,289], but the functional epigenetics consequence and accurate gene annotations remain to be investigated.

So far, limited functional human genetics studies have suggested a critical role of single nucleotide polymorphism (SNP)-imbedded *cis*-regulatory elements in regulating endothelial mRNA expression[255–258]. Systematic identification of CVD SNP-associated endothelial enhancers provides a unique opportunity to unbiasedly identify endothelial *cis*-regulatory elements prioritized for study and to elucidate novel regulatory mechanisms of CVD-associated variants. In combination, a vascular endothelial cell-specific promoter interactome would enable more accurate and functional annotation for these genetic variants.

To answer these fundamentally important questions, I integrated H3K27ac ChIP-seq, Promoter Capture Hi-C (PCHi-C), transcription factor ChIP-seq, transcriptomics and human genetics studies to systematically identify the SNP-enriched cistrome in vascular endothelial cells under well-defined hemodynamics associated with atherosclerosis. A cohort of endothelial typical-enhancers and super-enhancers were identified. We discovered that when compared to typical-enhancers, endothelial super-enhancers are enriched with genetic variants associated with cardiovascular diseases and binding sites for transcription factors key to endothelial functions. These super-enhancers preferentially contact to genes controlling endothelial homeostasis and vascular functions. We further identified two distinct cohorts of mechano-sensitive super-enhancers: unidirectional flow (UF)-enriched or disturbed flow (DF)-enriched super-enhancers. Many of these mechano-sensitive super-enhancers contain CVD-associated SNP(s), and the majority of them are physically contacted by promoters of flow-sensitive genes. CRISPR interference successfully validated the enhancer activity of a candidate UF-enriched super-enhancer in promoting the transcription of three anti-oxidant genes, and a DF-enriched super-enhancer in up-regulating two pro-thrombotic genes in endothelial cells. To this end, we successfully integrated multi-layer omics datasets to systemically characterize the mechano-sensitive epigenomic landscape in vascular endothelial cells under well-defined hemodynamics. These results highlight the regulatory role of CVD SNP-enriched super-enhancers in governing the flow-dependent endothelial transcriptome key to vascular homeostasis and diseases.

2.2 Materials and Methods

H3K27ac chromatin immuno-precipitation with whole genome sequencing (ChIP-seq) and RNA-seq. H3K27ac ChIP-seq and RNA-seq were conducted in low-passage Human

Aortic Endothelial Cells (HAECs, Lonza, Allendale, USA) subjected to 24-hr 'athero-prone' disturbed flow mimicking the hemodynamics measured in human carotid sinus or 'athero-protective' unidirectional representing the wall shear stress in human distal internal carotid artery, as described previously[131,290].

ChIP-seq analysis and identification of super-enhancers and typical-enhancers. Using Cutadapt[291], adapters were trimmed from the raw sequencing data of H3K27ac ChIP-seq. Reads were then aligned to the UCSC hg19 genome using Bowtie2[292] (version 2.3.4.3) with default parameters to generate SAM files. SAM files were filtered and converted to BAM files, followed by sorting and PCR duplicates removal using SAMtools[293] (version 1.6.0). Mapped reads were then organized into tag directories using the 'makeTagDirectory' command of HOMER[294] (version 4.10.0). Tag directories of 5 biological replicates from unidirectional flow were merged for IP and input samples, respectively. Similarly, tag directories of 6 biological replicates from disturbed flow were merged for IP and input samples, respectively.

Super-enhancers and typical-enhancers were identified using HOMER 'findPeaks -style super -L 0', in the merged IP tag directories against input tag for each experimental flow condition. In brief, super-enhancers and typical-enhancers were classified following the criteria established by the Young laboratory[260], and was described in the results section above. HOMER 'mergePeaks -d given' was used to combine the super-enhancers identified in HAECs exposed to two types of flows, which added up to 1,000 endothelial super-enhancers and similarly for the identification of 26,457 typical-enhancers. To plot the heatmaps of H3K27ac distribution, we generated the data matrix using HOMER 'annotatePeaks.pl -ghist'. Each enhancer together with the 10,000 bp surrounding its center was divided into 200 units, and the number of tags mapped to each unit was counted. Within each super- or typical-enhancer, the unit with the maximum

number of tag counts was aligned to the middle point of x-axis for visualization using MATLAB 'heatmap' function. Histograms were generated by taking the average of tag counts across all units at each enhancer locus.

To identify unidirectional flow (UF)- and disturbed flow (DF)-enriched endothelial super-enhancers, HOMER 'getDifferentialPeaks -F 1.2' was used to detect super-enhancers which have a ≥ 1.2-fold change of normalized tag count in HAECs in comparison between the UF and DF conditions (Poisson enrichment p-value ≤ 1e-4). The complementary set of super-enhancers out of the 1,000 were defined as core super-enhancers.

Motif enrichment analysis. Motif enrichment analysis was performed using HOMER 'findMotifGenome.pl' command in UF-enriched, DF-enriched and core super-enhancers, respectively. Option '-size given' was specified to find motifs using the exact size of each super-enhancer. HOMER randomly selected both size-matched and GC content-matched genomic regions as background and referred to it to discover enriched motifs in each type of super-enhancers.

Counting enhancers with transcription factor binding sites. ChIP-seq of transcription factors EGR, JUN, JUNB, or NFκB-p65 conducted in HAECs[245] were employed to map the transcription factor binding sites in endothelial super-enhancers and typical-enhancers identified in this study. To evaluate the proportions of super-enhancers and typical-enhancers that contain a transcription factor binding site, the normalized tag counts of each TF ChIP-seq along every SE and TE were calculated using HOMER 'annotatePeaks.pl'. For each TF ChIP-seq, the numbers of SEs and TEs that contain non-zero normalized tag counts were added up, which were then divided by the total numbers of SEs (1,000) and TEs (26,457), respectively, to calculate the

percentage. To examine the TF binding site density, the previously calculated normalized tag counts along each SE and TE were further divided by that enhancer length in bp.

Promoter Capture Hi-C (PCHi-C) and enhancer annotation. In situ Hi-C was performed as described by Rao et al[295]. Five million of HAECs were harvested from culture and then resuspended in 1x DPBS. To cross-link interacting DNA loci, 37% formaldehyde was added to the cells to a final concentration of 1% and carried out for 10 mins at room temperature. Cross-linked chromatin was digested using MboI endonuclease (New England Biolabs, R0147); the restriction overhangs were filled in and the DNA ends were marked with biotin-14-dATP (Life Technologies, 19524-016). To isolate captured fragments, the biotin-labeled DNA was then sheared and pulled down using Dynabeads MyOne Stretavidin T1 beads (Life Technologies, 65602). The in situ Hi-C library was amplified off the T1 beads with 6 cycles of PCR using Illumina primers (Illumina, 2007). The promoter-containing fragments were further isolated from the whole-genome Hi-C library as described by Montefiori et al[296]. The Hi-C library was hybridized to 81,735 biotinylated 120-mer custom RNA oligomers (CustomArray, Inc.) targeting promoter regions (4 probes/ RefSeq transcription start sites) and added to streptavidin-coated magnetic beads (Life Technologies, 65602). Subsequently, an 8-cycle PCR was performed to amplify the DNA bound to the beads captured by the biotinylated RNA. Each library was sequenced on a full lane of an Illumina HiSeq 4000 machine. Standard capture Hi-C analysis was performed as described previously[296]. Hi-C reads were aligned and filtered using HiCUP[297]. The computational pipeline CHiCAGO[298] which eliminates sequence capture bias was employed to identify genomic interactions. Only strong interactions with CHiCAGO scores ≥ 5 were selected for further analysis. Promoter-interacting regions from PCHi-C were then overlapped with H3K27ac-identified endothelial typical-enhancers and super-enhancers, and intersections were

selected using HOMER 'mergePeaks -prefix' and assigned back to their interacted promoters for further gene annotation.

The number of interactions that an SE or TE can form with promoters was calculated by counting the amount of overlaps of an SE or TE with the promoter-interacting regions detected in PCHi-C. The number of repetitive interactions of SEs or TEs with the same promoter was calculated as enhancer-gene contact frequency.

GWAS SNP enrichment analysis. The enrichment of disease-associated variants in endothelial super-enhancers and typical-enhancers identified in this study was examined using R package traseR[299]. SNP-trait associations were obtained from the combination of dbGaP and NHGRI GWAS Catalogs, and SNPs in linkage disequilibrium (LD, $r^2 > 0.8$) within 100 kb of the lead SNPs were obtained from 1000 Genome Project, which generated 78,247 unique LD trait-associated SNPs. Whole genome outside the enhancer regions were referred to as the background. The significant enrichment was examined using binomial test, with the null hypothesis being the probability of observing a base to be trait-associated SNP is the same in the enhancer regions as in their corresponding background regions. The test was performed for 33 GWAS classes and 573 GWAS traits. A statistical *q-value* < 0.05 and odds ratio > 1 were used as the threshold cutoffs for significant enrichment.

Refining super-enhancers that contain cardiovascular diseases (CVD)-associated GWAS SNP. The CVD GWAS traits were curated using the following keywords: cardiovascular (for cardiovascular disease), coronary artery/coronary heart (for coronary artery and heart disease), myocardial infarction (for myocardial infarction), atherosclerosis/plaque (for atherosclerosis), thrombo (for thrombosis), stroke (for stroke), heart failure/heart disease/heart defect (for heart disease), ventricular (for ventricular disease), atrial fibrillation (for atrial

fibrillation), blood pressure (for blood pressure), hypertension (for hypertension), valve (for valve defect), carotid (for carotid artery disease), and peripheral (for peripheral artery disease). CVD-associated SNPs were downloaded from NHGRI-EBI GWAS Catalog[300] (version 1.0.2), and the genomic coordinates were converted to hg19 using liftOver[301]. BEDTools intersect[302] was used to refine CVD SNP-containing super-enhancers.

Gene expression annotation using RNA-seq. RNA-seq results in HAECs subjected to well-defined hemodynamic forces were conducted and analyzed as described previously[290]. The Fragments Per Kilobase of transcript per Million mapped reads (FPKM) was used as the proxy for gene expression level in HAECs subjected to unidirectional flow or disturbed flow. The expression level of genes contacted to super-enhancers was compared to that of genes exclusively contacted to typical-enhancers; the FPKM under unidirectional flow and disturbed flow was averaged for each gene. For mechano-sensitive super-enhancers-contacted genes, the expression fold change of each gene in response to distinct hemodynamics was calculated as the ratio of its FPKM under unidirectional flow to its FPKM under disturbed flow and represented in a $\log_2$ scale.

Gene ontology analyses. Metascape[303] was used to identify enriched biological pathways of selected gene sets. Genes with promoters contacted to super-enhancers or exclusively contacted to typical-enhancers were further filtered to select only genes that were actively expressed (FPKM $\geq$ 12 in RNA-seq) in HAECs. Similar procedure was followed to identify enriched biological pathways of the genes exclusively contacted to UF-enriched SEs and genes exclusively contacted to DF-enriched SEs, with less stringent criteria to select actively expressed genes (FPKM $\geq$ 1 in RNA-seq).

CRISPR interference and RT-qPCR. Catalytically dead Cas9 (dCas9) was fused to KRAB repressor and transduced to HAECs using adenoviruses (addGene cat# 46911). One day after the dCas9-KRAB transduction, HAECs were transfected with 2-3 targeted sgRNAs (IDT, sequence shown below) or negative control sgRNAs (IDT, 1072544) using RNAiMAX (Life Technologies), and cultured in EGM-2 medium (Lonza) containing 4% dextran (for the following flow experiments). Non-targeting negative control guide RNA was purchased from IDT. SE-targeted sgRNAs were specifically designed on IDT to align to the CVD SNP-containing H3K27ac peaks. HAECs were then subjected to unidirectional flow or disturbed flow for 24 hours before RNA isolation.

Table 2.1. sgRNAs used in CRISPR interference assay to inhibit the candidate super-enhancers in human aortic endothelial cells.

	Targeting SE type	**Targeting SE location**	**sgRNA sequence**
sgRNA #1	UF-enriched SE	chr16_69412415-69482923	5'-GTGTCTACACCCCAGAAATG-3'
sgRNA #2	UF-enriched SE	chr16_69412415-69482923	5'-AATAAACTGGTGGGGAACCG-3'
sgRNA #3	DF-enriched SE	chr6_11605189-11618730	5'-ACTAGTTTCTTAGGCCCAAC-3'
sgRNA #4	DF-enriched SE	chr6_11605189-11618730	5'-ACCGAGGGAAGTGCTACCAC-3'
sgRNA #5	DF-enriched SE	chr6_11605189-11618730	5'-CTGCCAGTAATTTACGGAGC-3'

RNA was isolated from cells using NucleoZOL RNA isolation kits (Takara) and reverse transcribed using High-Capacity cDNA Reverse Transcription Kit (ThermoFisher). Quantitative mRNA expression was determined by RT-qPCR using SYBR Green MasterMix (Roche). The following primer (IDT) sequences were used.

Table 2.2. All primers used in RT-qPCR experiment to assess the transcriptional activity of candidate super-enhancers in human aortic endothelial cells.

Gene	**Forward primer**	**Reverse primer**
β-Actin	5'-TCCCTGGAGAAGAGCTACGA-3'	5'-AGGAAGGAAGGCTGGAAGAG-3'
GAPDH	5'-TGCACCACCAACTGCTTAGC-3'	5'-GGCATGGACTGTGGTCATGAG-3'
Ubiquitin	5'-ATTTAGGGGCGGTTGGCTTT-3'	5'-TGCATTTTGACCTGTTAGCGG-3'
NQO1	5'-GGCAGAAGAGCACTGATCGTA -3'	5'-TGATGGGATTGAAGTTCATGGC-3'
CYB5B	5'-ATGTCCGGTTCAATGGCGAC-3'	5'-CATGGATCACAAGCCACAGTT-3'
WWP2	5'-CAAAGCCCAAGGTGCATAATCG-3'	5'-CCAATGCGCTTCCCAGTCT-3'
EDN1	5'-AGAGTGTGTCTACTTCTGCCA-3'	5'-CTTCCAAGTCCATACGGAACAA-3'
HIVEP1	5'-GAACTTCGGAATCCCTTAAAGGT-3'	5'-AAGAACGGCGAAAGATGACTC-3'

2.3 Results

2.3.1 Endothelial super-enhancers are enriched with transcription factor binding sites.

The molecular identity of enhancers in endothelial cells under well-defined hemodynamics remains to be determined. We analyzed our whole-genome H3K27ac ChIP-seq[257] conducted in human aortic endothelial cells (HAECs) exposed to 24-hr atherosclerosis-promoting complex disturbed flow (DF) or atherosclerosis-protective pulsatile unidirectional flow (UF). Disturbed flow recreates the hemodynamics measured in human carotid sinus prone to atherogenesis and unidirectional flow represents the hemodynamics measured in human distal internal carotid artery resistant to atherosclerosis[304]. H3K27ac-identified enhancers within 12.5 kb of each other were stitched together to define a single entity, and ranked by increasing H3K27ac signal to separate super-enhancers (SEs) from typical-enhancers (TEs)[259,260]. As shown in Figure 2.1A, all enhancers are ranked along the *x-axis* according to the H3K27ac signaling plotted on the *y-axis*. Super-enhancers are defined as those to the right of the tangent point (slope =1) of the resulting curve. In total, we identified 1,000 super-enhancers and 26,457 typical-enhancers in HAECs under flows (Figure 2.1A). As predicted, the distribution of overall H3K27ac signal is higher in super-enhancers than in typical-enhancers both at each locus (Figure 2.1B) and on average (Figure 2.1C). The genome distributions of the typical-enhancers and super-enhancers are described in Figure 2.1D. Recent studies suggested that cell-type-specific enhancers are typically activated by unique combinations of a few transcription factors (TFs)[237]. We next characterized these endothelial super-enhancers and typical-enhancers by identifying the binding sites of key transcription factors in endothelial cells. Whole-genome endothelial

ChIP-seq results of ERG, JUN, JUB and NFκB-p65[245], key transcription factors regulating endothelial homeostasis and inflammation, were employed to identify TF binding sites in these endothelial enhancers. We detected a higher percentage of super-enhancers than typical-enhancers containing at least one binding site for these endothelial-enriched TFs (Figure 2.1E). For instance, the binding sites of ERG, a TF regulating endothelial lineage identity and endothelial homeostasis[305], were detected in 96% of super-enhancers compared with only 35% of typical-enhancers. To mitigate the length-dependent bias, as super-enhancers are on average longer in size than typical-enhancers, we applied a normalization to calculate the TF binding density by dividing the number of ChIP-seq tag counts mapped to each enhancer to its length (bp). The histogram showed that the distribution of super-enhancers was more skewed to the high TF binding density end than typical-enhancers for all TFs, suggesting a higher percentage of super-enhancers than typical-enhancers containing denser TF binding sites (Figure 2.1F). Taken together, these data suggest that in HAECs under flows, endothelial super-enhancers are more enriched with binding sites of key endothelial transcription factors compared to typical-enhancers.

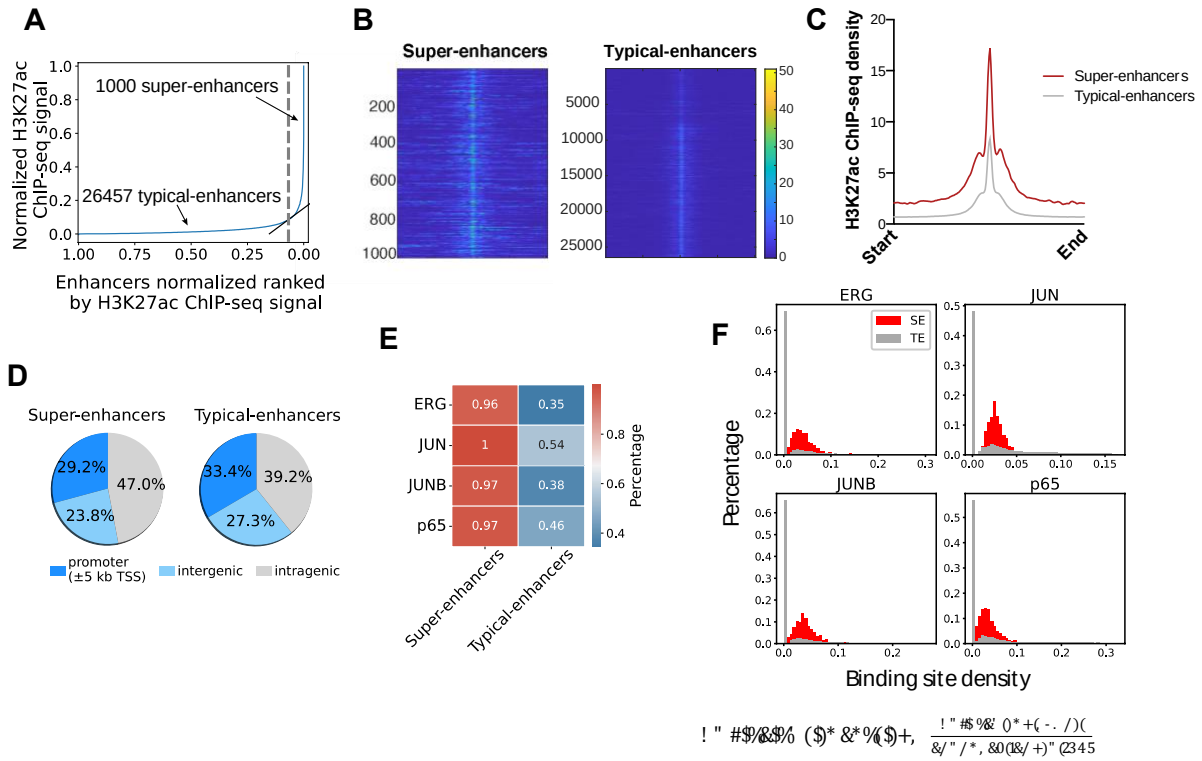

Figure 2.1. Endothelial super-enhancers are enriched with transcription factor binding sites. (A) Hemodynamics-regulated endothelial super-enhancers and typical-enhancers identified by H3K27ac ChIP-seq were ranked by increasing normalized H3K27ac signal. The cutoff slope = 1 is shown as black line and a horizontal gray dashed line passing the tangency point was shown to discriminate SEs from TEs. **(B)** Heatmaps of normalized H3K27ac tag counts along each of the 1,000 SEs (left) and 26,457 TEs (right). **(C)** Histogram of the averaged normalized H3K27ac tag counts along all 1,000 SEs and 26,457 TEs. **(D)** Pie charts of genomic distributions of SEs and TEs. **(E)** Heatmap of percentages of SEs and TEs containing transcription factor binding sites. **(F)** Histogram showing a higher percentage of SEs (red) than TEs (gray) contain denser transcription factor binding sites. X-axis: transcription factor binding sites density (the ChIP-seq tag counts at each enhancer locus normalized to that enhancer length). Y-axis: percentage of enhancers.

2.3.2 Endothelial super-enhancers are enriched with genetics variants associated with cardiovascular diseases.

We further examined the enrichment of disease-associated variants in these super-enhancers and typical-enhancers, using SNPs reported in the NCBI dbGaP[306] and NHGRI GWAS catalogs[307]. The enrichment analyses were conducted by testing the null hypothesis that the probability of observing a single base being a disease-associated SNP is the same inside as

outside of the genomic regions of the enhancers. We detected that cardiovascular diseases (CVD), among all 33 GWAS catalog human traits, is most significantly associated with the variants in super-enhancers compared to those in the background regions ($-log_{10}(q\text{-}value) = 5.23$, Figure 2.2A). The second most significant class on the list is body weights and measures, which is closely related with CVD (Figure 2.2A). On the contrary, variants resided in typical-enhancers are most significantly associated with digestive system diseases (Figure 2.2B). Although CVD ranked the second on the list, its q-value does not show marked difference from other disease categories including immune system diseases. This finding indicate that endothelial super-enhancers show distinct enrichment only with CVD-associated SNPs, whereas typical-enhancers do not have such preference. When comparing the odds ratio of detecting a variant in each category, consistently, it is more likely to observe a CVD SNP in super-enhancers (OR=1.5) than in typical-enhancers (OR=1.3) (Figure 2.2C). Further analyses focusing on the CVD traits demonstrated that CVD SNPs are enriched in both types of enhancers and the odds ratios are mostly higher for super-enhancers (Figure 2.2D). These results support the notion that disease-associated loci are enriched in *cis*-regulatory regions in corresponding disease-relevant cell types[237,259,308]. The enrichment of CVD SNPs (Figure 2.2A, C and D) along with binding sites of endothelial transcription factors (Figure 2.1E-F) in endothelial super-enhancers support their putative functions in regulating vascular homeostasis and diseases.

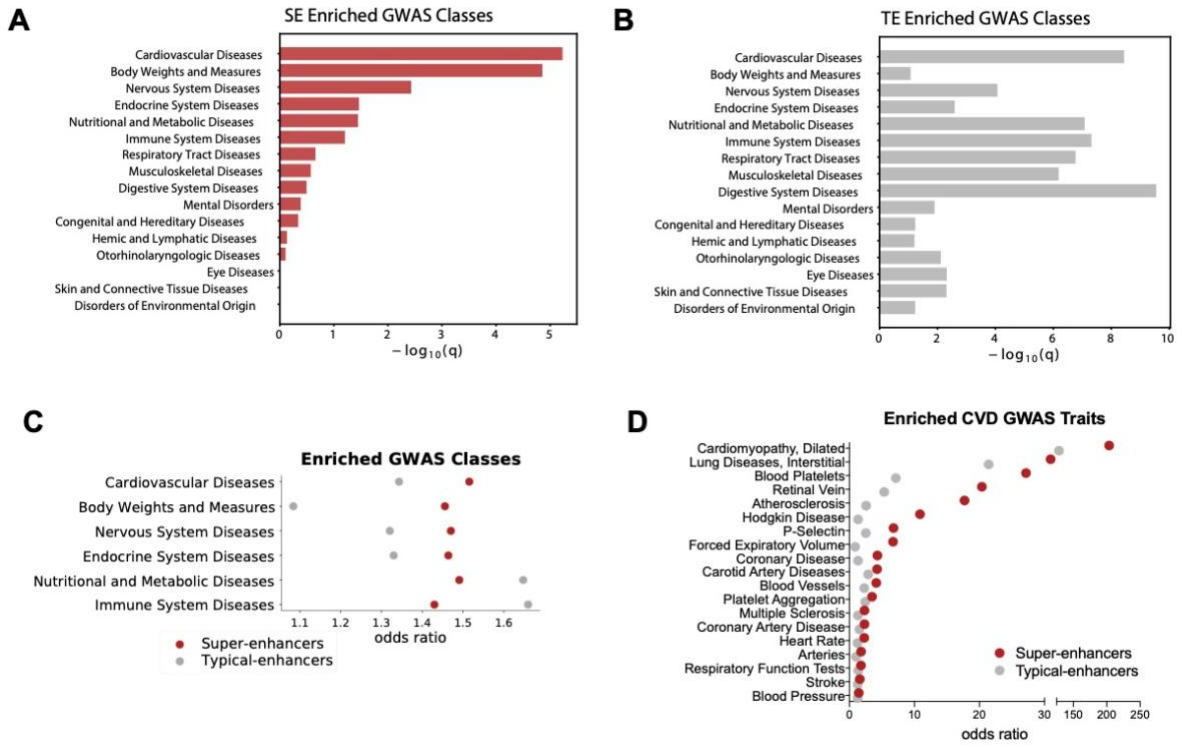

Figure 2.2. Endothelial super-enhancers are enriched with genetics variants associated with cardiovascular diseases. Top GWAS disease classes associated with SE-harboring SNPs **(A)** and TE-harboring SNPs **(B)** that shown by -log$_{10}$(*q-value*) from binomial test. **(C)** Top GWAS disease classes associated with SE-harboring SNPs ranked by *p-value* from binomial test. Dot plot shows the odds ratio of identifying these disease-associated SNPs inside vs. outside SEs (red), and inside vs. outside TEs (gray). **(D)** Odds ratio of identifying selective CVD-associated SNPs inside vs. outside SEs (red), and inside vs. outside TEs (gray).

2.3.3 Promoter Capture Hi-C (PCHi-C) demonstrated that endothelial super-enhancers preferentially contact to the promoters of EC-enriched genes.

Enhancers are proposed to control gene expression by forming physical contacts with target gene promoters, sometimes through long-range chromosomal interactions spanning significant genomic distances[309]. Although chromosome conformation capture techniques such as Hi-C[310] have been conducted in adult endothelial cells to probe the genome-wide mapping of long-range chromatin contacts[311–313], most Hi-C datasets have limited resolution (> 40 kb) and do

not precisely identify the enhancer-promoter interactions. High-resolution promoter capture Hi-C (PCHi-C) is developed based on Hi-C but the highly complex libraries were specifically enriched for promoter sequences to identify and interrogate physical interactions between *cis*-regulatory elements and all annotated promoters[314,315]. We conducted PCHi-C in HAECs to generate a three-dimensional (3D) endothelial chromatin organization focusing on the genome-wide detection of promoter-interacting *cis*-regulatory elements. In brief, we performed in-situ Hi-C[295,296] in HAECs and used the four-cutter restriction enzyme MboI to generate ligation fragments ~400-500 bp allowing enhancer-level resolution of promoter contacts. The Hi-C libraries were then enriched for promoter interactions by hybridization with a set of 81,735 biotinylated RNA probes ('baits') targeting 22,600 human RefSeq protein-coding promoters, followed by next-generation sequencing. The computational pipeline CHiCAGO[298] which eliminates sequence capture bias was employed to identify genomic interactions. PCHi-C captured 114,713 high-confidence interactions (CHiCAGO score ≥ 5) in HAECs of gene promoters with DNA fragments (Supplementary Table 3). CHiCAGO-analyzed PCHi-C results enable us to systematically and unbiasedly interrogate the H3K27-identified enhancers for their physically contacted promoters/genes.

By integrating the endothelial 3D genome organization and the H3K27ac-mapped endothelial enhancers, we identified that 2,353 gene promoters are physically contacted by at least one H3K27ac-identified super-enhancers. Meanwhile, 5,669 gene promoters are contacted by at least one typical-enhancer but not a super-enhancer. Gene ontology analyses showed that SE-contacted genes are enriched in endothelial- and vasculature-enriched biological processes such as response to oxygen levels, cell-substrate adhesion and blood vessel development, whereas TE-contacted genes are involved in general cellular pathways such as cellular

macromolecule biosynthesis and cellular protein catabolic process (Figure 2.3A). These results agree with the prevailing view that super-enhancers are instrumental to tissue-specific cellular functions[259,260]. Interrogation with the HAEC transcriptome[131] demonstrated that genes contacted by super-enhancers are on average more highly expressed than genes exclusively contacted by typical-enhancers (Figure 2.3B). The data support an emerging view that super-enhancers, when compared to typical-enhancers, confer higher transcriptional activation on targeted genes[260,269,316]. We also detected that on average an endothelial super-enhancer forms significantly more interactions with promoters than a typical-enhancer does (Figure 2.3C), a phenomenon that was reported in cancer cells[317]. Moreover, if we only count the contacts to the same promoter, our data showed a rightward skewing of super-enhancers compared to typical-enhancers in the histogram (Figure 2.3D), suggesting a higher proportion of super-enhancers contact to the same promoter repetitively. In other words, different regions within a super-enhancer tend to form simultaneous contacts to their targeted gene. This finding provides a potential mechanism explaining the higher transcriptional regulation activity of super-enhancers than typical-enhancers. Together, H3K27ac ChIP-seq, CHiCAGO-analyzed PCHi-C, and transcriptomics support the notion that endothelial super-enhancers are hyper-active regulatory domains which contact to promoters of highly expressed endothelial genes instrumental to key vascular functions. We then prioritized super-enhancers for further analyses and functional validations.

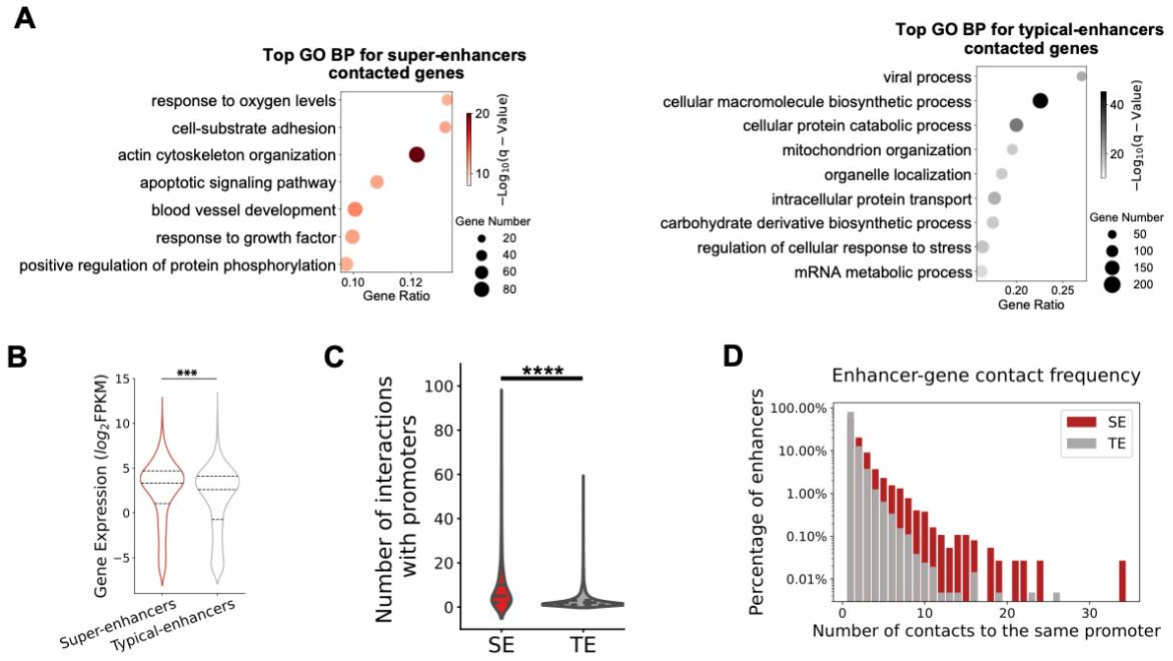

Figure 2.3. PCHi-C demonstrated that endothelial super-enhancers preferentially contact to the promoters of EC-enriched genes. (A) Gene ontology analysis showing top biological processes associated with highly expressed genes contacted to SEs (*left*) and TEs (*right*). **(B)** The expression level (FPKM) of SE-contacted genes (red) and TE-contacted genes (gray) in HAECs subjected to hemodynamic flows (average over UF and DF). **(C)** Hemodynamic-regulated SEs form significantly more interactions with promoters than TEs do in HAECs. **(D)** Percentage of SEs (red) and TEs (gray) that repetitively contact to a promoter. ****p-value* ≤ 0.001 and *****p-value* ≤ 0.0001 was determined by Student's t-test.

2.3.4 Unidirectional flow and disturbed flow induce distinct cohorts of endothelial super-enhancers.

Mechanical forces are major determinants of the endothelial transcriptomes but the identity of endothelial super-enhancers responding to distinct mechanical cues, such as different hemodynamics forces, remains to be determined. We thus set out to systematically identify flow-sensitive endothelial super-enhances by comparing the H3K27ac ChIP-seq results in HAECs subjected to 24-hr athero-protective unidirectional flow (UF) with those in cells exposed to

athero-prone disturbed flow (DF). We defined the "UF-enriched" super-enhancer as the total H3K27ac signal at one super-enhancer locus greater in HAECs under UF than DF (*p-value* ≤ 0.0001, Fold Change/FC ≥ 1.2) (Figure 2.4A). Similarly, we defined a "DF-enriched" super-enhancer if the total H3K27ac signal was greater under DF than UF (*p-value* ≤ 0.0001, FC ≥ 1.2) (Figure 2.4A). We defined these two clusters of super-enhancers as "flow-sensitive" super-enhancers. In contrast, we defined a "core" super-enhancer when at this given locus, the H3K27ac signal remains similar in HAECs under UF and DF. Using these criteria, we identified 152 UF-enriched super-enhancers, 183 DF-enriched super-enhancers, and 665 core super-enhancers in HAECs (Figure 2.4A). The genome distributions of the core and flow-sensitive endothelial super-enhancers are described in Figure 2.4B. We then performed motif analyses to identify the enriched TF binding motifs in each of these three classes of endothelial super-enhancers. Common TF motifs of NRF2 (a transcriptional activator) and BACH (a transcriptional suppressor) are identified in flow-sensitive and core endothelial super-enhancers (Figure 2.4C). This implied that both transcriptional activators and transcriptional suppressors may be involved in endothelial super-enhancers activity, which is consistent with the previously reported roles of NRF2 and BACH in driving key endothelial functions such as proliferation, migration, apoptosis, and inflammation[318–323]. ETS binding motif is enriched only in the UF-enriched super-enhancers whereas the binding motif of NFκB-p65 are only enriched in the DF-enriched super-enhancers (Figure 2.4C). Notably, ETS-1 is induced in endothelial cells under UF[324] and a cooperative action of ETS and KLF2 (a key TF to maintain endothelial quiescence under UF) has been reported[325]. Meanwhile, the major role of NFκB-p65 in endothelial inflammation induced by disturbed flow has been well established[326–328]. These results characterized the flow-sensitive endothelial enhancers as a function of hemodynamics key to the

protection or susceptibility to atherosclerosis. These finding also support the proposed model that the combinatorial effects of transcription factor bindings on super-enhancers are key to cell type-specific and context-dependent gene expression/ biological functions such as cell plasticity[244,245,260,329].

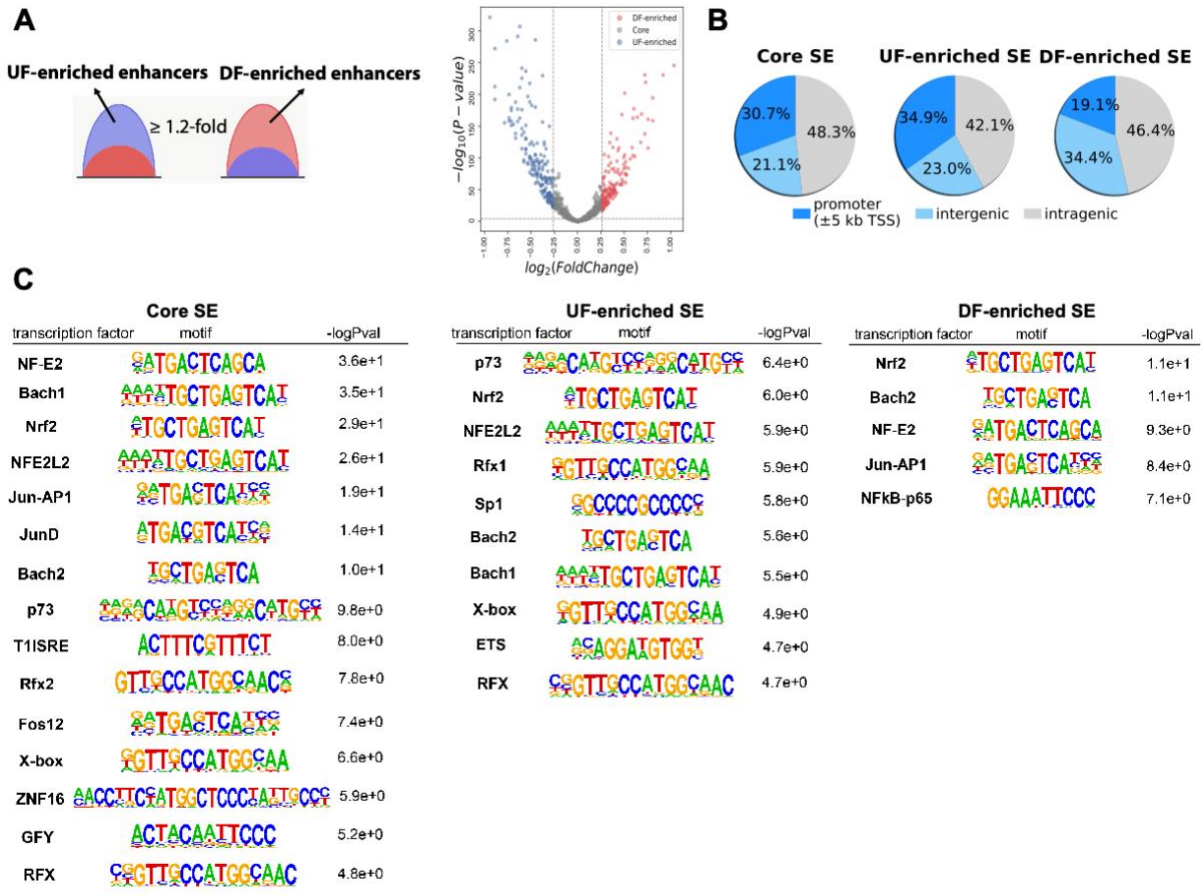

Figure 2.4. Unidirectional flow and disturbed flow induce distinct cohorts of endothelial super-enhancers. (A) Identifying mechano-sensitive SEs and Core SEs by comparing H3K27ac in HAECs subjected to UF and DF at each SE locus. *Left*: schematic plot for identification of mechano-sensitive SEs using fold change of H3K27ac signal ≥ 1.2; *Right*: volcano plot showing $\log_2$(fold change) vs. -$\log_{10}$(p-value) of differential H3K27ac enrichment at each SE locus in response to DF vs. UF. UF-enriched SEs (blue dots) were selected by $\log_2$(fold change) ≤ -0.263; **Figure 2.4. continued.** DF-enriched SEs (red dots) were selected by $\log_2$(fold change) ≥ 0.263; Core SEs (partially gray dots) were selected by |$\log_2$(fold change)| < 0.263; statistical significance -$\log_{10}$(p-value) ≥ 4 was used as cutoff. **(B)** Pie charts of genomic distributions of each cluster of SEs. **(C)** Enriched transcription factor binding motifs within each cluster of SEs.

2.3.5 Flow-sensitive endothelial super-enhancers physically contact a cohort of promoters, the expression of which is dynamically regulated by hemodynamic forces.

To probe possible biological functions of these flow-type specific endothelial super-enhancers, we employed the PCHi-C results to identity a list of endothelial genes, promoters of which are physically contacted by UF-enriched or DF-enriched super-enhancers. We further selected promoters/genes that are actively expressed in HAECs under flow, by integrating with our RNA-seq dataset[131] to only choose genes with FPKM ≥ 1 under either type of flow. 249 endothelial promoters/genes are physically contacted by UF-enriched super-enhancers whereas 280 endothelial promoters/genes are contacted by DF-enriched super-enhancers (Figure 2.5A). Very few (18) endothelial promoters are contacted by both UF- and DF-enriched super-enhancers (Figure 2.5A). Gene ontology analyses demonstrated that genes contacted to flow-sensitive super-enhancers participate in biological functions key to endothelial mechano-transduction pathways. Specifically, endothelial genes exclusively contacted by UF-enriched super-enhancers are enriched in biological processes such as actin filament assembly and small GTPase signaling (Figure 2.5B). Genes exclusively contacted by DF-enriched super-enhancers are implicated in biological functions of endothelin receptor signaling pathway, tight junction organization, and vasculature development (Figure 2.5B). We next hypothesized that flow-type specific super-enhancers could drive endothelial gene transcription as the function of the flow waveforms in a coordinated fashion. To test this hypothesis, we interrogated the list of flow-sensitive endothelial super-enhancers along with their targeted genes (identified by PCHi-C) with the transcriptome dataset conducted in HAECs subjected to the same UF and DF conditions. RNA-seq results demonstrated that the transcription of genes contacted by UF-enriched super-enhancers tended to be up-regulated by UF (median $\log_2 FC < 0$, DF/UF),

whereas those contacted by DF-enriched super-enhancers tended to be up-regulated by DF (median $\log_2$FC > 0, DF/UF; Figure 2.5C). The genome-wide loci contacted by flow-sensitive super-enhancers and flow-sensitive transcriptome in HAECs were plotted in the circos plot in Figure 2.5D. Inner circle links are PCHi-C-detected intra- and inter-chromosomal interactions. Physical connections between UF-enriched super-enhancers and gene promoters are labeled in blue and physical connections between DF-enriched super-enhancers and promoters are labeled in red. The majority of chromosomal interactions between flow-sensitive super-enhancers and endothelial promoters are intra-chromosomal and only a few interactions were inter-chromosomal. The outer circle represents histograms of mRNA levels (FPKM) of flow-sensitive genes detected by RNA-seq (*q-value* ≤ 0.05) in HAECs subjected to 24-hr UF or DF. Blue histograms represent the mRNA levels of flow-sensitive genes in HAECs under UF and red histograms show the mRNA levels in HAECs under DF. Overall, flow-regulated endothelial genes are largely located in genomic loci contacted by flow-sensitive super-enhancers, supporting their functions in regulating the endothelial mechano-sensitive transcriptome.

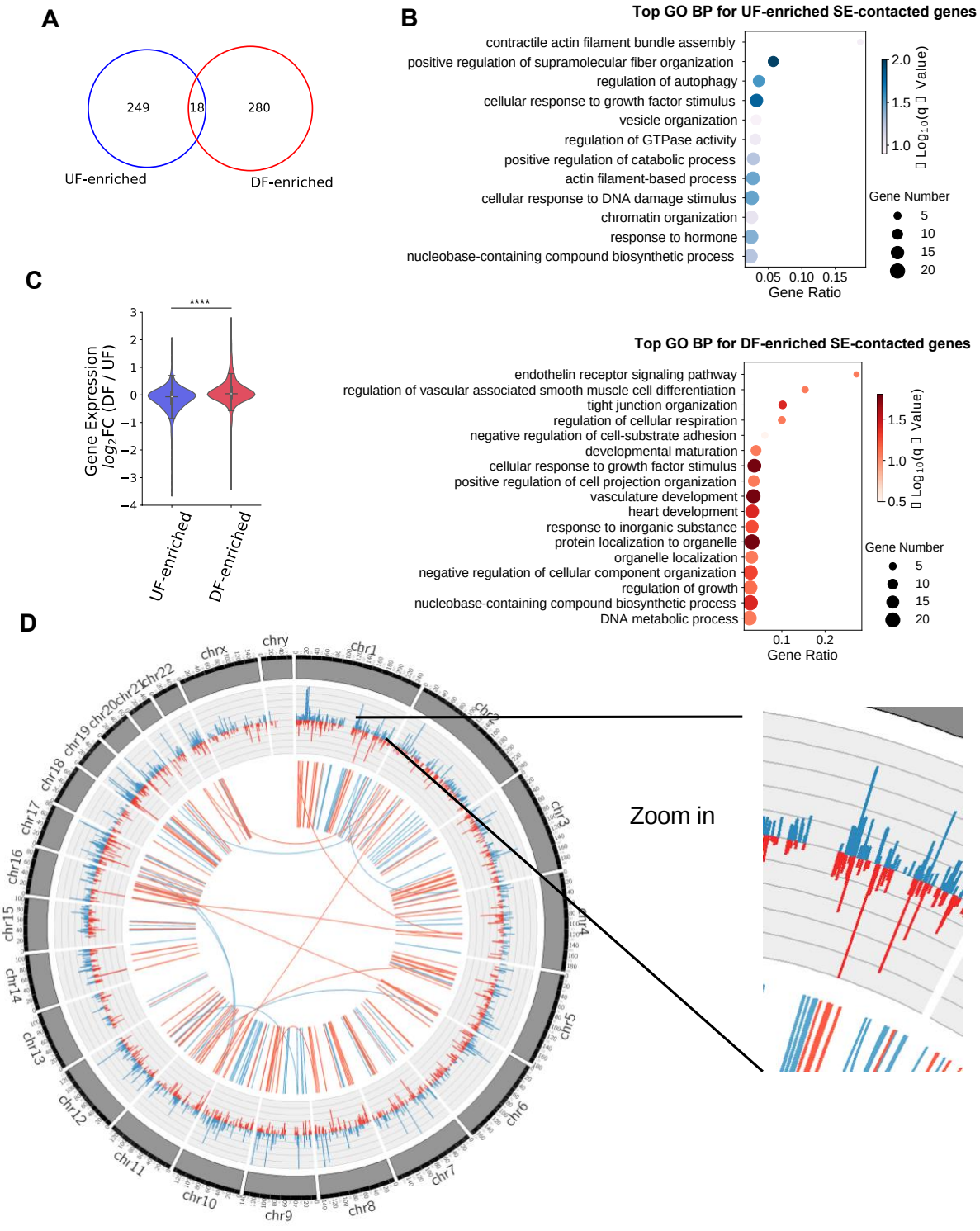

Figure 2.5. Mechano-sensitive super-enhancers preferentially contact the promoters of mechano-sensitive genes to regulate their transcription. (A) Venn diagram showing the number of genes that exclusively contact to UF-enriched SE or to DF-enriched SE, and genes that simultaneously contact to both type of SE. **(B)** Gene ontology analysis showing top

Figure 2.5. continued. biological processes associated with highly expressed genes contacted to UF-enriched SEs (*top*) and DF-enriched SEs (*bottom*). **(C)** Hemodynamics-regulated transcription fold change (DF/UF) of genes contacted to UF-enriched SEs vs. DF-enriched SEs. **(D)** Circos plot illustrates the genome-wide loci contacted by flow-sensitive super-enhancers and flow-sensitive transcriptome in HAECs. *Inner circle links*: PCHi-C-detected intra- and inter-chromosomal interactions. Physical connections between UF-enriched super-enhancers and gene promoters are labeled in blue and physical connections between DF-enriched super-enhancers and promoters are labeled in red. *Outer circle histograms*: RNA-seq-detected expression levels (FPKMs) of flow-sensitive genes (*q-value* ≤ 0.05) in HAECs subjected to 24-hr UF or DF. Blue histograms represent the mRNA levels of flow-sensitive genes in HAECs cultured under UF and red histograms show the mRNA levels in HAECs cultured under DF. Overall, flow-regulated endothelial genes are largely located in genomic loci contacted by flow-sensitive super-enhancers. ****p-value ≤ 0.0001 was determined by Student's t-test.

2.3.6 A cohort of endothelial flow-sensitive super-enhancers contain CVD GWAS SNPs and contact promoters of flow-sensitive genes in HAECs.

To refine flow-sensitive endothelial super-enhancers for investigation of their biological functions, we assessed their enrichment of GWAS SNPs associated with cardiovascular diseases curated from NHGRI-EBI GWAS Catalog[300]. Moreover, PCHi-C in HAECs was used to identify the physical interaction of these CVD SNP-imbedded super-enhancers to specific endothelial promoters. Our analyses identified 10 UF-enriched super-enhancers and 24 DF-enriched super-enhancers which all contain at least one cardiovascular trait-associated GWAS SNP and physically contact at least one endothelial promoter. Figure 2.6A and 2.6B detail the genomic locations of these flow-sensitive endothelial super-enhancers along with the number of imbedded SNPs, their associated CVD traits, and their connected gene promoters. The majority of these flow-sensitive super-enhancers contact multiple genes. To further probe the regulatory functions of these super-enhancers, we integrated the RNA-seq results from HAECs under UF and DF, and found a large number of genes contacted by these CVD SNP-embedded flow-sensitive super-enhancers are also transcriptionally regulated by hemodynamic forces. Particularly, transcription

levels of genes contacted by UF-enriched super-enhancers are largely increased by UF (Figure 2.6A) whereas transcripts of genes contacted by DF-enriched super-enhancers are mostly elevated by DF (Figure 2.6B). Taken together, the integration of H3K27ac ChIP-seq, GWAS, PCHi-C, and RNA-seq identified a cohort of CVD SNP-containing flow-sensitive endothelial super-enhancers which physically contact to multiple promoters of flow-sensitive genes.

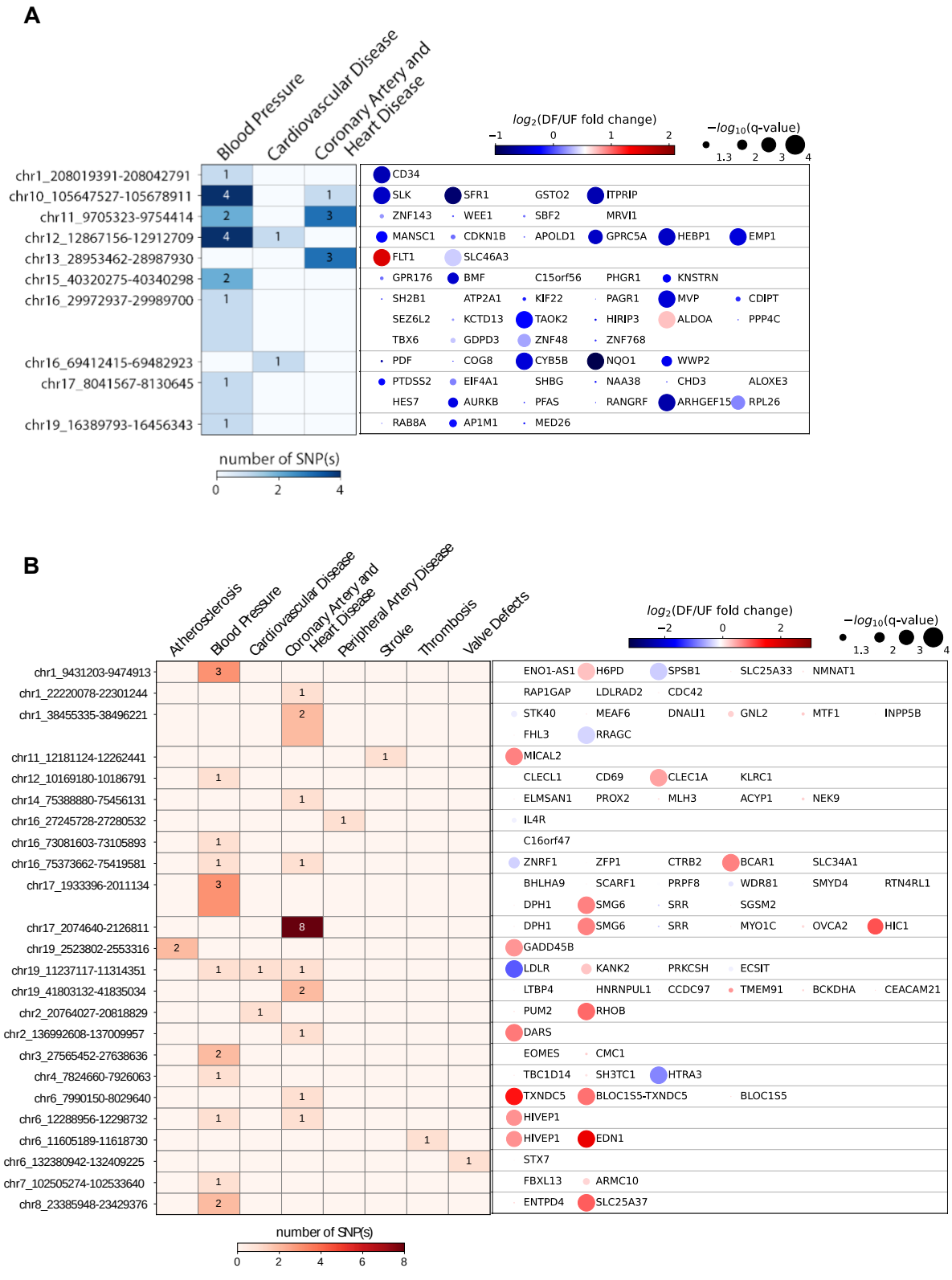

Figure 2.6. Refining functional mechano-sensitive super-enhancers. Heatmaps summarizing UF-enriched SEs **(A)** and DF-enriched SEs **(B)** harboring CVD-associated GWAS SNP(s) and

Figure 2.6. continued. the hemodynamics-regulated expression fold change of these SE-contacted genes. *Left heatmaps:* The color and number both represent the amount of CVD SNPs that reside in each super-enhancer locus. The CVD trait associated with the SE-harboring GWAS SNP was located on the top. *Right heatmaps:* Color of the dots represents the gene expression fold change in HAECs subjected to DF compared to UF; blue ($log_2FC < 0$): upregulated by UF; red ($log_2FC > 0$): upregulated by DF. Size of the dots represents the statistical significance (*q-value*) of gene expression fold change.

2.3.7 UF-enriched super-enhancer chr16: 69412415-69482923 up-regulates UF-induced anti-oxidant genes NQO1, CYB5B and WWP2 in HAECs.

Sequencing-based identification of super-enhancers requires experimental validation[330,331]. Therefore, we set out to determine the regulatory function of a UF-enriched super-enhancer in regulating gene expression in HAECs. We prioritized chr16: 69412415-69482923 for investigation for the following reasons. Firstly, GWAS have demonstrated that chr16: 69412415-69482923 harbors a genetic variant rs75086474 strongly associated with CVD. Specifically, UK Biobank identified that SNP rs75086474 is significantly associated with CVD (*p-value* = 6E-10)[332] and with vascular/heart problems diagnosed by doctor (*p-value* = 4.7E-10)[333]. Secondly, super-enhancer analyses in HAECs under athero-relevant flows showed that the H3K27ac activity in chr16: 69412415-69482923 is markedly increased by UF when compared to DF (Figure 2.7A). Thirdly, PCHi-C and CHiCAGO demonstrated that chr16: 69412415-69482923 physically contacts five promoters in HAECs: Polypeptide Deformylase (PDF), Component Of Oligomeric Golgi Complex 8 (COG8), NAD(P)H:quinone oxidoreductase 1 (NQO1), Cytochrome B5 Type B (CYB5B) and WW Domain Containing E3 Ubiquitin Protein Ligase 2 (WWP2). Fourthly, RNA-seq in HAECs detected three (NQO1, CYB5B and WWP2) of these five genes were transcriptionally upregulated in HAECs subjected to UF compared to DF (Figure 2.7B). Consistent with the increased H3K27ac activity under UF, our data of Assay for Transposase-Accessible Chromatin using sequencing (ATAC-seq) demonstrated that the

chromatin accessibility at chr16: 69412415-69482923 is increased in HAECs under UF when compared to DF (Figure 2.7A).

Notably, NQO1, CYB5B and WWP2 not only are all induced by UF but also implicated in the anti-oxidant endothelial phenotype associated with UF. NQO1 acts both as a quinone reductase and a superoxide reductase, which protects against endothelial inflammation and spontaneous hypertension[334–336]. CYB5B forms a reducing system with cytochrome b5 reductase type 3 (CYB5R3) and NADH to protect against oxidative stress[337]. WWP2 modulates the ubiquitination of Septin4 to protect against oxidative stress-induced endothelial injury and vascular remodeling[338]. Thus, we hypothesize this UF-enriched super-enhancer can promote endothelial quiescence through co-regulating the transcription of these three genes.

To test the regulatory role of chr16: 69412415-69482923 in endothelial NQO1, CYB5B and WWP2 expression, we used CRISPR interference (CRISPRi) to suppress the activity of targeted *cis*-regulatory elements[339] and their contacted promoters[340]. Specifically, we transduced HAECs subjected to 24-hr UF with dCas9-KRAB carrying adenovirus, followed by transfection of a pair of sgRNAs targeting the H3K27ac peak surrounding CVD GWAS SNP rs75086474. We found that rs75086474-targeted sgRNAs significantly reduced the mRNA expression of NQO1, CYB5B and WWP2 when compared to cells transfected with non-targeting sgRNA (Figure 2.7C). These results validate the regulatory activity of one super-enhancer chr16: 69412415-69482923 in up-regulating multiple key anti-oxidant genes in endothelial cells under UF.

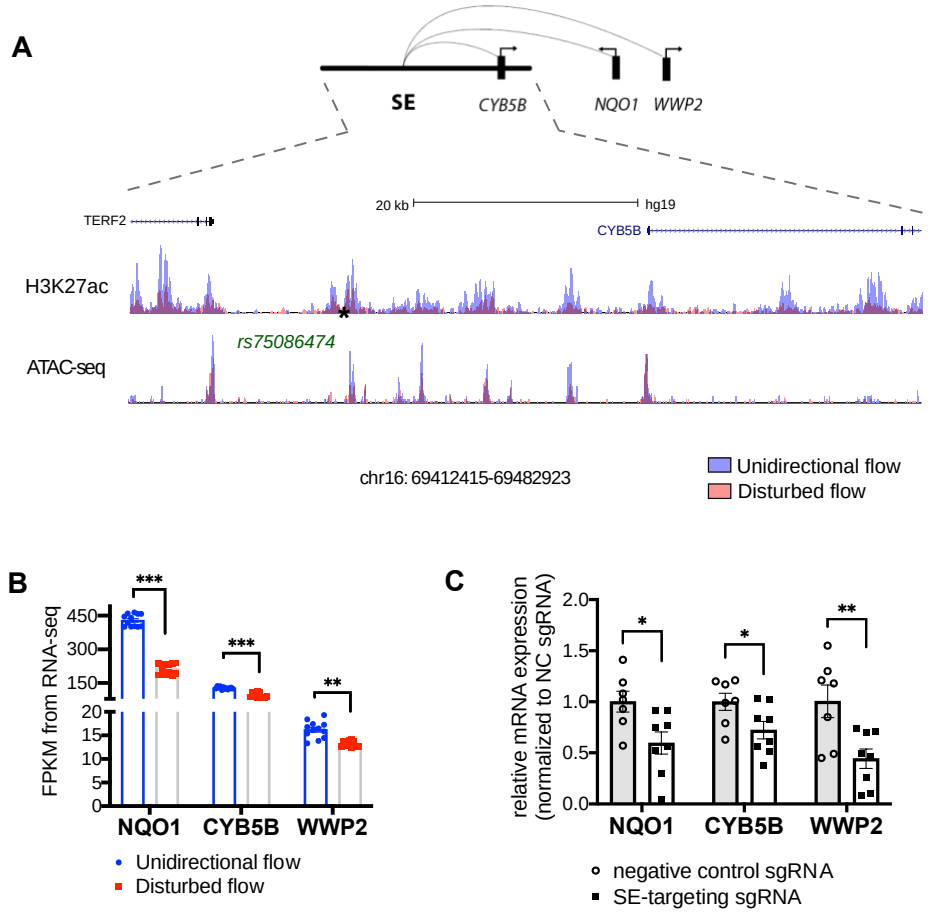

Figure 2.7. A UF-enriched super-enhancer positively regulates the transcription of three genes contributing to HAECs quiescence. (A) Genome track of UF-enriched SE chr16:69412415-69482923 (hg19) which has higher H3K27ac signal under UF (blue) than under DF (red), contacted to the promoters of three UF-induced genes and harbors one GWAS SNP (labeled as *****) associated with cardiovascular disease. The chromatin accessibility at this UF-enriched super-enhancer is also increased in HAECs cultured under UF when compared to DF. **(B)** Transcriptions of NQO1, CYB5B and WWP2 were significantly induced in HAECs subjected to UF compared to DF from RNA-seq. **(C)** CRISPRi targeting this UF-enriched SE significantly reduced the transcription of NQO1, CYB5B and WWP2 in HAECs subjected to 24-hr UF. n = 7-10; Data represents mean ± SEM. **p-value* ≤ 0.05 and ***p-value* ≤ 0.01 were determined by Student's t-test.

2.3.8 DF-enriched super-enhancer chr6: 11605189-11618730 functionally up-regulates DF-induced EDN1 and HIVEP in HAECs.

Similarly, we then prioritized a DF-induced endothelial super-enhancer chr6: 11605189-11618730 for functional investigation. H3K27ac ChIP-seq indicated that the chr6: 11605189-11618730 enhancer activity is significantly induced by DF in HAECs (Figure 2.8A). Chr6: 11605189-11618730 harbors a GWAS SNP rs113092656 which is significantly associated with thrombosis[341]. In agreement with the H3K27ac results, our ATAC-seq showed that the chromatin accessibility of chr6: 11605189-11618730 is markedly increased in DF-exposed HAECs when compared to cells under UF (Figure 2.8A). CHiCAGO-analyzed PCHi-C in HAECs demonstrated that chr6: 11605189-11618730 physically contacts the promoter regions of endothelin-1 (EDN1) and Members of the ZAS family, ZAS1 (HIVEP1). The transcriptional levels of EDN1 and HIVEP1 are both significantly induced in HAECs by DF when compared to UF (Figure 2.8B).

Endothelin-1 is primarily produced by endothelial cells, and functions as one of the most potent vasoconstrictors in humans[342]. EDN1 contributes to CVD and thrombosis through both a paracrine fashion to promote vascular smooth muscle cell-mediated vasoconstriction[342,343] and remodeling[344,345], as well as an autocrine mechanism to inhibit eNOS expression[346,347] while increasing von Willebrand factor (vWF)[348]. The regulation of EDN1 by a flow-sensitive super-enhancer was not previously proposed. HIVEP1 belongs to the HIVEP family which are DNA-binding proteins containing several zinc fingers[349]. Increased endothelial HIVEP1 has been linked to elevated endothelial platelet adhesion[350] and genetic variants at the HIVEP1 locus are associated with venous thrombosis[351,352]. In addition, plasma HIVEP1 level is positively associated with the occurrence of venous thromboembolism[353].

We then conducted CRISPRi experiment to test the causal role of DF-induced super-enhancer chr6: 11605189-11618730 in regulating EDN1 and HIVEP1 transcription in HAECs

under DF. Specifically, we designed three sgRNAs to target the H3K27ac peak surrounding rs113092656. Our data suggested that when compared to the non-targeting sgRNA, rs113092656-targeted sgRNAs significantly reduced the transcription of EDN1 and HIVEP1 in HAECs under 24-hr DF (Figure 2.8C). H3K27ac ChIP-seq, ATAC-seq, PCHi-C, and CRISPRi experiments collectively demonstrate that chr6: 11605189-11618730 functions as a DF-induced super-enhancer to up-regulate endothelial expression EDN1 and HIVEP.

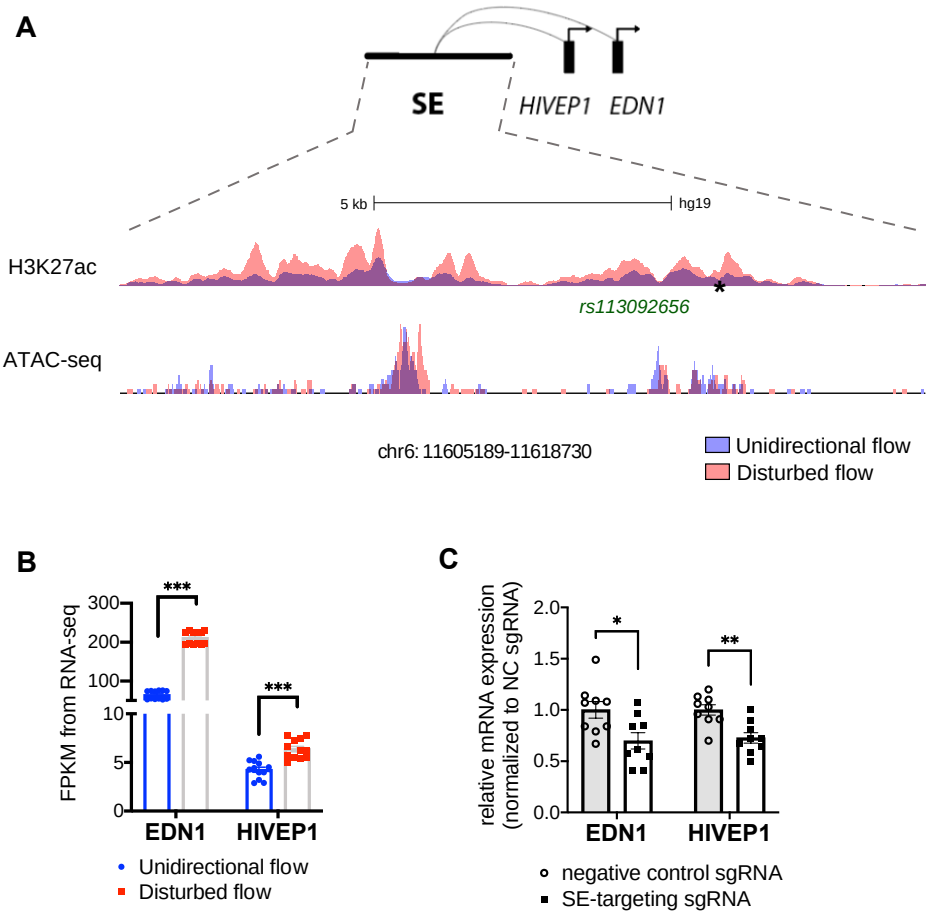

Figure 2.8. A DF-enriched super-enhancer positively regulates the transcription of two genes contributing to HAECs activation. (A) Genome track of DF-enriched SE chr6: 11605189-11618730 (hg19) which has higher H3K27ac signal under DF (red) than under UF (blue), contacted to the promoters of two DF-induced genes and harbors one GWAS SNP (labeled as *****) associated with thrombosis. The chromatin accessibility at this DF-enriched super-enhancer is also increased in HAECs cultured under DF when compared to UF. **(B)**

Figure 2.8. continued. Transcriptions of EDN1 and HIVEP1 were significantly induced in HAECs subjected to DF compared to UF from RNA-seq. **(C)** CRISPRi targeting this DF-enriched SE significantly reduced the transcription of EDN1 and HIVEP1 in HAECs subjected to 24-hr DF. n = 6; Data represents mean ± SEM. **p-value* ≤ 0.05 and ***p-value* ≤ 0.01 were determined by Student's t-test.

2.4 Discussion

Super-enhancers have emerged as prominent *cis*-regulatory elements to orchestrate the majority of cell-type-specific patterns of gene expression critical to the biological processes in development[262,263], disease progression and tissue damage[264–266]. Mechano-transduction mechanisms are instrumental to embryonic and organ development as well as the physiological control of tissue homeostasis[354]; nevertheless, the molecular identity of mechano-sensitive super-enhancers remains poorly understood. Endothelial mechano-sensing mechanisms are crucial regulatory controls of vascular homeostasis and diseases[26,355–357]. Here, we provide the first characterization of typical-enhancers and super-enhancers in endothelial cells subjected to well-defined hemodynamic forces by integrating multi -omics datasets including H3K27ac ChIP-seq, transcription factor ChIP-seq, Promoter Capture Hi-C, GWAS, and RNA-seq. We report that compared to typical-enhancers, super-enhancers are enriched with the binding sites of multiple key endothelial transcription factors and GWAS genetic variants associated with cardiovascular diseases. The overall mRNA expression of endothelial genes which are physically contacted by super-enhancers is higher when compared to genes contacted by typical-enhancers. Super-enhancer-contacted genes in HAECs are enriched in biological processes related to endothelial specification and vascular functions. We also characterized a cohort of endothelial super-enhancers which are specifically activated by athero-protective unidirectional flow or by athero-susceptible disturbed blood flow. Genes contacted by UF-enriched super-enhancers overall have

higher transcriptional levels in endothelium under UF while genes contacted by DF-enriched super-enhancer largely have higher transcriptional levels in cells under DF. CRISPRi was employed to functionally demonstrate the enhancer activity of one UF-enriched and one DF-enriched candidate endothelial super-enhancer, both of which contain a CVD genetic variant and physically contact promoters of flow-sensitive genes. To this end, we successfully integrated multi-layer -omics to systematically identify the *cis*-regulatory architecture of the flow-sensitive endothelial epigenome, particularly super-enhancers, as a function of hemodynamic forces instrumental to vascular hemostasis and disease.

Our H3K27ac ChIP-seq results identified 1,000 super-enhancers and 26,457 typical enhancers in endothelial cells subjected to blood flows. These results support the notion that super-enhancers represent less than 5% of the enhancers in a cell[260,316,358]. Analyses of the genomic locations demonstrate that these endothelial super-enhancers preferentially locate in intragenic regions and distribute less in intergenic and promoter-adjacent regions compared to endothelial typical-enhancers. The preferred intragenic genomic localization of endothelial super-enhancers is also reported in ATAC-seq-identified super-enhancers in vascular endothelium from human atherosclerotic lesion[246]. Since the abovementioned study was conducted in isolated blood vessels where the blood flow was absent after the endarterectomy operations, our new results provide a complementary open data resource for endothelial enhancers in cells under well-defined hemodynamics.

Large-scale human genetics studies have evidently established the association of common genetic variants with human diseases. Recent discoveries demonstrated that disease-associated loci are enriched in tissue-specific regulatory regions including enhancers in corresponding disease-relevant cell types[246,255,359,360]. Consistently, GWAS studies on CVD identified that over

90% of these genetic variants are located in the noncoding genome[77,249], and a few candidate CVD variants have been shown to exert biological functions by modulating the activities of *cis*-regulatory elements, particularly enhancers in the cell types key to the CVD pathogenesis. For instance, rs17293632 in the CAD locus 15q24.1 is associated with the chromatin accessibility of an enhancer and consequent SMAD3 expression in human coronary artery smooth muscle cells[361]. The enhancer variant rs12740374 at CVD locus 1p13 influences low-density lipoprotein cholesterol (LDL-C) level by regulating sortilin 1 (SORT1) expression in hepatocytes[360]. Here we showed that endothelial super-enhancers are enriched with CVD SNPs, supporting the emerging importance of genetic contribution to the arterial wall-specific mechanisms in CVD[362]. Given the critical role of endothelial mechano-transduction in CVD pathogenesis, this study provides a roadmap and public datasets for future studies to identify the causal CVD variant/gene and elucidate the underlying molecular mechanisms, which are ongoing challenges in the post GWAS era[77]. Indeed, our previous candidate approaches have identified that rs17114036, a common noncoding SNP strongly associated with CVD, is located in a flow-sensitive endothelial enhancer that modulates the expression of PLPP3 (phospholipid phosphatase 3) which maintain endothelial quiescence and monolayer integrity under UF[258,290].

Transcriptional enhancers control the spatial-temporal expression of the target genes through physical contact[309]. Analyses of coordinated activation of enhancers and promoters by chromatin accessibility assay without the experimental information of the three-dimensional genome organization have been employed to identify putative active enhancers in vascular cells[246]3/31/2023 3:40:00 PM. Here we advance the endothelial functional genomics studies by conducting the Promoter Capture Hi-C (PCHi-C) assay which enables the genome-wide identification of distal promoter-interacting regions for all known promoters. Hi-C was

developed to identify the entire ensemble of chromosomal interactions within a cell population and has been conducted in human umbilical vein endothelial cells (HUVECs) and HAECs[311,312]. Based on this, PCHi-C was further developed to specifically map the genome-wide promoter-interacting DNA sequences by enriching the promoter-containing ligation products from Hi-C libraries using tens of thousands biotinylated RNA 120-mers to pull down fragments containing all annotated promoters[314,315]. PCHi-C has been successfully conducted in many cell types[267,296,314,315,363–366] but not in human endothelial cells. Our PCHi-C results in HAECs analyzed by CHiCAGO[298], a computational pipeline which accounts for sequence capture , successfully identified the whole-genome 3D ensemble of promoter-interacting region in human endothelium. The PCHi-C data allow us to further refine the H3K27ac-implicated enhancers by assigning their contacted promoters. Our results demonstrate that super-enhancer-contacted promoters are enriched in genes associated with endothelial and vascular biological processes (e.g. response to oxygen levels and blood vessel development) while typical-enhancer-contacted genes are involved in more general cellular pathways (e.g. Golgi vesicle transport and translation), further supporting the proposed role of super-enhancers in determining cell fate and cell type-specific gene expression patterns[259,260]. Our results show that super-enhancer-contacted endothelial genes are overall more highly expressed than typical-enhancer-contacted genes (Figure 2.3B), evidencing the predicted function of super-enhancers to confer higher expression on their target genes compared to typical-enhancers[259,260,316,358]. One possible mechanism, like what has been discovered in cancer cells[317] is that individual endothelial super-enhancers, when compared to typical-enhancers, contact more frequently with a given target promoter (Figure 2.3D). Our PCHi-C dataset in HAECs can be used in junction with the Hi-C results in HUVECs and HAECs[311,312] to construct a basic architecture of the endothelial 3D genome regardless of

stimuli since higher-order structural reorganizations of chromatin interaction are more dynamic and detectable in gametogenesis, early embryonic development, lineage commitment and cell differentiation but not in differentiated cells[367]. Assays detecting histone marks and chromatin accessibility, such as H3K27ac ChlP-seq and ATAC-seq, are more dynamically regulated in differentiated cells can then be used to detect the local chromatin alterations modulated by biochemical and biomechanical cues.

Super-enhancers are implicated in functions related to tissue-specific or developmental stage-specific manner[259,262,263], and our results further demonstrate their dynamic regulation by atherosclerosis-relevant hemodynamic forces. Endothelial genes physically contacted by UF-enriched super-enhancers are preferentially up-regulated by UF whereas genes contacted by DF-enriched super-enhancers are favorably up-regulated by DF, which point to coordinated action of super-enhancer activity and targeted gene transcription as a function of blood flow types. Distinct transcription factor binding motifs were identified between the UF-enriched and DF-enriched super-enhancers. These results collectively suggest a plausible mechanism that flow-sensitive endothelial transcriptome, at least partially, is attributable to the combinatorial activation or inactivation of enhancers and transcription factors, a model proposed to drive the context-dependent regulation of genes required for specialized functions of macrophages[368]. Binding sites for ETS-1, a transcription factor implicated in endothelial responses to unidirectional flow[324,325], are particularly enriched in the UF-enriched endothelial super-enhancers. In contrast, binding sites of pro-inflammatory transcription factors Jun/AP1 and NFκB-p65[326–328,369] are enriched in the DF-enriched endothelial super-enhancer. This is consistent with previous observation in endothelial cells that a much higher density of p65 motifs was found in TNFα-gained SEs than in TNFα-lost SEs[244]. These data also support the recently

emerging condensate model for gene regulation[331,370,371] that super-enhancers cooperatively assemble a dynamically regulated high density of transcriptional apparatus. Future studies are required to further dissect the detailed molecular controls of distinct combinations of transcription factors and super-enhancers in regulating endothelial responses to a wide range of biomechanical cues (shear stress, cyclic stretch, etc.) in different vascular beds.

Although genome-wide epigenetic studies and motif analyses promote the genome-wide discovery of super-enhancers, chromatin and transcription factor profiling alone do not ascertain enhancer activity. Functional assays are critical to verify the enhancer activity and eliminate false discoveries[372]. To do so, we have prioritized two omics-identified flow-sensitive endothelial super-enhancers for functional dissection to determine their enhancer activity on target gene expression. chr16: 69412415-69482923 is a UF-enriched while chr6: 11605189-11618730 is a DF-induced endothelial super-enhancer identified by H3K27ac ChlP-seq and ATAC-seq. Both super-enhancers contain genetic variants associated with CVD whereas their enhancer activities have not been experimentally determined. The activities of these two flow-sensitive super-enhancers are supported by PCHi-C, which identified physical looping to promoters of flow-regulated endothelial genes. In agreement with the chromatin profiling and 3D endothelial genome architecture, CRISPR interference experiments demonstrated the UF-enriched super-enhancer chr16: 69412415-69482923 is critical to maintain the elevated expression of NQO1, CYB5B and WWP2 in endothelial cells under UF. Meanwhile, DF-enriched super-enhancer chr6: 11605189-11618730 regulates the elevated endothelial expression of EDN1 and HIVEP1 under DF. Functional identification of these two flow-sensitive super-enhancers further support the notion that a single super-enhancer can impact a complex regulatory network and consequent physiological processes by coordinated activations on functionally connected genes, a model

proposed in other gene regulatory mechanisms such as microRNAs[326,373,374]. The proposed functions of NQO1, CYB5B and WWP2 in promoting the anti-oxidant endothelial phenotype have been well established[335,337,338] whereas EDN1 and HIVEP1 are implicated in the pro-inflammatory and pro-thrombotic endothelial function[342–348,350,353]. The presence of the respective CVD-associated SNPs (rs75086474 and rs113092656) in these two flow-sensitive endothelial super-enhancers suggest a possible convergence of CVD genetic predisposition and mechano-transduction mechanisms on enhancer activities, a phenomenon described in the CVD SNP rs17114036 located in a flow-sensitive endothelial enhancer[257]. Nevertheless, whether rs75086474 and rs113092656 are the causal SNPs and the plausible underlying molecular mechanisms remain unknown. This will be the subject of future studies.

Cellular transcriptional responses to bio-mechanical stimuli are critical to embryogenesis, organ development and patho-physiological control of tissues. The endothelial transcriptome is tightly and dynamically regulated by blood flow which is a major regulator of vascular network morphogenesis, vascular tone control, vascular structure and localization of pathological vascular remodeling[26,355,356]. Atherosclerosis and stenosis largely initiate and develop in arterial regions at which local disturbed flow activates endothelial cells, whereas unidirectional flow promotes the anti-inflammatory and anti-oxidant endothelial phenotype. Employing multi-layer omics approaches, we systematically characterized the chromatin architecture, particularly enhancers, in endothelial cells under well-defined hemodynamics. In summary, our results elucidate the identity and highlight the importance of super-enhancers as CVD SNP-enriched *cis*-regulatory elements contributing to the flow-regulated endothelial transcriptome that are key to vascular health and disease.

CHAPTER THREE: MECHANO-SENSITIVE LACTATE DEHYDROGENASE A (LDHA) REGULATES ENDOTHELIAL EPIGENOME AND ATHEROSCLEROSIS

3.1 Introduction

Atherosclerotic plaques preferentially develop at sites of arteries where local disturbed flow (DF) activates endothelium[375–377]. In contrast, the straight parts of arteries are exposed to unidirectional flow (UF) which promotes endothelial quiescence that is resistant to plaque formation[375–377]. Despite the focal nature of atherogenesis, current treatments to atherosclerosis primarily target systematic risk factors. Investigating novel molecular mechanisms that link DF to focal plaque formation is crucial as it may provide potential targets for local therapeutics.

Metabolism has emerged as a central control of endothelial functions, and recent studies demonstrated that endothelial metabolism is tightly regulated by hemodynamics[378–381]. Specifically, glycolysis contributes 75-85% of ATP generation in endothelium[127]. Studies conducted by Fang lab and others have collectively shown that glycolysis is significantly increased in endothelial cells subjected to disturbed flow compared to cells exposed to unidirectional flow or static conditions[378]. However, the role of DF-induced endothelial glycolysis in atherosclerosis remains poorly understood.

Previously, we detected an upregulation of the glycolytic gene Lactate Dehydrogenase A (LDHA) in human aortic endothelial cells (HAECs) that were subjected to disturbed flow compared to cells under unidirectional flow (Figure 3.1A); however, the putative role of LDHA in endothelial mechano-transduction and atherogenesis is completely unknown. In this study, I tested the hypothesis that disturbed flow increases the glycolytic enzyme Lactate Dehydrogenase A to promote endothelial activation and atherosclerosis.

3.2 Materials and Methods

Regulatory. Animal studies were approved by the Institutional Animal Care and Use Committee (ACUP #72567) at the University of Chicago. Cells, viral vectors and DNA-based vectors were approved by the Institutional Biosafety Committee (IBC #1512).

Inducible and conditional KO mouse models. A novel inducible mouse line was bred in which Ldha can be conditionally deleted in adult endothelium. $Ldha^{fl/fl}$ mice[382] (#030112, The Jackson Lab) were crossed with Cdh5(PAC)-CreERT2 mice[383] (from Dr. Ralf Adams) to generate $Ldha^{fl/fl}$-Cdh5-CreERT2 mice. In parallel, mice with Cdh5-CreERT2 genotype will serve as the control group. Mouse genotypes were confirmed by PCR using the following primers: $Ldha^{fl/fl}$ forward 5'- CTGAGCACACCCATGTGAGA -3' and reverse 5'-AGCAACACTCCAAGTCAGGA -3'; Cdh5-CreERT2 forward 5'-GCCTGCATTACCGGTCGATGCAACGA -3' and reverse 5'-GTGGCAGATGGCGCGGCAACACCATT -3'. To induce Cre expression, starting from week 5, mice from all groups will be injected (intraperitoneal) daily with 80 mg/kg tamoxifen for 7 consecutive days.

Atherosclerotic mouse models. (1) Adeno-Associated-Virus-9 (AAV9)-PCSK9 (Proprotein Convertase Subtilisin/Kexin type 9) overexpression model. Starting at week 8 (two weeks after injection completion), mice from all groups were injected once via tail vein with AAV9-packaged vector containing the PCSK9 gene. 1E11 vector genome copies (VG) were diluted in sterile PBS for injection, and right after the injection, mice were fed with high-fat diet (Harlan Envigo TD88137) containing 21% fat (wt/wt) for 12 weeks until week 20 of age. Mice from all groups were fasted overnight prior to being drawn blood from and sacrificed. **(2)**

ApoE$^{-/-}$ model. Ldha$^{fl/fl}$-Cdh5-CreERT2 mice were crossed with ApoE$^{-/-}$ C57BL/6J mice (#002052, The Jackson Lab) to generate Ldha$^{wt/fl}$-Cdh5-CreERT2 -ApoE$^{wt/-}$ mouse line (F1) and then Ldha$^{fl/fl}$-Cdh5-CreERT2 -ApoE$^{-/-}$ (F2) and Cdh5-CreERT2-ApoE$^{-/-}$ mouse lines (F2). Mouse genotypes were confirmed by PCR using the following primers: ApoE$^{-/-}$ common 5'-GCCTAGCCGAGGGAGAGCCG -3', wildtype reverse 5'-TGTGACTTGGGAGCTCTGCAGC -3' and mutant reverse 5'- GCCGCCCCGACTGCATCT -3'. Starting at week 8 (two weeks after injection completion), mice from all groups were fed on high-fat diet (Harlan Envigo TD88137) containing 21% fat (wt/wt) for 3 months. Mice from all groups were fasted overnight prior to being drawn blood from and sacrificed.

Plasma cholesterol measurement. At the time of the mice being sacrificed, whole blood was collected in EDTA-treated Eppendorf tube, and maintained on ice before centrifuged at 3,000 x *g* for 15 mins to collect plasma. Cholesterol concentration was measured using Amplex® Red Cholesterol Assay Kit (Invitrogen, A12216).

Mouse plaque lesion analysis. The tissue collection, treatment and analysis were conducted following lab's previous studies[78,384]. After euthanasia and perfusion, mouse aorta and heart were collected. Aorta was fixed in 4% paraformaldehyde for 15 mins, followed by Oil Red O staining (Sigma-Aldrich, 01391) for 15 mins. Heart was fixed in 4% paraformaldehyde overnight, sequentially immersed in 30% sucrose overnight, and in optimal cutting temperature compound (OCT): 30% sucrose mixture solution (1:1) overnight before embedded in OCT. The embedded frozen samples were sectioned to 8-μm thickness and stained with Oil Red O for 15 mins. The plaque areas were calculated using ImageJ [385]. The atherosclerosis in the *en face* aorta was calculated as the percentage (plaque area relative to the total aorta area), whereas in the aortic root was presented as the absolute plaque area on each cryosection.

Intimal RNA isolation from carotid arteries. The isolation was conducted following lab's previous study [384]. After euthanasia and perfusion, mouse carotid arteries were collected. Each carotid lumen was inserted into a 29-gauge insulin syringe filled with 350 uL of QIAzol lysis reagent (Qiagen, 79306), and then quickly flushed to collect intima RNA. The rest of the carotid artery tissue was then homogenized in a new tube with 350 uL of QIAzol to collect RNA from media and adventitia. Total RNA was extracted in accordance with the manufacturer's instructions.

Immunofluorescence staining. Mouse aorta was collected after perfusion with prechilled PBS and 4% paraformaldehyde, then dissected to remove excess tissues and cut open to get endothelium exposed on the top. The *en face* aorta was sequentially permeabilized in 0.2% Triton-X in PBS for 10 mins, incubated in blocking buffer of Tris-buffered saline (TBS) containing 10% bovine serum albumin (BSA) and 2.5% Tween 20 for 1 hour, stained with primary antibody at 4°C overnight, washed with TBS containing 2.5% Tween 20, stained with secondary antibody (and CD31-488-conjugated Ab) at dark for 1 hour, and washed with TBS containing 2.5% Tween 20. The aorta was then submerged in the mounting solution (Abcam, ab104139) on glass slide and flattened for imaging.

Table 3.1. List of antibodies for immunofluorescence staining.

Antibody	**Company**	**Catalog #**	**Dilution**
LDHA	Proteintech	21799-1-AP	1:100

Table 3.1. continued.

Mouse CD31/PECAM-1 Alexa Fluor® 488-conjugated Antibody	R&D systems	FAB6874G	1:100
H3K18la	PTM Biolabs	1406	1:100
Goat Anti-Rabbit, Alexa Fluor™ 488	Invitrogen	A11034	1:400
Goat Anti-Rabbit, Alexa Fluor™ 594	Invitrogen	A11037	1:400

Cell culture. Human aortic endothelial cells (Lonza, CC-2535) were cultured in EGM-2 (Lonza, CC-3156) supplemented with SingleQuots (Lonza, CC-4176) and 1% antibiotic-antimycotic (Gibco, 15240062) at 37°C with 5% CO_2, and being used from passage 5 to 9 for all experiments.

Application of athero-relevant flows. HAECs were subjected to 24-hr 'athero-susceptible' disturbed flow mimicking the hemodynamics measured in human carotid sinus or 'athero-protective' unidirectional representing the wall shear stress in human distal internal carotid artery, as described previously [131,290].

siRNA transfection. siRNA targeting LDHA (Qiagen, SI02663535), LDHB (Qiagen, SI03038014), and JCAD (Horizon, L-026476-02-0005) were transfected to HAECs to knockdown LDHA, LDHB and JCAD, respectively. The transfection was performed using Lipofectamine RNAiMAX (Life Technologies, 13778150) following manufacturer's instruction. The optimal working concentration of siRNA targeting LDHA (50 nM) LDHB (5 nM) and

JCAD (50 nM) were selected from preliminary titration with RT-qPCR as the readout and used in all experiments. Non-targeting siRNA (Qiagen, 1027310) were transfected in the same concentrations as its counterpart siRNA to serve as the negative control. Cells were transfected 24 hours after seeding and treated with siRNA for 48 hours before harvesting.

LDHA inhibition using GSKA. GSK 2837808A (GSKA) (Tocris, 5189) was dissolved in DMSO and applied to HAECs at a final concentration of 5, 10, or 20 uM for 48 hours to inhibit LDHA activity. DMSO with the same amount served as the control.

LDHA overexpression. The plasmid of LDHA (NM_001165415) fused with Myc-DDK tag in the pCMV6-Entry vector was purchased from Origene (RC228206). pCMV6-Entry vector carrying Myc-DDK tag was adopted as the control (Origene, PS100001). PCR was performed to amplify the two plasmids using primers below. To generate the mRNA, *in vitro* transcription was performed from the PCR products of each vector, using the mMESSAGE mMACHINE™ T7 ULTRA Transcription Kit (Invitrogen, AM1345-5) followed by the MEGAclear™ Transcription Clean-Up Kit (Invitrogen, AM1908). The purified mRNA products were transfected to HAECs using Lipofectamine™ MessengerMAX™ reagent (Invitrogen, LMRNA015) following manufacturer's protocol, and cultured for 8 hours before harvested.

Table 3.2. Primers used to amplify the PCR products for T7 *in vitro* transcription (for the amplification of both LDHA and control plasmids).

Name	**Sequence**
T7_promoter_Forward	5'- cgaaatTAATACGACTCACTATAGGG -3'
pCMV6_IVT_Reverse	5'- TATTAGGACAAGGCTGGTG -3'

RNA extraction and real-time quantitative PCR. For *in vitro* studies, total RNA was extracted from HAECs using either NucleoZOL RNA Isolation Kit (Takara) or GenElute™

Mammalian Total RNA Miniprep Kit (Sigma, RTN350-1KT) following manufacturer's protocol. RNA was reverse transcribed using High-Capacity cDNA Reverse Transcription Kit (Applied Biosystems, 4368813). For *in vivo* studies, total RNA was extracted from tissues using QIAzol (Qiagen, 79306) according to manufacturer's protocol. Reverse transcription was performed using the Maxima First Strand cDNA Synthesis Kit (Thermo Scientific, K1642). The RT-qPCR of both *in vitro* and *in vivo* studies were conducted using LightCycler® 480 SYBR Green I Master (Roche, 04887352001) according to manufacturer's protocol. The cDNA amount of each gene of interest was quantified by normalizing to the geometric mean of the cDNA amount of β-Actin, GAPDH and Ubiquitin in each sample.

Table 3.3. RT-qPCR primers.

Gene name	**Forward primer 5'-3'**	**Reverse primer 5'-3'**
Human primers		
β-Actin	TCCCTGGAGAAGAGCTACGA	AGGAAGGAAGGCTGGAAGAG
GAPDH	TGCACCACCAACTGCTTAGC	GGCATGGACTGTGGTCATGAG
Ubiquitin	ATTTAGGGGCGGTTGGCTTT	TGCATTTTGACCTGTTAGCGG
LDHA	TGGAACCAAAAGGAATCGGGA	CGATTCCGGATCTCATTGCC
JCAD	CCTGGAACTGGGAATGAGTATG	GTACTGAACGAAGCCGTCATAG
CYR61	CGGCTCCCTGTTTTTGGAATG	GGGTTTCTTTCACAAGGCGG
CTGF	CTCGCGGCTTACCGACTG	GGCTCTGCTTCTCTAGCCTG
IL6	TGCAATAACCACCCCTGACC	GTGCCCATGCTACATTTGCC
IL8	TGTGCCTTGGTTTCTCCTTT	GCTTCCACATGTCCTCACAA
VCAM1	TCCCTACCATTGAAGATACTGGAAA	GCTGACCAAGACGGTTGTATCTC

Table 3.3. continued.

Mouse primers		
mβ-Actin	GATCAAGATCATTGCTCCTCCTG	AGGGTGTAAAACGCAGCTCA
mGAPDH	TGCACCACCAACTGCTTAGC	GGCATGGACTGTGGTCATGAG
mUbiquitin	AGTGACGAGAGGCTTTGTCC	CGAAGATCTGCATTTTGACCTGT
mLDHA	GACTTGGCGGATGAGCTTGC	GGAGATCCATCATCTCGCCC
mLDHB	AGTCTCCCGTGCATCCTCAA	AGGGTGTCCGCACTCTTCCT
mJCAD	TGACGCTGCAGCATGTATAG	CGACCTGCATCTCTCTGATTT
mCTGF	GGGCCTCTTCTGCGATTTC	ATCCAGGCAAGTGCATTGGTA
mCYR61	CTGCGCTAAACAACTCAACGA	GCAGATCCCTTTCAGAGCGG

Western blot. For *in vitro* studies, whole cell extracts were harvested with UREA lysis buffer containing 8M deionized urea, 1% SDS, 10% glycerol, 60 mM Tris-HCl, 5% betamercaptoethanol (all chemicals from Sigma-Aldrich) as previously described[131]. For *in vivo* studies, aortas were dissected to remove the attached tissues, and then homogenized in cold UREA lysis buffer with a Polytron rotor-stator homogenizer. The protein lysis was separated by 15% (for Pan Kla and histone modification bands) or 12% handcasting Bis-Tris Protein Gels, followed by transferred to 0.2 um (for Pan Kla and histone modification bands) or 0.45 um PVDF membrane (Millipore) using Biorad Gel Transfer System (Biorad). The membrane was sequentially blocked in TBS with 5% BSA and 0.1% Tween20 (TBST) for an hour, incubated with primary antibody in TBST at 4°C overnight, washed with TBST, incubated with secondary antibody in TBST at room temperature for one hour, and washed with TBST. Bands were then detected with ECL peroxidase substrate (Pierce). The image processing and quantification was performed in ImageLab (Biorad). Bands were segmented into equal area, and the adjusted

volume of each band was obtained after subtracting global background. The relative protein expression was calculated by dividing the adjusted volume of protein of interest to the adjusted volume of the internal control (b-actin, b-tubulin or H3).

Table 3.4. List of antibodies for Western blot.

Antibody	**Company**	**Catalog #**	**Dilution**
LDHA	Proteintech	21799-1-AP	1:3000
LDHB	Abcam	ab85319	1:5000
Pan Kla	PTM Biolabs	1401RM	1:2000
H3K18la	PTM Biolabs	1406	1:2000
H3K18ace	Abcam	ab1191	1:1000
JCAD	Sigma	HPA017956	1:1000
Flag	Cell Signaling	CS8146S	1:1000
β-actin	Abcam	ab6276	1:3000
β-tubulin	Cell Signaling	86298S	1:1000
Histone H3	Abcam	ab12079	1:1000
Mouse Anti-Rabbit IgG, HRP	Invitrogen	31464	1:3000
Goat Anti-Mouse IgG, HRP	Calbiochem	401253	1:5000

Lactate supplementation. Sodium L-lactate (Sigma, 71718) was dissolved in PBS and supplemented to cells at a final concentration of 50 mM for 24 hours before cells were harvested.

Single-cell laconic assay. The detailed protocol was described in previous publications[386,387]. To summarize, HAECs were seeded in ibidi chamber to confluency, and

transduced with Ad5 adenovirus carrying the Laconic plasmid which consists of an mTFP-Venus FRET pair and bacterial transcription factor LldR [388] (ad-Lac). The transduction was performed at 50 multiplicity of infection (MOI) in the mix of EGM2 medium and Opti-MEM (Thermo Fisher, 11058021) at 1:1 ratio, with 3 uL/mL GeneJammer (Agilent, 204130). One hour after the transduction, the medium was replaced with EGM-2. Six hours after the replacement, HAECs were added with DMSO or GSKA.

The LPR assay was performed on an Olympus IX-71 microscope with ×10 objective, two days after the ad-Lac transduction. HAECs were starved in Fluorobrite MEM (Gibco, A1896701) for an hour. The assayed chamber was injected with 10 mM glucose in ECB, then after 3 minutes, 10 mM glucose and 500 uM pCMBA in ECB. The fluorescence of mTFP and Venus was captured with exposures between 100–300 ms/frame every 2 seconds until assay completed. Intracellular lactate was determined by the FRET signal, and LPR was calculated as the ratio of $\Delta \log_{10}$lactate over Δtime as described previously[386].

L-Lactate colorimetric assay. HAECs were cultured in 10-cm dishes for a day to reach 90% confluency, and then treated with either siRNA or DMSO/GSKA for 48 hours before the assay. Before the assay, cells were starved in seahorse basal DMEM media (Agilent, 103334-100) supplemented with 2 mM glutaMAX (Gibco, 35050061) and 5 mM HEPES (Corning, 25-060-CI), and cultured at 37 °C in the non-CO_2 incubator for 1.5 hours. Then each sample was supplemented with D-glucose (Sigma, G8270) at a final concentration of 10 mM, and incubated for another 20 mins before harvesting. Cells were centrifuged at 1,000 g at 4 °C for 5 mins for pellet collection, and resuspended in lactate assay buffer (Biovision, K627-100) to vortex thoroughly. Sonication was performed using Biorupter for 2.5 mins, followed by centrifugation at 13,000 g at 4 °C for 5 min for supernatant collection. Deproteinization was performed using

10,000 MW filter column (Millipore, UFC501096), and lactate colorimetric assay was conducted using kit (Biovision, K627-100) following manufacturer's protocol.

Seahorse respiratory assay. Glycolysis stress test was performed using XFe96 Extracellular Flux Analyzer (Agilent). HAECs were seeded at a density of 10,000 cells/well on the Seahorse plate for a day and then treated with either siRNA or DMSO/GSKA for 48 hours before the assay. One the day of the seahorse assay, cells were equilibrated in seahorse basal DMEM media (Agilent, 103334-100) supplemented with 2 mM glutaMAX (Gibco, 35050061) and 5 mM HEPES (Corning, 25-060-CI), and cultured at 37 °C in the non-CO_2 incubator for 1 hour. The assay was performed by subsequentially injecting 10 mM D-glucose (Sigma, G8270), 1 uM oligomycin (Sigma, 495455) and 100 mM 2-DG (Sigma, D8375).

RNA-seq. HAECs were seeded in 6-well plates for a day to reach 90% confluency, and then transfected with either negative control siRNA or siLDHA as described above. One day post transfection, culture media was switched to flow media (culture media supplemented with 4% dextran (Sigma, 31392)), and HAECs were subjected to either unidirectional flow or disturbed flow for 24 hours. Total RNA was then isolated in Trizol using Direct-zol RNA MiniPrep kit (Zymo, R2053) with in-column DNaseI digestion.

The RNA quality was assessed by 2100 Bioanalyzer (Agilent). Sequencing was done on Illumina HiSeq 4000 with paired-end 100 bp read length. Quality of reads was assessed using fastQC. Reads were aligned to the reference genome hg19 using hisat2[389] (version 2.1.0). Transcriptome were then assembled using Cufflinks (version 2.2.1), merged by Cuffmerge (version 2.2.1), and differentially expressed genes were identified using Cuffquant (version 2.2.1) followed by Cuffdiff (version 2.2.1)[390]. FDR 0.05 was used as cut-off for differentially expressed genes.

H3K18la ChIP-seq. Native ChIP-seq was conducted following previous studies[277]. HAECs were seeded in 10-cm dishes at 90% confluency, followed by 10 uM DMSO or GSKA treatment the next day and cultured for 48 hours before harvesting. Multiple dishes were combined for harvesting to reach 1.5E7 cells in each condition. MNase digestion was performed with 1000 U MNase (NEB M0247S) after dose optimization to enrich mononucleosomes and dinucleosomes. The immunoprecipitation was performed at 4 °C for overnight by incubating 20-30 ug of nucleosome with 4 ug H3K18la antibody (PTM-1406) in each condition, after taking out 10% of samples to serve as inputs. Native protein A Sepharose beads (Sigma, GE17-5280-01) were then added to the IP samples and incubated at 4 °C for 2 hours to pull down the antibody-antigen complexes, followed by sequential wash in TSE I (0.1% SDS, 1% Triton X-100, 2 mM EDTA, 20 mM Tris-HCl pH 8.0, 150 mM NaCl), TSE II (0.1% SDS, 1% Triton X-100, 2 mM EDTA, 20 mM Tris-HCl pH 8.0, 500 mM NaCl), buffer III (0.25 M LiCl, 1% NP-40, 1% deoxycholate, 1 mM EDTA, 10 mM Tris-HCl pH 8.0) and TE buffer (1 mM EDTA, 10 mM Tris-HCl pH 8.0). The immunoprecipated DNA were eluted using elution buffer (0.1M NaHCO3, 1% SDS), followed by RNase A (Invitrogen, 12091021) and Protease K (Invitrogen, AM2546) digestion, and being cleaned using QIAquick PCR purification kit (Qiagen, 28106).

ChIP library was constructed using TruSEQ Chip-SEQ library prep kit (Illumina) and sequenced on NovaSEQ6000 with paired-end of 100 bp. Quality of reads was assessed using fastQC. Reads were aligned to the reference genome hg38 using BWA with default parameters to generate SAM files. SAM files were filtered and converted to BAM files, followed by sorting and PCR duplicates removal using SAMtools[293]. Peaks were called using MACS2[391] by comparing IP samples with their inputs (FDR ≤ 0.05), then counted using DiffBind dba[392] to identify consensus peaks across all three biological replicates from each treatment condition.

Occupancy difference was determined by comparing DMSO- with GSKA-treated groups. The genomic distribution of the peaks and their adjacent genes were annotated using ChIPseek[393].

3.3 Results

3.3.1 Endothelial LDHA is significantly induced by disturbed flow both *in vitro* and *in vivo*.

First, the RNA-seq result was validated by RT-qPCR and Western blot to measure the expression of glycolytic gene LDHA both *in vitro* and *in vivo*. For the *in vitro* system, HAECs were exposed to 24-hour's DF or UF using a dynamic flow device[304] which faithfully recreated 1) *in vitro* DF mimicking hemodynamics measured in athero-susceptible human carotid sinus *in vivo*, or 2) *in vitro* UF mimicking hemodynamics measured in athero-protective human distal carotid artery *in vivo*. As a result, the expression of LDHA was higher in HAECs subjected to DF compared with UF at both mRNA and protein levels (Figure 3.1B-C). Meanwhile, no differential expression of Lactate Dehydrogenase B (LDHB) was detected between these two groups of cells (Figure 3.1C), which is consistent with the RNA-seq results (Figure 3.1A).

To compare the flow effect *in vivo*, mouse aorta was dissected and separated into two segments: the aortic arch (AA) that has mainly been exposed to disturbed flow and descending thoracic aorta (DA) that has mainly been exposed to unidirectional flow (illustration shown in Figure 3.1D). The tissues were then homogenized in protein lysis buffer and Western blot was performed. The results showed that the protein expression of LDHA was higher in AA than in DA (Figure 3.1E), indicating that LDHA expression was induced by DF. However, one caveat of this whole tissue measurement is that the aorta consists of a heterogeneous cell population, and therefore the upregulation of LDHA by DF may not necessarily resulted from endothelium. To

address this concern, immunofluorescence staining was conducted in *en face* mouse aorta, with the endothelium exposed at the top of the tissue and localized using an endothelial-specific surface marker, CD31. The data suggested that LDHA expression was higher in the DF-exposed aortic endothelium (inner curvature of AA) than in UF-exposed aortic endothelium. Taken together, these findings reveal that disturbed flow promotes endothelial LDHA expression both *in vitro* and *in vivo*.

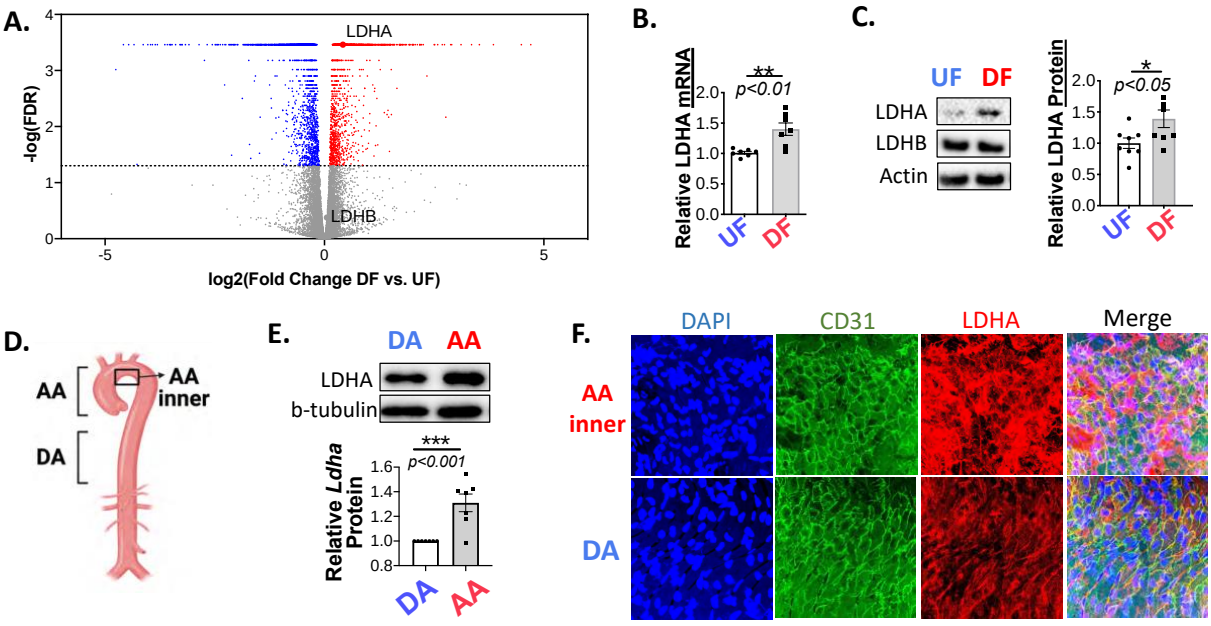

Figure 3.1. Disturbed flow induces endothelial LDHA expression both *in vitro* and *in vivo*. **(A)** Volcano plot of gene expression fold change detected in 24-hour's DF- vs. UF-exposed HAECs. FDR ≤ 0.05 is used as the cutoff to define differentially expressed genes. The transcription of LDHA is significantly higher in HAECs under DF compared to under UF (fold change = 1.34, FDR = 3.45 x 10^{-4}), while LDHB transcription is not significantly regulated by flow. **(B)** RT-qPCR detected LDHA was transcriptionally elevated in HAECs under 24-hour's DF than UF (n = 7). **(C)** Western blot showed the protein level of LDHA but not LDHB was elevated in HAECs under 24-hour's DF compared to UF (n = 8). **(D)** Illustration figure of mouse aorta dissection according to the hemodynamic exposure. AA (aorta arch) and AA inner (inner curvature of aorta arch) are areas exposed to DF, while DA (descending thoracic aorta) is areas exposed to UF. **(E)** Western blot using dissected mouse aortas showed the protein level of LDHA is higher in aorta arch than in descending thoracic aorta. The protein level of LDHA in AA was normalized to its level in DA in each mouse, respectively (n = 7). **(F)** Immunofluorescence staining in mouse *en face* aorta showed the LDHA expression in endothelial cells localized at the inner curvature of aorta arch is higher than those localized at descending thoracic aorta. *p ≤ 0.05, **p ≤ 0.01 were determined by two-tailed Student's t-test.

3.3.2 Endothelial LDHA acts as a transcriptional regulator of a cohort of atherogenic genes.

To investigate the function of DF-induced endothelial LDHA, siRNA was adopted to inhibit LDHA expression in HAECs that were cultured under DF for 24 hours. The cells were then isolated for RNA-seq experiment, with scramble siRNA serving as a non-targeting control delivered to HAECs in the same culture condition.

Analysis of the sequencing data revealed that 1,087 genes were significantly differentially expressed in siLDHA- vs. scramble siRNA-treated cells. The large number of differentially expressed genes suggests that LDHA is an important transcriptional regulator in DF-exposed HAECs. Among these genes, 581 were downregulated while 506 were upregulated by LDHA inhibition. Gene Ontology (GO) analyses were performed to summarize the functions of siLDHA-suppressed genes, which were demonstrated to be enriched in biological processes including immunity (innate immune response and response to interferon-gamma), cardiovascular system development (response to oxygen levels, blood vessel development, heart development and tissue morphogenesis), and atherosclerosis-related processes (myeloid leukocyte activation and regulation of cell adhesion) (Figure 3.2A). Specifically, genes involved in atherosclerosis include pro-inflammatory genes CYR61 and CTGF, selectin SELP, hypoxia-inducible factor EPAS1, and endothelial junctional protein JCAD (Figure 3.2B). On the contrary, LDHA inhibition also up-regulated lung Krüppel-like Factor (KLF2), a dominant transcription factor regulating endothelium quiescence (Figure 3.2B). In summary, our RNA-seq data show that inhibiting LDHA in HAECs reduces the transcription of multiple atherogenic genes, suggesting

that LDHA acts as a transcription regulator in atherogenesis. However, the molecular mechanism linking LDHA to endothelial transcriptome remodeling is still not understood.

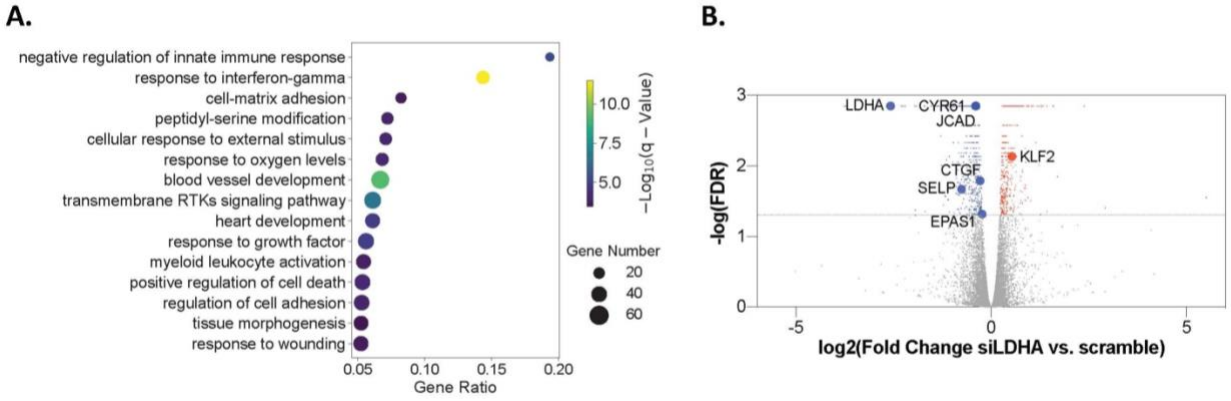

Figure 3.2. Endothelial LDHA acts as transcriptional regulator of a cohort of atherogenic genes. (A) Top Gene Ontology biological processes of siLDHA-downregulated genes detected by RNA-seq in 24-hour's DF-exposed HAECs. **(B)** Volcano plot of gene expression fold change detected in siLDHA- vs. scramble siRNA-treated HAECs cultured under 24-hour's DF. FDR ≤ 0.05 is used as the cutoff to define differentially expressed genes. siLDHA significantly reduced the transcription of LDHA (fold change = 0.17, FDR = 1.42 x 10^{-3}), JCAD (fold change = 0.76, FDR = 1.42 x 10^{-3}), CYR61 (fold change = 0.76, FDR = 1.42 x 10^{-3}), CTGF (fold change = 0.82, FDR = 1.63 x 10^{-2}), SELP (fold change = 0.59, FDR = 2.13 x 10^{-2}) and EPAS1 (fold change = 0.85, FDR = 4.82 x 10^{-2}), while up-regulated the transcription of KLF2 (fold change = 1.44, FDR = 7.36 x 10^{-3}).

3.3.3 Inhibiting endothelial LDHA reduces lactate production rate, intracellular lactate level and extracellular acidification.

Next, I set out to investigate how this metabolic enzyme impacts the transcription network in endothelial cells. Although the lactate dehydrogenase activity of LDHA, which converts pyruvate to lactate, is well known in multiple cell types[397–399], its role in aortic endothelial cells has not been studied. To investigate the capability of endothelial LDHA in regulating lactate production, three *in vitro* assays were conducted in cultured HAECs. First, lactate production rate (LPR) was measured at single-cell level using a Förster resonance energy transfer (FRET) image-based approach that was developed by our lab [386,387]. HAECs were transduced with

laconic adenovirus following the protocol and treated with either GSK 2837808A (GSKA), a small compound that selectively inhibits the protein activity of LDHA (IC_{50} values are 2.6 nM for LDHA and 43 for LDHB) or DMSO. Compared to the DMSO group, HAECs treated with 10 uM and 20 uM of GSKA had reduced LPR (Figure 3.3A; no statistical significance at 10 uM of GSKA which is likely due to the small number of cells), indicating that LDHA regulates the rate of lactate production in HAECs.

Next, lactate level was measured in HAECs in bulk using a colorimetric assay kit. As expected, the reduced LPR in HAECs treated with GSKA resulted in significantly less intracellular lactate than their counterparts treated with DMSO (Figure 3.3B).

Moreover, the extracellular lactate level was measured using the seahorse glycolysis stress test as a surrogate. Compared to DMSO treatment, HAECs treated with GSKA had significantly lower levels of glycolysis, as well as less glycolytic capacity and glycolytic reserve (Figure 3.3C-D). These data indicate that the reduced lactate production by LDHA inhibition also led to decreased extracellular acidification rate (ECAR) from HAECs. Taken together, these data reveal that endothelial LDHA acts as the glycolytic enzyme to regulate lactate production.

However, one limitation of these experiments is that the inhibition effect of GSKA was not exclusive to LDHA but also affected LDHB and possibly other proteins, making it difficult to conclude that lactate production regulation was solely due to LDHA. Alternatively, a more specific inhibition approach using siRNA was adopted to target LDHA (siLDHA). Surprisingly, siLDHA did not reduce either the intracellular lactate level or the extracellular acidification rate (Figure 3.3E-F). Even inhibiting both LDHA and LDHB using siRNAs did not mimic the GSKA effect in these two readouts (Figure 3.3E-F). This may be due to the high expression level of these two genes, especially LDHA, in endothelial cells. Unlike the potent inhibitor GSKA, the

siRNAs only partially suppressed the expression of these two genes (Figure 3.3G), and thus the siRNA-treated cells may still retain sufficient LDHA(B) for normal intracellular lactate levels and lactate secretion. Alternatively, a more sensitive approach such as metabolomics may be used to test the effect of siLDHA on lactate regulation. Completely knocking out LDHA using CRISPR-Cas9 in endothelial cells may serve as a more effective model to test the function of LDHA exclusively.

Based on my previous data showing no alteration in LDHB expression by hemodynamics (Figure 3.1A and C), it is reasonable to hypothesize that in hemodynamics-exposed endothelial cells, LDHA is the limiting factor in determining the enzyme's tetramer ratio (LDHA vs. LDHB) and thus the favored reaction direction that contributes to DF-induced glycolysis and cell activation. Therefore, in the following studies, GSKA will be used to effectively perturb LDHA activity and study its function in HAECs.

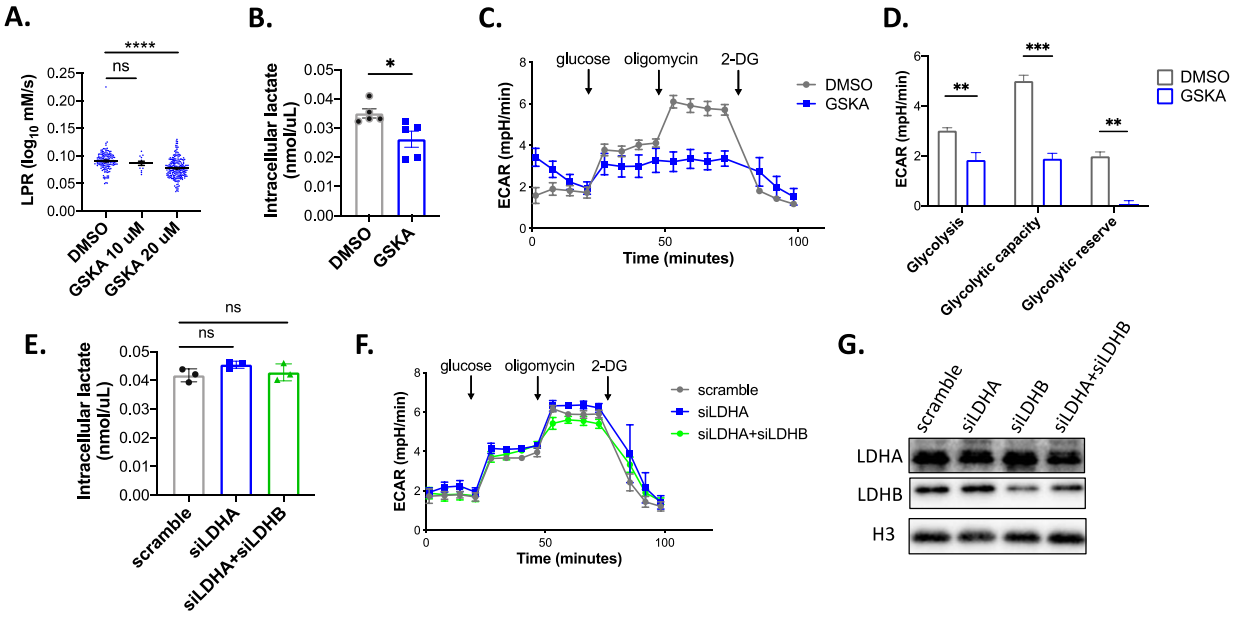

Figure 3.3. LDHA regulates lactate production in human aortic endothelial cells. (A) Inhibiting LDHA protein by 48-hour's GSKA treatment reduced lactate production rate in HAECs, measured by FRET-based single cell laconic assay (n = 151, 12 and 220 for DMSO-, 10 uM GSKA-, and 20 uM GSKA-treated cells, respectively). **(B)** Colorimetric assay detected

Figure 3.3. continued. GSKA reduced intracellular lactate level of HAECs (n = 5). **(C)** Seahorse glycolytic stress test detected GSKA reduced extracellular acidification rate (ECAR) of HAECs (n = 4 and 3 for DMSO- and GSKA-treated cells, respectively). Arrows indicate consequent injection of glucose, oligomycin and 2-DG. **(D)** Under glycolytic stress test, HAECs treated with GSKA showed reduced glycolysis, glycolytic capacity and reserve when compared to HAECs treated with DMSO. **(E)** Colorimetric assay showed HAECs transfected with siRNA targeting LDHA (siLDHA) or LDHA and LDHB together (siLDHA + siLDHB) did not have a difference in their intracellular lactate level from their counterparts transfected with scramble siRNA (n = 3). **(F)** Seahorse glycolytic stress test showed HAECs transfected with siLDHA or siLDHA+siLDHB did not have a difference in their ECAR from cells transfected with scramble siRNA (n = 4). **(G)** Western blot showed siLDHA and siLDHB only partially reduced the protein levels of LDHA and LDHB, respectively, in HAECs. *$p \leq 0.05$, **$p \leq 0.01$, ***$p \leq 0.001$, and ****$p \leq 0.0001$ were determined by one-way ANOVA for within-group comparison, and by two-tailed Student's t-test (correct for multiple comparisons using Holm-Sidak method) for between-group comparison.

3.3.4 LDHA modifies histone lysine lactylation in HAECs.

LDHA-derived lactate has been reported to be a precursor for histone lysine lactylation (Kla), a post-translational modification found in human, mouse, plant and fungal[277,400–409]. Specifically, the lactylation on histone 3 lysine 18 site (H3K18la) at gene promoter regions has been demonstrated to promote transcription[277,402]. Therefore, I hypothesized that endothelial LDHA-induced atherogenic transcription is also mediated by this mechanism, despite the fact that the existence of Kla and specifically H3K18la in endothelial cells is to be determined.

To test this hypothesis, I first investigated whether LDHA-derived lactate can also be used to make Kla in endothelial cells. The existence of Kla in HAECs was examined using an antibody that can probe for pan lysine lactylation modifications (Figure 3.4A). Furthermore, a decreased pan Kla level was observed in response to 48 hour's GSKA treatment in a dose-dependent manner (Figure 3.4A), suggesting that endothelial Kla is regulated by LDHA. Although not as dramatic as GSKA treatment, siLDHA also led to a reduction of pan Kla level in HAECs cultured under either 24 hours of UF or DF (Figure 3.4B). Notably, the expression level of pan Kla was positively correlated with LDHA expression in response to flows, with the

LDHB expression remained constant (Figure 3.4B), demonstrating that pan Kla regulation in HAECs is dependent on LDHA.

Next, the specific lactylation at the H3K18 site was examined in HAECs. Compared to DMSO treatment, suppressing LDHA activity in HAECs using GSKA dramatically decreased the level of lactylation but not the acetylation at the H3K18 site (Figure 3.4C). The same reduction was also observed in the siLDHA-treated HAECs that were cultured either under static, UF or DF (Figure 3.4D), indicating that endothelial regulation of H3K18la is dependent on endogenous LDHA. Similarly, the H3K18la level was positively associated with the level of LDHA in response to flows (Figure 3.4D), although more replicates are needed to determine the statistical correlation. Interestingly, the difference in H3K18la between cells treated with siLDHA and scramble siRNA was most distinct when they were subjected to DF compared to those under UF or static. This may be due to the demand for modifying lactylation at H3K18 being the highest in DF-exposed cells, thus LDHA perturbation is the most sensitive, also explaining why LDHA is transcriptionally increased by DF to fulfill this supply. It is reasonable to hypothesize that this elevated H3K18la modification by DF-induced LDHA may contribute to flow-governed transcriptome remodeling, such as up-regulating atherogenic genes.

To further validate this LDHA-regulated H3K18la modification is through lactate, sodium L-lactate (NaLac) was supplemented in the medium of HAECs for 24 hours followed by Western blot. DMSO-treated cells gained relatively more H3K18la modifications after the addition of NaLac in comparison to PBS (Figure 3.4E), suggesting that exogeneous lactate can modestly boost the baseline level of global H3K18la in HAECs. Furthermore, 24-hour NaLac supplementation markedly restored the GSKA-suppressed H3K18la (Figure 3.4E), indicating this histone marker uses LDHA-derived lactate as the precursor and can be dynamically and

reversely regulated. To support this conclusion, HAECs were transfected with a human LDHA mRNA construct to boost lactate production, and a higher amount of H3K18la was observed compared to cells transfected with control mRNA (Figure 3.4F).

Taken together, these findings demonstrate that in vascular endothelial cells, LDHA-derived lactate is not a waste product but rather a precursor for protein lysine lactylation, including H3K18la in the chromosome. As H3K18la has been shown to promote cell-type-specific transcriptome in multiple types of cells and tissues[277,402], my data support the possibility that this marker participates in endothelial LDHA-directed gene transcription.

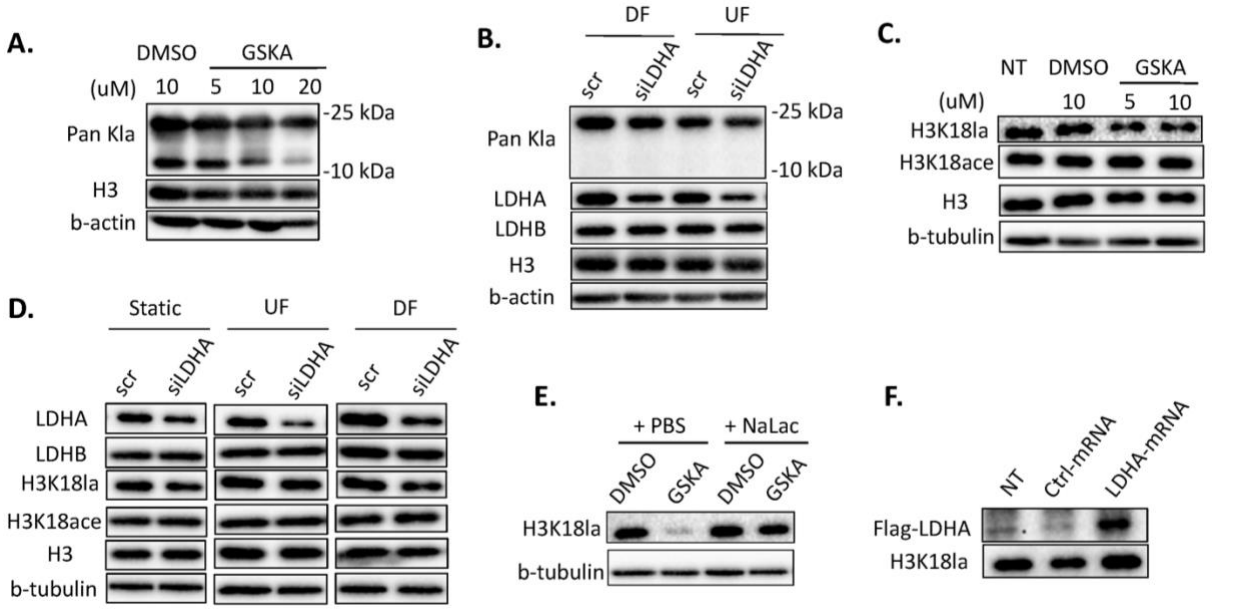

Figure 3.4. LDHA regulates histone lysine lactylation in human aortic endothelial cells detected by Western blots. (A) HAECs treated with GSKA for 48 hours had dose-dependent lower pan Kla level compared to HAECs treated with DMSO. **(B)** Pan Kla level was increased in HAECs cultured under 24-hour's DF compared to UF, and the modification was suppressed by siLDHA in comparison to scramble siRNA (scr) transfection. **(C)** H3K18la level was reduced in HAECs treated with GSKA compared to those with DMSO. **(D)** H3K18la but not H3K18ace level was decreased by siLDHA compared to scramble siRNA transfection in HAECs cultured under either 24-hour's static, UF or DF. **(E)** Sodium L-lactate (NaLac) supplementation restored the GSKA-inhibited H3K18la modification in HAECs compared to PBS supplementation. **(F)** LDHA mRNA transfection increased H3K18la modification in HAECs compared to the transfection using control mRNA.

3.3.5 Disturbed flow induces H3K18la modification in mouse aortic endothelium *in vivo*.

To investigate the potential role of endothelial H3K18la modification in atherogenesis *in vivo*, mouse aorta was dissected to assess if the H3K18la level was responsive to atherosclerosis-relevant flows. As previously described, the mouse aorta was separated into two segments: the aortic arch (AA) and descending thoracic aorta (DA). The aorta tissues were then homogenized in protein lysis buffer and loaded for Western blot. Consistent with the trend of LDHA expression, the level of H3K18la was higher in the DF-exposed AA region than in the UF-exposed DA region (Figure 3.5A). To further localize endothelial cells, *en face* mouse aorta was used and a higher H3K18la level in AA inner curvature than in DA was consistently detected (Figure 3.5B). These finding imply that the DF-induced LDHA expression in mouse endothelium resulted in a gain of H3K18la modification. Taken together, these *in vivo* data further support the hypothesis that endothelial LDHA is an atherogenic transcription regulator.

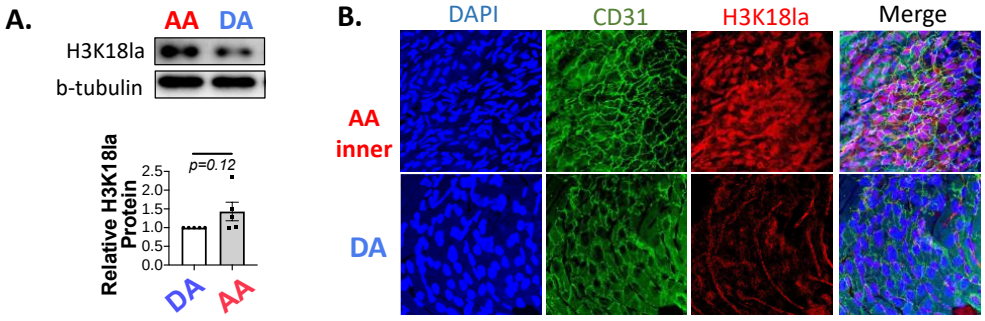

Figure 3.5. Disturbed flow induces H3K18la modification in mouse aortic endothelium *in vivo*. (A) Western blot suggested there was a higher trend of H3K18la modification in the aorta arch than in the descending thoracic aorta (n = 4). **(B)** Immunofluorescence *en face* staining suggested the H3K18la level was higher in endothelium located at inner curvature of aorta arch than those located at descending thoracic aorta. P-value was determined by two-tailed Student's t-test.

3.3.6 Constructing inducible mouse line with LDHA conditionally knockout from vascular endothelium.

To further examine the function of endothelial LDHA *in vivo*, an inducible mouse line was chosen that allows for the conditional deletion of LDHA in adult endothelium. $Ldha^{fl/fl}$ mice[382] (#030112, The Jackson Lab) were crossed with Cdh5(PAC)-CreERT2 mice[383] (from Dr. Ralf Adams) to generate $Ldha^{fl/fl}$-Cdh5-CreERT2 mice. Following tamoxifen injection, Ldha mRNA was significantly reduced in the endothelium-enriched intima isolated from carotid arteries of $Ldha^{fl/fl}$-Cdh5-CreERT2 mice ($LDHA^{iEC\text{-}KO}$) compared to control Cdh5-CreERT2 mice ($CDH5^{Cre}$) (Figure 3.6A). Notably, we did not detect any difference in Ldha expression in the non-endothelial layers (media and adventitia) of the blood vessel between $LDHA^{iEC\text{-}KO}$ and $CDH5^{Cre}$ mice (Figure 3.6A), demonstrating the specificity of our conditional knock-out model. Therefore, we have established a mouse line that enables the study of LDHA's effect exclusively in vascular endothelial cells.

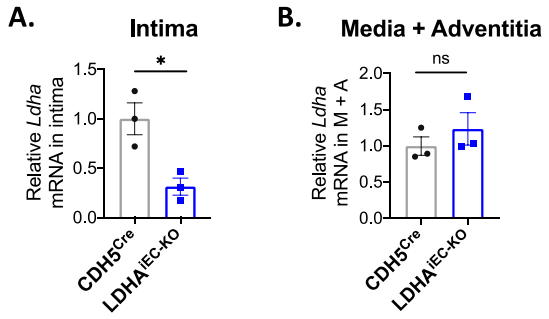

Figure 3.6. Constructing inducible mouse line with LDHA conditionally knockout from vascular endothelium. (A) RT-qPCR result showed Ldha transcription in the carotid artery intima was significantly reduced in the $LDHA^{iEC\text{-}KO}$ mice than in the $CDH5^{Cre}$ mice after tamoxifen injection (n = 3). **(B)** RT-qPCR result showed Ldha transcription in the carotid artery media and adventitia was not changed between the $LDHA^{iEC\text{-}KO}$ mice and the $CDH5^{Cre}$ mice after tamoxifen injection (n = 3). *$p \leq 0.05$ was determined by two-tailed Student's t-test.

3.3.7 Endothelial LDHA deficiency reduces atherosclerosis in AAV9-PCSK9 overexpressed mice.

To test the hypothesis that endothelial LDHA causatively regulates atherogenesis, atherosclerosis was induced in the conditional knock-out mice by the injection of Adeno-

Associated-Virus-9 (AAV9) viruses carrying PCSK9 (Proprotein Convertase Subtilisin/Kexin type 9) and a 12-week high-fat diet (HFD)[410]. The study design is illustrated in Figure 3.7A. PCSK9 overexpression promotes atherogenesis by suppressing the recycling of low-density lipoprotein receptor (LDLR) back to the membrane of liver cells, consequently leading to excess cholesterol in the plasma[410,411].

To measure plaque formation, the *en face* aorta and the cryosection of aortic root were both stained with Oil Red O. The data suggested AAV9-PCSK9 overexpression together with a 12-week HFD was sufficient to promote atherogenesis in *male* mice (Figure 3.7B and C). The ratio of lesion area to the total aorta area was smaller in $LDHA^{iEC\text{-}KO}$ mice than $CDH5^{Cre}$ mice (Figure 3.7B). Consistently, fewer lesions were formed at the aortic root region in $LDHA^{iEC\text{-}KO}$ mice than $CDH5^{Cre}$ mice (Figure 3.7C). Although the sample size was small (n = 4-5 for *en face* staining; n = 3 for aortic root staining), these preliminary data showed a statistical difference (**$p \leq 0.01$ and *$p \leq 0.05$, respectively) of plaques formed between genotypes, supporting the causal role of endothelial LDHA in atherogenesis in male mice.

The body weights of $CDH5^{Cre}$ mice and $LDHA^{iEC\text{-}KO}$ mice were similar after 12 weeks of HFD and post-18 hour fasting (Figure 3.7D). However, the total cholesterol level in the plasma was significantly lower in $LDHA^{iEC\text{-}KO}$ mice (Figure 3.7E). These observations indicate that the athero-protective role of $LDHA^{iEC\text{-}KO}$ may not directly result from the lower proinflammatory activity of aortic endothelial cells, but may also indirectly attribute to an amelioration of hyperlipidemia. One possible mechanism for the observed effects of deleting endothelial LDHA is that it may result in insufficient vasculature support in major organs involved in lipid metabolism, such as the liver and adipose tissues [412–414]. To further investigate the impact of $LDHA^{iEC\text{-}KO}$ on inflammation reduction, we plan to perform functional assays, such as

leukocyte-endothelium adhesion assays[395,396], using endothelial cells isolated from LDHA^{iEC-KO} and CDH5^{Cre} mice.

Our RNA-seq data indicate that LDHA regulates the transcription of multiple endothelial inflammatory markers, which supports the hypothesis that LDHA^{iEC-KO} may at least partially ameliorate endothelial activation during atherosclerosis initiation.

However, we noted one limitation of the AAV-PCSK9 model used in our study, which only induced atherosclerosis to a modest extent. Specifically, in subsequent replication batches of the experiment, we were unable to induce plaques formation in most female mice regardless of their genotypes (data not shown). This gender discrepancy may be explained by a previous study showing that adeno-associated virus transduction to the liver was less efficient in female than in male mice[415]. Therefore, we decided to adopt an alternative mouse model to further validate the atherogenic role of endothelial LDHA.

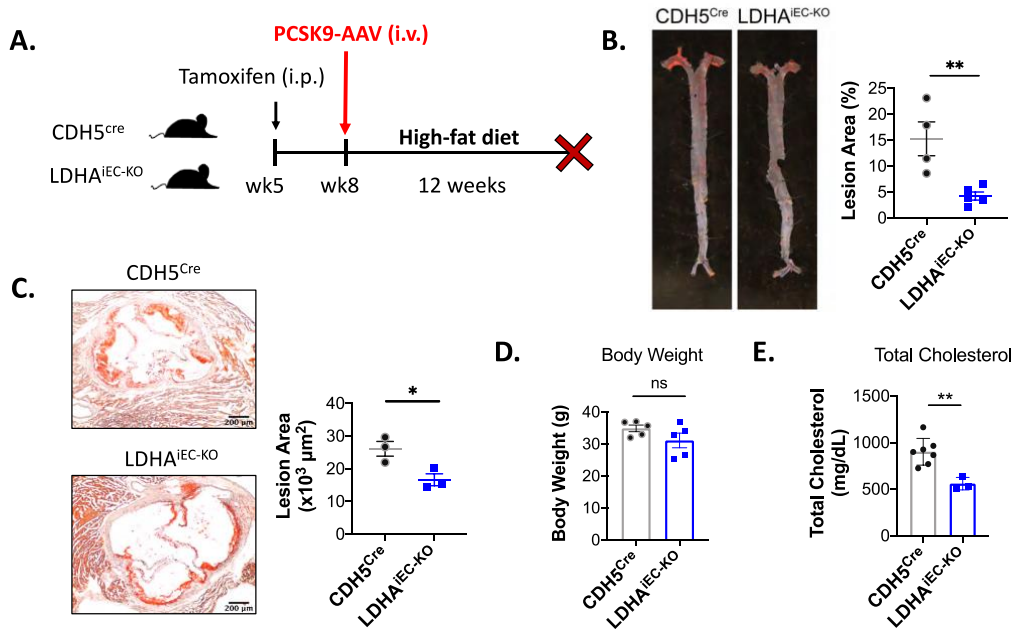

Figure 3.7. Endothelial LDHA deficiency reduces atherosclerosis in AAV9-PCSK9 overexpressed mice. (A) Study design of the AAV9-PCSK9 atherosclerosis mouse model. At week 5, tamoxifen was delivered to LDHA^{iEC-KO} and CDH5^{Cre} mice each day for 7 consecutive days through intraperitoneal injection (i.p.). Starting from week 8, these mice were injected with

Figure 3.7. continued. AAV9-PCSK9 through tail vein, and fed on high-fat diet for 12 weeks before sacrificed for plaque characterization. **(B)** Oil Red O staining on *en face* aorta showed fewer lesions were formed in the $LDHA^{iEC\text{-}KO}$ mice than the $CDH5^{Cre}$ mice (n = 5 and 4, respectively; male mice only). **(C)** Oil Red O staining on the aortic root cryosectioning showed fewer lesions were formed in the $LDHA^{iEC\text{-}KO}$ mice than the $CDH5^{Cre}$ mice (n = 3; male mice only). **(D)** The body weights were similar between $CDH5^{Cre}$ mice and $LDHA^{iEC\text{-}KO}$ mice after AAV9-PCSK9 injection and 12-week's high-fat diet (n = 5; male mice only). **(E)** The plasma cholesterol level was higher in $CDH5^{Cre}$ mice than $LDHA^{iEC\text{-}KO}$ mice after AAV9-PCSK9 injection and 12-week's high-fat diet (n = 3 and 7, respectively; male mice only). $*p \leq 0.05$ and $**p \leq 0.01$ were determined by two-tailed Student's t-test.

3.3.8 Endothelial LDHA deficiency reduces atherosclerosis in $ApoE^{-/-}$ mice.

To further validate the atherogenic role of LDHA, another mouse model with homozygous deletion of apolipoprotein E (ApoE) was adopted. ApoE constitutes chylomicrons, VLDL and LDL to facilitate the delivery and clearance of plasma cholesterol by the liver, and its deficiency induces hypercholesterolemia thus driving atherosclerosis[416,417]. To select for $Ldha^{fl/fl}$-Cdh5-CreERT2- $ApoE^{-/-}$ mouse line in generation F2, $Ldha^{fl/fl}$-Cdh5-CreERT2 mice were bred into $ApoE^{-/-}$ background. The mice with the Cdh5-CreERT2- $ApoE^{-/-}$ genotype were used as the control group. Starting from week 5, tamoxifen was injected into mice once a day consecutively for a week to generate $ApoE^{-/-}$-$LDHA^{iEC\text{-}KO}$ and $ApoE^{-/-}$-$CDH5^{cre}$ genotypes. Two weeks post-injection completion, atherogenesis was activated by feeding both groups with HFD for 3 months before harvesting their tissues for characterization. The study design is illustrated in Figure 3.8A.

Oil Red O was used to stain the *en face* aorta, and a considerable amount of plaques were detected in the control ($ApoE^{-/-}$-$CDH5^{cre}$) mice from both genders (Figure 3.8B and C), validating a successful induction of atherosclerosis using this $ApoE^{-/-}$ model. By comparison, fewer lesions were detected in the aortas from $ApoE^{-/-}$-$LDHA^{iEC\text{-}KO}$ than those from $ApoE^{-/-}$-$CDH5^{cre}$ mice, and this significant reduction was consistently observed in both male (n = 3 and 6, $**p \leq 0.01$) and female groups (n = 3, $*p \leq 0.05$) (Figure 3.8B and C). Although more

replicates are needed for both genders, these preliminary data demonstrated that endothelial LDHA deficiency suppressed aortic plaques formation in $ApoE^{-/-}$ mice.

In this study, the body weights of $ApoE^{-/-}$-$LDHA^{iEC\text{-}KO}$ and $ApoE^{-/-}$-$CDH5^{cre}$ mice were measured both before and after a 3-month HFD. Similar to the AAV9-PCSK9 model, we did not detect any differences in their body weights after HFD feeding (Figure 3.8D). To account for individual and litter variations, we calculated the percentage body weight gain for each mouse after vs. before the HFD treatment, and we still did not detect a difference between the two genotypes (Figure 3.8E). These findings were consistent for mice of both genders.

Furthermore, we collected the plasma from these mice after 3 months of HFD and 18 hours of fasting for lipid measurement. Interestingly, endothelial LDHA deficiency significantly suppressed the HFD-induced plasma cholesterol gain in female $ApoE^{-/-}$ mice (Figure 3.8F, $^{**}p \leq 0.01$, n = 2-4). Although not statistically significant, likely due to small sample size ($p = 0.08$, n = 2), a similar difference was also observed in the male mice. These data suggest a possible mechanism of endothelial LDHA contributing to atherogenesis by regulating lipid metabolism, in addition to its direct role in advancing endothelial inflammation. And as mentioned in the previous section, further experiments are needed to distinguish the two mechanisms.

Overall, the preliminary results from both AAV9-PCSK9 and $ApoE^{-/-}$ mouse models demonstrate the causal role of endothelial LDHA in atherogenesis and support LDHA as a potential target for the “local” treatment of endothelial dysfunction in vascular diseases. However, the pathway linking LDHA to downstream atherogenic transcriptome remains unknown. Based on the RNA-seq and Western blot data above, we hypothesized LDHA acts as an epigenetic activator of atherogenic genes by modifying H3K18la marks on their genome. We will test this hypothesis in the studies below.

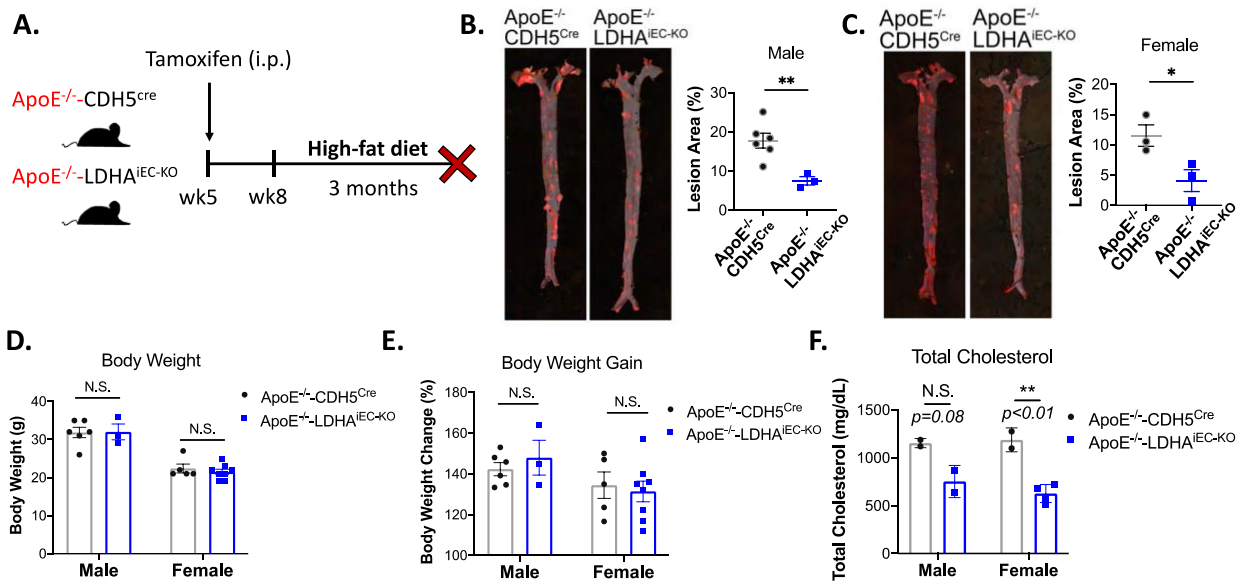

Figure 3.8. Endothelial LDHA deficiency reduces atherosclerosis in ApoE-/- mice. (A) Study design of the ApoE$^{-/-}$ atherosclerosis mouse model. At week 5, tamoxifen was delivered to ApoE$^{-/-}$-LDHA^{iEC-KO} and ApoE$^{-/-}$-CDH5^{cre} mice each day for 7 consecutive days through intraperitoneal injection (i.p.). Starting from week 8, these mice were fed on high-fat diet (HFD) for 3 months before sacrificed for plaque characterization. **(B)** Oil Red O staining on *en face* aorta showed fewer lesions were formed in the ApoE$^{-/-}$-LDHA^{iEC-KO} than the ApoE$^{-/-}$-CDH5^{cre} male mice (n = 3 and 6, respectively). **(C)** Oil Red O staining on *en face* aorta showed fewer lesions were formed in the ApoE$^{-/-}$-LDHA^{iEC-KO} than the ApoE$^{-/-}$-CDH5^{cre} female mice (n = 3). **(D)** The body weights were similar between ApoE$^{-/-}$-LDHA^{iEC-KO} and ApoE$^{-/-}$-CDH5^{cre} in both genders, after 3-month's HFD (n = 3 and 6 for male mice; n = 8 and 5 for female mice). **(E)** The 3-month's HFD-induced body weight gain was similar between ApoE$^{-/-}$-LDHA^{iEC-KO} and ApoE$^{-/-}$-CDH5^{cre} in both genders (n = 3 and 6 for male mice; n = 8 and 5 for female mice). **(F)** The plasma cholesterol level in the ApoE$^{-/-}$-CDH5^{cre} mice showed a higher trend than that in the ApoE$^{-/-}$-LDHA^{iEC-KO} mice in both genders, after 3-month's HFD (n = 2 for male mice; n = 4 and 2 for female mice). *p ≤ 0.05 and **p ≤ 0.01 were determined by two-tailed Student's t-test (correct for multiple comparisons using Holm-Sidak method).

3.3.9 Endothelial LDHA regulates the transcription of atherogenic gene JCAD, likely through H3K18la modification.

Our RNA-seq results demonstrate that suppressing LDHA reduced the transcription of multiple atherogenic genes, including a coronary artery disease (CAD)-associated GWAS gene junctional cadherin 5 associated (JCAD), which encodes an endothelial cell-cell junction protein[418,419] (Figure 3.8A). In addition to JCAD, the transcription of its two downstream targets

connective tissue growth factor (CTGF) and cysteine-rich angiogenic inducer 61 (CYR61), was also downregulated by siLDHA (Figure 3.8A). Consistently, Western blot showed the LDHA inhibitor GSKA dramatically reduced JCAD expression in HAECs cultured under DF (Figure 3.9B). Previous studies showed global knockout and endothelial deficiency of JCAD both suppressed atherosclerosis formation in ApoE$^{-/-}$ mice after 10 weeks or 12 weeks of a high-fat diet[420,421]. The atherogenic function of JCAD has been demonstrated to be through the upregulation of an inflammatory transcriptome, which is partially dependent on the YAP/TAZ Hippo pathway[420–422]. Interestingly, JCAD is also a mechano-sensitive gene as its transcription is elevated in endothelial cells subjected to DF compared to UF[420], making JCAD a promising candidate linking the DF-induced LDHA to atherogenesis. In support of this hypothesis, using RT-qPCR, I also detected consistent siLDHA-dependent downregulation of other JCAD's downstream proinflammatory targets, including cytokines interleukin 6 (IL6) and interleukin 8 (IL8), and vascular cell adhesion molecule 1 (VCAM1) (Figure 3.9C).

In alignment with the *in vitro* results, mice with endothelial LDHA deficiency also showed a trend of reduced transcription of JCAD and its targets CTGF and CYR61 in their vascular intima (Figure 3.9D). However, there is no statistical difference between genotypes determined by multiple t tests, likely due to the small sample size (n = 3) and large variation in gene expression baseline among individuals. Therefore ,more biological replicates are needed to validate the endothelial regulation of LDHA on JCAD *in vivo*.

Based on the previous data, I hypothesized LDHA controls JCAD transcription through modifying H3K18la. I first tested this hypothesis by supplementing GSKA-treated HAECs with the lactylation substrate NaLac and harvested the protein for Western blot. NaLac addition restored the GSKA-inhibited JCAD expression (Figure 3.9E), indicating that the regulation of

LDHA on JCAD expression is dependent on lactate and likely through H3K18la modification at its promoter or enhancer region. To test if the marker is directly modified at these sites, a Chromatin Immunoprecipitation sequencing (ChIP-seq) assay was conducted in HAECs using an H3K18la antibody, following the protocol established by Zhang *et al*[277] and described above. Furthermore, these HAECs were treated with either DMSO or GSKA to evaluate the H3K18la distribution as a function of LDHA activity.

The quality of ChIP-seq samples was checked and analyzed following the procedures described in the Methods section. Occupancy analysis using DiffBind[392] suggests a peak located at JCAD promoter in both DMSO- and GSKA-treated HAECs (Figure 3.9F), indicating the direct modification of H3K18la at this locus. However, to validate that this lactylation is LDHA-dependent, the relative H3K18la level between DMSO- and GSKA-treated HAECs needs to be compared by affinity analysis, which will be conducted as part of the future research.

Taken together, these preliminary results supported our hypothesis that endothelial LDHA upregulates the transcription of the CAD GWAS gene JCAD, likely through installing more H3K18la at its promoter or enhancer. This modification may contribute to the causal role of endothelial LDHA in atherogenesis.

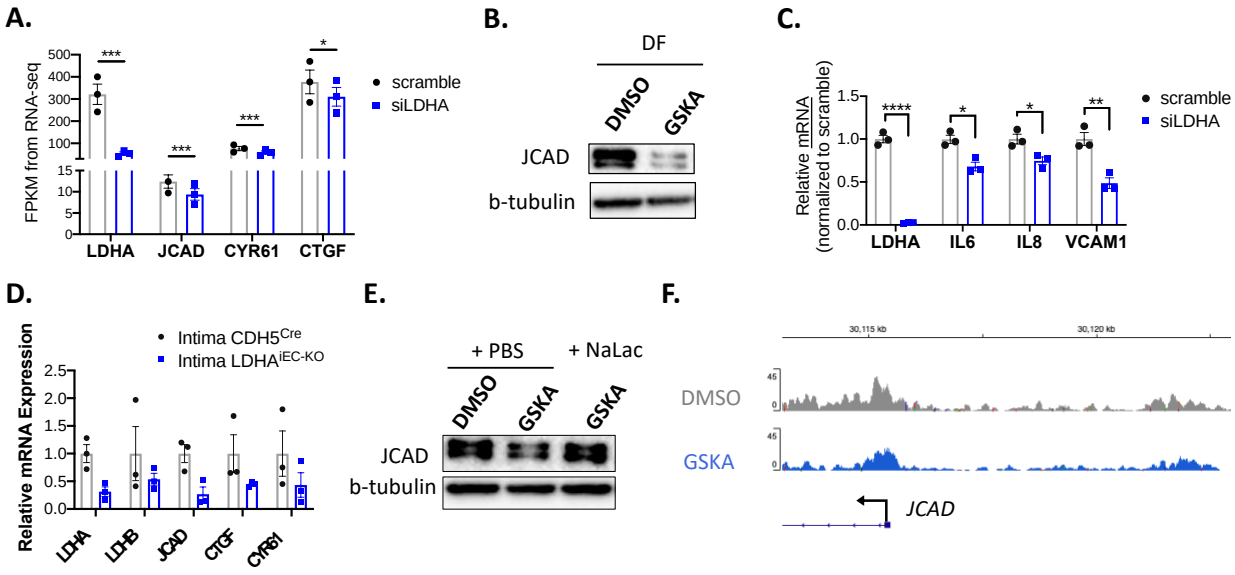

Figure 3.9. Endothelial LDHA regulates the transcription of atherogenic gene JCAD, likely through H3K18la modification. (A) RNA-seq showed inhibiting LDHA using siRNA (siLDHA) significantly reduced the mRNA of LDHA, JCAD, CYR61 and CTGF compared to scramble siRNA, in HAECs cultured under 24-hour's DF (n = 3). **(B)** Western blot suggested inhibiting LDHA using GSKA dramatically suppressed JCAD expression in HAECs cultured under 24-hour's DF. **(C)** RT-qPCR demonstrated HAECs transfected with siLDHA had significantly lower transcription of LDHA, IL6, IL8 and VCAM1 compared to those transfected with scramble siRNA (n = 3). **(D)** RT-qPCR showed endothelial LDHA deficiency showed a trend of transcription reduction of LDHA, LDHB, JCAD, CTGF and CYR61 in mouse intima (n = 3). **(E)** Western blot suggested NaLac supplementation restored the GSKA-inhibited JCAD expression in HAECs compared to PBS addition. **(F)** Genome tracks demonstrated the modification of H3K18la at JCAD promoter in HAECs treated either with DMSO or GSKA (peaks have been normalized to the input with MACS2 using FDR ≤ 0.05).

3.3.10 H3K18la is widely modified at endothelial genome.

In addition to detecting the modification of JCAD, we conducted a genome-wide analysis of H3K18la peaks in human aortic endothelial cells. A total number of 60,920 peaks were found to be concurrently existed in both DMSO- and GSKA-treated HAECs, 8,600 peaks exclusively presented in DMSO-treated HAECs but were missing in GSKA treatment, and 6,149 peaks exclusively presented in GSKA-treated but not in DMSO-treated cells (Figure 3.10A). These results suggest that H3K18la modification occurs in the majority (80%) of these genome loci, regardless of LDHA activity. These peaks were then assigned to their most-adjacent

promoters/genes, which generated 18,156 (for overlapped peaks), 5,626 (for DMSO-only peaks) and 4,509 (for GSKA-only peaks) genes, respectively. However, affinity analysis needs to be performed to compare the relative lactylation amount at each locus in response to alteration in LDHA activity. Nevertheless, our findings showed that higher levels of H3K18la (DMSO treatment) marked more genes than lower H3K18la (GSKA treatment), consistent with what had been observed in M1 polarization macrophages[277].

Next, we annotated the genome features that these peaks distributed in. The fraction of peaks within promoter regions was the highest (~30%) for the overlapped peaks, but it dropped to < 20% for peaks that exclusively presented in DMSO- or GSKA-treated cells (Figure 3.10B). In contrast, the fraction of peaks within noncoding (intronic and intergenic) regions was the highest (~65%) for the treatment-specific peaks, but it dropped to 50% for overlapped peaks (Figure 3.10B). These findings are in line with the notion that promoter-overlapped H3K18la peaks are more stable through differentiation, while the lactylation in putative distal enhancers (largely intronic and intergenic) is more dynamically regulated[402].

Figure 3.10. H3K18la is widely modified at endothelial genome. (A) Venn diagram of H3K18la peaks shared by HAECs treated with 48-hour's DMSO or GSKA. Occupancy analysis detected 60,920 H3K18la peaks were co-present in HAECs treated with DMSO and GSKA, while 8,600 and 6,149 peaks exclusively presented in DMSO- or GSKA-treated HAECs, respectively. **(B)** Genomic distribution features of H3K18la peaks that were overlapped, or exclusively present in DMSO- or GSKA-treated HAECs. For both panel (A) and (B), only consensus peaks that were detected from all 3 biological replicates in each condition were taken into account.

3.4 Discussion

Vascular homeostasis and pathology are tightly regulated by mechanical forces generated by hemodynamics. One unique feature of atherosclerosis-associated cardiovascular diseases is that plaques preferentially develop at arterial sites of curvature and branching where disturbed flow occurs[27–29]. Previous studies showed one major signaling pathway in response to hemodynamics is through endothelial metabolism: disturbed flow (DF) promotes endothelial glycolysis while inhibiting OXPHOS and consequently contributes to the development of atherosclerosis[131]. But the mechanism linking DF-induced glycolysis to endothelial activation remained uncovered. Because our previous data showed that compared to UF, DF significantly elevated the transcription of a critical glycolytic enzyme LDHA in human aortic endothelial cells, we set out to explore the function of endothelial LDHA in the setting of hemodynamics-induced atherogenesis. Here, I discovered LDHA plays a causal role in atherogenesis *in vivo*, by constructing two mouse models with endothelial LDHA deficiency. I further demonstrated endothelial LDHA regulates the transcription of several genes implicated in atherosclerosis, including a CAD GWAS gene JCAD and its downstream proinflammatory markers. Importantly, my preliminary results showed that LDHA promotes JCAD transcription through producing lactate, which is possibly used for H3K18la modification at its promoter or enhancer. Taken together, my studies demonstrated a key glycolytic enzyme regulates the DF-induced endothelial atherogenic transcriptome through a novel epigenetic mechanism (Figure 3.11).

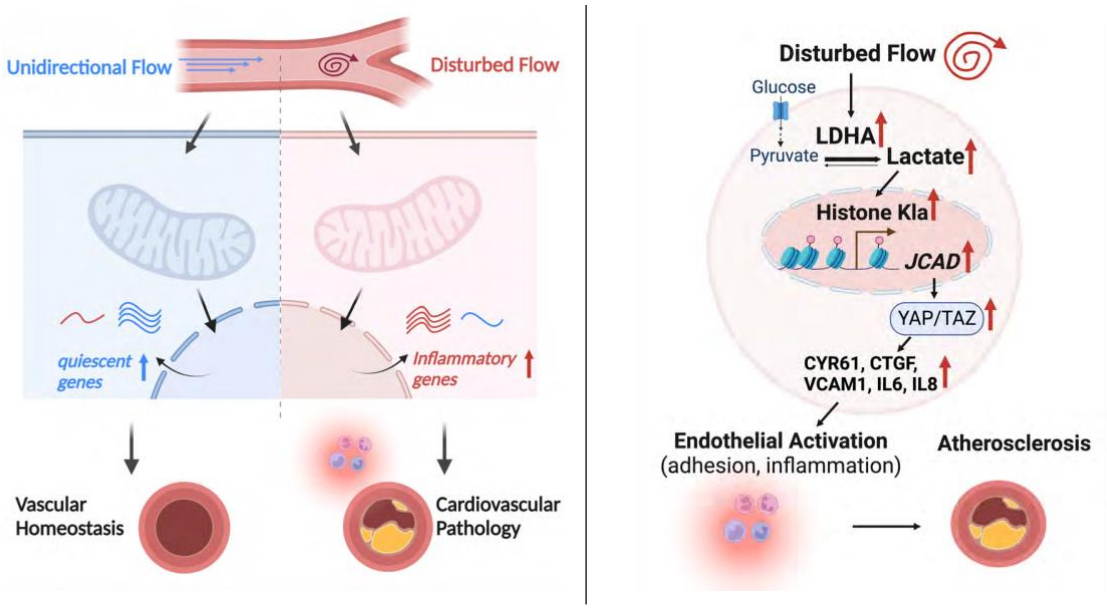

Figure 3.11. The proposed model. *Left:* Hemodynamics-governed endothelial metabolism and epigenome signaling that contribute to the vascular homeostasis or pathology. *Right*: The proposed intracellular pathway underlying the disturbed flow-induced endothelial activation and atherosclerosis formation.

Metabolism has emerged as a central control of endothelial functions and recent studies demonstrated that endothelial metabolism is tightly regulated by hemodynamics[378–381]. Endothelial cells are mostly glycolytic with a relatively small contribution of ATP generation from OXPHOS, and exhibit the Warburg effect, or, utilization of glycolysis in the presence of high concentrations of oxygen[131,215,423,424]. Importantly, mechanical forces including shear stress are able to reprogram endothelial metabolism[130,131,161]. The metabolic activity, throughput of glycolysis and the TCA cycle, all have profound effects on endothelial pathophysiology.

LDHA serves as a crucial glycolytic enzyme by catalyzing the reduction of pyruvate to L-lactate, with concomitant oxidation of NADH to NAD^+. In many cell types, LDHA also acts as an important epigenetic regulator on cell plasticity and phenotypes, through altering the level of its associated metabolites such as acetyl-CoA, NAD^+, and L-lactate[277,425,426]. In our lab's previous studies, the upregulation of LDHA was consistently detected in endothelial cells by

disturbed flow; however, its putative role in endothelial mechano-transduction and atherogenesis is completely unknown. My studies provide a new molecular insight elucidating the role of endothelial LDHA in disturbed flow-induced vascular dysfunction and diseases in three aspects.

First of all, my work identified a novel atherogenic function of an essential metabolic enzyme in endothelial cells. From multiple methods such as RNA-seq, RT-qPCR and Western blot, I found that the expression of endothelial LDHA was induced by DF compared to UF both *in vitro* and *in vivo*. Inhibiting LDHA by siRNA could downregulate multiple atherogenic genes including JCAD, CTGF, CYR61, SELP, IL6, IL8 and VCAM1. It is well known that JCAD (or KIAA1462) codes for endothelial junctional protein, and five different mutations in JCAD have all been reported by GWAS to be significantly associated with coronary artery disease and myocardial infarction in multi-ethnic groups[74,419,427,428]. The most well-characterized function of JCAD is its interaction and inhibition of large tumor suppressor kinase 2 (LAST2) to activate YAP/TAZ signaling, which subsequently upregulates the transcription of several inflammatory genes including CTGF, CYR61 and VCMA1[421,422]. CTGF induces atherosclerosis by serving as a chemoattractant to facilitate monocytes migration[429,430]. CYR61 is a biomarker of acute myocardial injury, and its expression is significantly induced in human atherosclerosis lesions compared to normal arteries[431,432]. It is suggested that CYR61 contributes to atherogenesis through its angiogenic function by promoting plaque neovascularization[431]. P-selectin assists with monocytes capture and rolling at endothelium[433]. Subsequently, IL-6 and IL-8 stimulate monocytes activation and coagulation[434–436], while VCAM-1 promotes their arrest and firm adhesion to the endothelium layer before transmigration[437]. These steps together give rise to atherosclerosis initiation[25]. Beyond these *in vitro* studies, two atherosclerosis mouse models were constructed with AAV9-PCSK9 overexpression and ApoE$^{-/-}$, respectively, to demonstrate that

endothelial LDHA deficiency ($LDHA^{iEC\text{-}KO}$ vs. $CDH5^{cre}$) significantly ameliorated plaques formation in mouse aorta. These findings collectively demonstrated the causal role of endothelial LDHA in atherogenesis. Nevertheless, one of the future directions is to validate this finding with more biological replicates in both genders. Besides using Oil Red O to stain fat deposit on *en face* aorta, more comprehensive characterizations of atherosclerosis development are needed. These include but not limited to processing the cryosections of aortic root to conduct: Verhoeff elastin staining for the assessment of intima-to-media ratio and maximum intima thickness, picrosirius red staining and Oil Red O staining for detection of collagen content and lipid deposition, and smooth muscle actin and CD45 immunostaining for the examination of smooth muscle cell migration[438–440]. More importantly, CD68 and Mac2 will be adopted to stain for monocytes/macrophages[381,441] to verify the *in vitro* endothelial adhesion as a function of LDHA deletion.

Secondly, my studies revealed a novel epigenetic modulation in endothelial cells by which the DF-induced LDHA could modify lactylation on histone lysine sites across the genome. Three assays were adopted to demonstrate that endothelial lactate production was sensitive to LDHA perturbation. Lactate has been shown to be associated with inflammatory diseases, as the physiological level of lactate in human blood and healthy tissues is around 2 mM, but it can rise up to 30 mM at inflamed tissues[170,171]. In support of it, a study using carotid endarterectomy from human patients also showed lactate concentration is positively correlated with the atherosclerosis severity[172]. These findings led to my hypothesis that the atherogenic function of endothelial LDHA is executed through its product lactate. Recently, lactate has been uncovered to have an epigenetic role by metabolized into lactyl-CoA and then added to the histone lysine residues to activate gene transcription[277], but whether this modification exists in endothelial cells has been

unknown. My studies for the first time uncovered the presence of lactylation and specifically H3K18la in aortic endothelial cells *in vitro* and *in vivo*. Furthermore, using ChIP-seq, I detected the genome-wide distribution of these H3K18la marks whose occupancy are also largely altered by the endogenous LDHA activity, indicating this epigenetic modification may be involved in a universal but also state-specific transcriptome regulation in endothelial cells. One future direction is to correlate H3K18la with gene transcription by integrating with our siLDHA RNA-seq dataset, which will allow us to predict lactylation-dependent transcriptome that directly respond to hemodynamics-regulated LDHA. One discrepancy in my data is that the two LDHA inhibition methods did not achieve the same effects on lactate production but both showed suppression on downstream pan Kla and H3K18la levels. One possible explanation is that, the difference in lactate production is more difficult to capture compared to the lactylation amount, due to lactate as an intermediate metabolite could be rapidly converted to pyruvate and lactyl-CoA or even transported extracellularly, while the post-translational lactylation would be more stably maintained. Therefore, the screenshot of lactate production could be sensitive to the more potent LDHA perturbation compound GSKA but not to siLDHA/B. This discrepancy has also been reported previously that the global H3K18la levels may not correlated with the small endogenous metabolic shift in the cells/tissues, but is correlated with the large lactate surplus by lactate supplementation[402]. Collectively, my work demonstrated an endogenous LDHA-dependent epigenetic modification in endothelial cells.

Lastly, I established a mechanistic model based on these preliminary data that endothelial LDHA modulates the transcription of a CAD GWAS gene JCAD through lactylation modification. Using RNA-seq, RT-qPCR and Western blot, we consistently detected that DF-induced LDHA could upregulate the expression of JCAD and its downstream targets in HAECs.

Further in the mouse intima, we observed endothelial LDHA deficiency tended to reduce the transcription of JCAD and its targets CYR61 and CTGF, although more biological replicates and downstream targets are needed to validate this pathway *in vivo*. After lactate supplied, the GSKA-suppressed JCAD expression was restored in HAECs, suggesting the transcriptional regulation of LDHA on JCAD is lactate-dependent. Furthermore, a concurrent higher expression of H3K18la and JCAD was detected in the DF-exposed arterial sites compared to their UF-exposed counterparts (Figure 3.1E-F and 3.5), establishing a positive association of mechano-sensitive H3K18la and JCAD. The direct modulation of H3K18la on JCAD was further validated by the ChIP-seq assay, where a peak localized at JCAD promoter was consistently found from all biological replicates. Again, affinity analysis is needed to test whether this modulation relied on endogenous LDHA activity by comparing the read counts aligned to JCAD promoter region between DMSO- and GSKA-treated groups. In addition to the promoter region, H3K18la peaks were also found to be present at one intronic and five distal intergenic regions of JCAD, and these regions were marked exclusively in the DMSO-treated but not GSKA-inhibited HAECs (genome tracks not shown). These findings indicate that H3K18la may modulate JCAD transcription through a *cis*-regulation mechanism, and this possibility will be further discussed in Chapter Four. Altogether, my studies uncovered a novel mechano-transduction signaling pathway through metabolism-mediated epigenome, which may provide significant implications in precisely targeting activated endothelium to treat “local” vascular diseases.

CHAPTER FOUR: DISCUSSIONS AND FUTURE DIRECTIONS

4.1 Summary

Mechanical signals from hemodynamics are sensed by endothelial cells to reprogram their transcriptome through two independent yet interconnected pathways: metabolism and epigenome. Specifically, atherosclerosis-prone disturbed flow activates the glycolytic outputs and re-distributes the active histone marks, including H3K27ac, which are correlated to the activation of the endothelial proinflammatory transcriptome. Nevertheless, several fundamental questions remain to be addressed for us to fully understand the highly organized coordination of these mechano-transduction processes, including how the individual *cis*-regulatory elements work synergistically to control transcription and how glycolysis participates in the atherosclerosis-relevant hemodynamics regulation.

In my doctoral studies, I set out to address these two questions from multiple perspectives by adopting various approaches including computational analyses, *in vitro* molecular and cell-based assays, and *in vivo* transgenic mouse models. In my studies in Chapter Two, I integrated multi-omics datasets to identify mechano-sensitive super-enhancers. I found these super-enhancers can orchestrate the flow of biological information from DNA sequences and genetic variation in the 3D genome to the functional transcriptome. In Chapter Three, I demonstrated the causal role of endothelial glycolytic enzyme LDHA in atherogenesis and provided preliminary data to uncover the mechanism that disturbed flow upregulates LDHA to induce histone lactylation, thus the transcription of several atherogenic genes.

4.2 *In vivo* relevance of mechano-sensitive super-enhancers

For my studies in Chapter Two, the super-enhancers were identified from H3K27ac ChIP-seq performed in human aortic endothelial cells cultured *in vitro* under specific flow devices. Although the shear stress patterns generated from these flow devices were well-designed to faithfully recreate the hemodynamics measured in the human carotid artery *in vivo*[304], we could not rule out the possibility that the true *in vivo* blood flow-induced super-enhancer remodeling would be different. In other words, the *in vitro* observations may be artificial, which is likely if we consider (1) the *in vivo* hemodynamics exposure is more chronic compared to the 24-hour's culture *in vitro*, and (2) the interactions of endothelial cells with their *in vivo* microenvironments such as blood immune cells were missing in our system.

Therefore, future studies using animal models could be conducted to investigate the *in vivo* relevance of these mechano-sensitive super-enhancers. For instance, mouse arterial endothelial cells exposed to UF or DF in the partial carotid ligation models could be isolated[289,442] for H3K27ac ChIP-seq or CUT&Tag[443] (to accommodate low cell numbers). Alternatively, similar assays could be performed using mouse aortic endothelial cells isolated from the UF-exposed descending thoracic aorta and the DF-exposed aortic arch, respectively. The corresponding *in vivo* transcriptomics data are already available[444] to enable integration analysis. The PCHi-C experiment may also be achievable after enriching the number of cells by expanding aortic endothelial cells *in vitro* or pooling more samples[445]. Although we expect a discrepancy between mouse and human epigenome, exploring the *in vivo* relevance of these mechano-sensitive super-enhancers would be valuable to validate our findings in a more physiologically relevant setting. Besides, such investigations will promote our understanding of whether and to what extent this mechano-transduction mechanism is evolutionarily conserved.

4.3 Interaction of metabolism and mechano-sensitive super-enhancers

As previously discussed in this dissertation, metabolism and epigenome closely interact to control gene transcriptions synergistically[446,447]. One example is that glucose- or fatty acids-derived acetyl-CoA serves as the substrate for histone acetylation. Therefore, it is reasonable to hypothesize that the H3K27ac-defined super-enhancer architectures are also sensitive to intracellular bioenergetic shifts. In support of this hypothesis, a study showed that many super-enhancers in human pancreatic islets have glucose-dependent activity[267]. Investigating the dictation of metabolic changes on super-enhancer remodeling may expand our understanding of the upstream regulatory mechanism of this dynamic cistrome. It may also elucidate how metabolic signals are translated to modify cell identity and how genetic variants converge with environmental factors to exert their activity. However, whether the mechano-sensitive super-enhancer landscapes in endothelial cells are also governed by their hemodynamics-induced metabolic changes has not been characterized.

To test this hypothesis, we could perturb the flow-induced metabolic shift in endothelial cells, such as DF-induced glycolysis, followed by super-enhancer identification. A significant amount of super-enhancer remodeling is expected by glycolysis perturbation, as acetyl-CoA synthesis from glucose will be affected. It is also expected that inhibiting glycolysis will broadly reduce the acetylation levels at DF-enriched super-enhancers while boosting the signals at UF-enriched ones, explaining the previous observations that the endothelial proinflammatory transcriptome is largely suppressed, whereas the quiescent transcriptome is upregulated by glycolysis inhibition, such as interfering HIF-1α[173] or LDHA in my studies. In addition to acetyl-CoA, the availability of NAD^+ is also expected to be impacted by glycolysis disruption, which contributes to histone deacetylation by activating sirtuins.

Other metabolites may also indirectly involve in writing the super-enhancers. For instance, the genome distribution of H3K27ac has been suggested to be positively correlated with that of H3K18la[402] and negatively associated with several histone lysine trimethylations[448]. Therefore, it is likely the hemodynamics-induced metabolic changes may affect lactylation and methylation to alter H3K27ac distribution indirectly. Because the global H3K18la location highly resembles that of H3K27ac[402], we could also use our current H3K18la ChIP-seq data to identify super-enhancer surrogates and test the effect of glycolysis inhibition (GSKA vs. DMSO).

4.4 Characterizing the atherogenic role of endothelial LDHA *in vitro* and *ex vivo*

My studies in Chapter Three demonstrated the atherogenic role of endothelial LDHA by showing that 1) endothelial LDHA deficiency reduced plaques formation in two different mouse models and 2) LDHA inhibition downregulates the transcription of a cohort of proinflammatory genes from the RNA-seq performed in cultured HAECs. However, it has not been characterized how this LDHA-driven inflammation transcriptome changes endothelial functions. In other words, a more complete link between our *in vitro* and *in vivo* observations needs to be established.

Future work could be performed to illustrate the atherogenic role of endothelial LDHA *in vitro* and *ex vivo.* First, a leukocyte-endothelium adhesion assay could be performed as previously described[395,396] together with LDHA perturbation. This experiment will allow us to test the hypothesis that the inflammatory transcriptome reduction by LDHA suppression can consequently ameliorate the DF-induced endothelial activation. Similarly, this assay could be conducted on endothelial cells isolated from either the lung[449] or aorta[450] of mice with intact

LDHA or endothelial LDHA deficiency. Should this hypothesis be true, cells isolated from $LDHA^{iEC\text{-}KO}$ mice would recruit fewer leukocytes to adhere than cells from $CDH5^{cre}$ mice. Secondly, *in vitro* atherosclerosis platforms such as organ-on-chip can be adopted to characterize the function of endothelial cells and their interaction with other atherogenic participants, including the immune cells[451]. Based on this model, HAECs with different LDHA levels could be cultured with their phenotypes further compared. Moreover, since endothelial-derived lactate also has an angiocrine function on surrounding cells[165], this co-culture device may enable us to investigate the potential effect of endothelial-derived lactate on other vascular components such as smooth muscle cells and macrophages which also contribute to atherosclerosis development. Thirdly, to directly compare the inflammatory activity of endothelial cells from $LDHA^{iEC\text{-}KO}$ with those from $CDH5^{cre}$ mice, flow cytometry-based analysis could be performed to quantify the LDHA downstream inflammatory markers.

4.5 Further validating the regulation of endothelial LDHA-derived lactate on histone lactylation

Lactate dehydrogenase is made of four subunits, with the most common ones being LDH-M and LDH-H encoded by LDHA and LDHB genes, respectively. As LDHA has a higher affinity for pyruvate while LDHB favors more in converting lactate, different combinations of these two subunits in the lactate dehydrogenase isoenzymes determine the direction of this redox reaction[452]. Although LDHB is highly expressed (the FPKM is higher than LDHA) in human aortic endothelial cells based on our RNA-seq data, its transcription is not altered by hemodynamics. Therefore, we concluded that only LDHA is the limiting factor in determining this hemodynamics-induced endothelial glycolysis shift, thus the downstream lactylation

alteration. This perspective was also supported by my data showing that exclusively inhibiting LDHA by siRNA was sufficient to reduce the global pan Kla and H3K18la levels (Figure 3.4). However, it does not exclude the possibility of LDHB contributing to these modifications. Interestingly, previous studies in cancer cells suggested that only the double deletion of LDHA and LDHB was sufficient to reduce lactate production, but the single disruption of either gene was not[277,453]. This dependency may also exist in endothelial cells, although we could not demonstrate that from our current data due to the incomplete interference effect of siRNAs (Figure 3.3E-G). A future direction would be using CRISPR-Cas9 to completely knock out these two genes separately or simultaneously in endothelial cells to distinguish their functions.

My data suggested that the GSKA-inhibited histone lactylation was restored by supplementing sodium L-lactate compared to cells added with PBS. However, we could not rule out the possibility that this NaLac-driven epigenetic modification is not from lactic acid but indirectly from sodium, as excess Na^+ may also induce multiple downstream processes in endothelial cells, such as increasing their oxidative stress and cell stiffness[454]. It is possible that these consequences could indirectly impact the activity of writers, readers, and erasers or the supply of endogenous lactate to affect histone lactylation. To rule out the potential contribution from Na^+, we should include better controls for NaLac, such as sodium chloride, to replace PBS in future experiments.

4.6 Further validating the LDHA-mediated JCAD transcription model

My studies demonstrated that endothelial JCAD expression depends on LDHA-derived lactate (Figure 3.9E), which I proposed is through H3K18la modification at the promoter of JCAD. As a direct piece of evidence to support this hypothesis, my ChIP-seq data detected the

presence of H3K18la peaks at the promoter of JCAD in all biological replicates. In addition, my preliminary finding (Figure 3.1E-F and 3.5) and previous studies[421] collectively indicated that the levels of H3K18la and JCAD were concordantly higher at DF-exposed than UF-exposed arterial endothelium. Nevertheless, colocalizing these two markers in the same sample, either by Western blot or *en face* staining, is needed to validate their expression correlation.

Nevertheless, we could not rule out other mechanisms underlying the LDHA-regulated JCAD expression. First, the LDHA-dependent H3K18la modulation of JCAD is not at its promoter but at other noncoding regions, such as its enhancers. This hypothesis is based on the observation from the ChIP-seq data that besides the promoter, H3K18la peaks also occupy one intronic and several distal intergenic regions of JCAD. To test this hypothesis, affinity analysis comparing the DMSO- and GSKA-treated samples is able to refine differentially modified regions. Besides, perturbation assays including CRISPR-activation and -interference targeting the potential regulatory region followed by RT-qPCR would allow us to validate their function *in vitro*. Secondly, the lactylation of JCAD is likely to be modified on other histone lysine sites rather than H3K18. Although H3K18la is mostly well characterized, lactylation can also be installed at many more lysine sites on histone 2A, 2B, 3 and 4[277]. However, the transcription regulatory role has only been demonstrated for H3K18la but not other lactylation markers, making it hard to challenge this H3K18la model. Still, we could exclude the possible modification of other histone lactylation marks by using specific antibodies to immunoprecipitate their associated chromatins, followed by qPCR to detect the JCAD promoter. Lastly, LDHA may upregulate JCAD through indirectly modifying Kla on other proteins/histones or through other lactate-dependent mechanism rather than Kla. These hypotheses could be supported should the affinity analysis and the *in vitro* perturbation assays

fail to detect a difference of histone lactylation at JCAD between DMSO- and GSKA-treated groups. Alternative modulators linking LDHA-derived lactate to JCAD transcription need to be discovered.

4.7 Systematic characterization of endothelial H3K18la modification

Beyond JCAD, a genome-wide distribution of H3K18la was also detected, a portion of which was sensitive to the endogenous endothelial LDHA activity. These observations indicate H3K18la may be responsible for some universal functions as well as LDHA-dependent state specification in endothelial cells. In support of this, it has recently been reported that H3K18la preferentially marks tissue-specific promoters and cell-state-specific enhancers[402]. Therefore, future work is needed to comprehensively characterize and distinguish the functions of these universal and LDHA-sensitive H3K18la peaks in endothelial cells, including annotating their contacted genes by integrating with the endothelial Promoter Capture Hi-C dataset. Based on previous findings, only genes co-marked with all H3K18la, H3K27ac, and H3K4me3 at their promoters are enriched in tissue-specific pathways, whereas genes missing H3K18la modification are not. Therefore, we could refine functional gene targets by overlapping the H3K18la ChIP-seq with the datasets of these active histone markers. A systematic analysis could also be performed to refine functional *cis*-regulatory elements that may be involved in endothelial state transition (DF-associated high LDHA vs. UF-associated low LDHA). Such analysis can be achieved by correlating the lactylation marks with other epigenetic profiles such as H3K27ac and chromatin accessibility, and with the transcription readouts from RNA-seq.

BIBLIOGRAPHY

1. World Health Organization. *World Health Organization-Cardiovascular diseases (CVDs)*. https://www.who.int/news-room/fact-sheets/detail/cardiovascular-diseases-(cvds).
2. Centers for Disease Control and Prevention, National Center for Health Statistics. *CDC WONDER Online Database website* https://wonder.cdc.gov/mcd-icd10.html (2022).
3. Tsao, C. W. *et al.* Heart Disease and Stroke Statistics-2022 Update: A Report From the American Heart Association. *Circulation* **145**, e153–e639 (2022).
4. Agency for Healthcare Research and Quality. https://meps.ahrq.gov/mepsweb/data_stats/download_data_files.jsp.
5. Roth, G. A. *et al.* Global Burden of Cardiovascular Diseases and Risk Factors, 1990–2019. *Journal of the American College of Cardiology* **76**, 2982–3021 (2020).
6. Wellcome Trust Case Control Consortium. Genome-wide association study of 14,000 cases of seven common diseases and 3,000 shared controls. *Nature* **447**, 661–678 (2007).
7. Chen, Z. & Schunkert, H. Genetics of coronary artery disease in the post-GWAS era. *J Intern Med* **290**, 980–992 (2021).
8. Clinical Guidelines on the Identification, Evaluation, and Treatment of Overweight and Obesity in Adults--The Evidence Report. National Institutes of Health. *Obes Res* **6 Suppl 2**, 51S-209S (1998).
9. Colditz, G. A., Willett, W. C., Rotnitzky, A. & Manson, J. E. Weight gain as a risk factor for clinical diabetes mellitus in women. *Ann Intern Med* **122**, 481–486 (1995).
10. Koh-Banerjee, P. *et al.* Changes in body weight and body fat distribution as risk factors for clinical diabetes in US men. *Am J Epidemiol* **159**, 1150–1159 (2004).
11. Guh, D. P. *et al.* The incidence of co-morbidities related to obesity and overweight: a systematic review and meta-analysis. *BMC Public Health* **9**, 88 (2009).
12. Klein, S., Gastaldelli, A., Yki-Järvinen, H. & Scherer, P. E. Why does obesity cause diabetes? *Cell Metabolism* **34**, 11–20 (2022).
13. Piché, M.-E., Tchernof, A. & Després, J.-P. Obesity Phenotypes, Diabetes, and Cardiovascular Diseases. *Circ Res* **126**, 1477–1500 (2020).
14. Higgins, L. J. & Rutledge, J. C. Inflammation associated with the postprandial lipolysis of triglyceride-rich lipoproteins by lipoprotein lipase. *Curr Atheroscler Rep* **11**, 199–205 (2009).
15. Schwartz, E. A. & Reaven, P. D. Lipolysis of triglyceride-rich lipoproteins, vascular inflammation, and atherosclerosis. *Biochim Biophys Acta* **1821**, 858–866 (2012).
16. Ting, H. J. *et al.* Triglyceride-rich lipoproteins prime aortic endothelium for an enhanced inflammatory response to tumor necrosis factor-alpha. *Circ Res* **100**, 381–390 (2007).

17. Mapanga, R. F. & Essop, M. F. Damaging effects of hyperglycemia on cardiovascular function: spotlight on glucose metabolic pathways. *American Journal of Physiology-Heart and Circulatory Physiology* **310**, H153–H173 (2016).

18. Aronson, D. & Rayfield, E. J. How hyperglycemia promotes atherosclerosis: molecular mechanisms. *Cardiovasc Diabetol* **1**, 1 (2002).

19. Hall, J. E., do Carmo, J. M., da Silva, A. A., Wang, Z. & Hall, M. E. Obesity-Induced Hypertension: Interaction of Neurohumoral and Renal Mechanisms. *Circ Res* **116**, 991–1006 (2015).

20. Johansson, B. B. Hypertension mechanisms causing stroke. *Clin Exp Pharmacol Physiol* **26**, 563–565 (1999).

21. Escobar, E. Hypertension and coronary heart disease. *J Hum Hypertens* **16**, S61–S63 (2002).

22. Wang, Z. & Nakayama, T. Inflammation, a link between obesity and cardiovascular disease. *Mediators Inflamm* **2010**, 535918 (2010).

23. Howard, G. *et al.* Insulin Sensitivity and Atherosclerosis. *Circulation* **93**, 1809–1817 (1996).

24. Ginsberg, H. N. Insulin resistance and cardiovascular disease. *J Clin Invest* **106**, 453–458 (2000).

25. Libby, P. *et al.* Atherosclerosis. *Nat Rev Dis Primers* **5**, 56 (2019).

26. Gimbrone, M. A. & García-Cardeña, G. Endothelial Cell Dysfunction and the Pathobiology of Atherosclerosis. *Circ Res* **118**, 620–636 (2016).

27. Davies, P. F., Civelek, M., Fang, Y. & Fleming, I. The atherosusceptible endothelium: Endothelial phenotypes in complex haemodynamic shear stress regions in vivo. *Cardiovascular Research* Preprint at https://doi.org/10.1093/cvr/cvt101 (2013).

28. Gimbrone, M. A. & García-Cardeña, G. Endothelial Cell Dysfunction and the Pathobiology of Atherosclerosis. *Circulation Research* (2016) doi:10.1161/CIRCRESAHA.115.306301.

29. Hahn, C. & Schwartz, M. A. Mechanotransduction in vascular physiology and atherogenesis. *Nature Reviews Molecular Cell Biology* Preprint at https://doi.org/10.1038/nrm2596 (2009).

30. Moore, K. J., Sheedy, F. J. & Fisher, E. A. Macrophages in atherosclerosis: a dynamic balance. *Nat Rev Immunol* **13**, 709–721 (2013).

31. Stary, H. C. *et al.* A definition of initial, fatty streak, and intermediate lesions of atherosclerosis. A report from the Committee on Vascular Lesions of the Council on Arteriosclerosis, American Heart Association. *Circulation* **89**, 2462–2478 (1994).

32. Wolf, D. & Ley, K. Immunity and Inflammation in Atherosclerosis. *Circ Res* **124**, 315–327 (2019).

33. Bennett, M. R., Sinha, S. & Owens, G. K. Vascular Smooth Muscle Cells in Atherosclerosis. *Circ Res* **118**, 692–702 (2016).

34. Pugliese, G., Iacobini, C., Fantauzzi, C. B. & Menini, S. The dark and bright side of atherosclerotic calcification. *Atherosclerosis* **238**, 220–230 (2015).

35. Badimon, L. & Vilahur, G. Thrombosis formation on atherosclerotic lesions and plaque rupture. *J Intern Med* **276**, 618–632 (2014).

36. Quillard, T., Franck, G., Mawson, T., Folco, E. & Libby, P. Mechanisms of erosion of atherosclerotic plaques: *Current Opinion in Lipidology* **28**, 434–441 (2017).

37. Kakadiya, J. Causes, symptoms, pathophysiology and diagnosis of atherosclerosis–a review. *PharmacologyOnline* **3**, 420–442 (2009).

38. Folsom, A. R. *et al.* Community prevalence of ideal cardiovascular health, by the American Heart Association definition, and relationship with cardiovascular disease incidence. *J Am Coll Cardiol* **57**, 1690–1696 (2011).

39. Stampfer, M. J., Hu, F. B., Manson, J. E., Rimm, E. B. & Willett, W. C. Primary prevention of coronary heart disease in women through diet and lifestyle. *N Engl J Med* **343**, 16–22 (2000).

40. Stamler, J. *et al.* Low Risk-Factor Profile and Long-term Cardiovascular and Noncardiovascular Mortality and Life Expectancy: Findings for 5 Large Cohorts of Young Adult and Middle-Aged Men and Women. *JAMA* **282**, 2012 (1999).

41. Berry, J. D. *et al.* Lifetime risks of cardiovascular disease. *N Engl J Med* **366**, 321–329 (2012).

42. Ford, E. S., Zhao, G., Tsai, J. & Li, C. Low-risk lifestyle behaviors and all-cause mortality: findings from the National Health and Nutrition Examination Survey III Mortality Study. *Am J Public Health* **101**, 1922–1929 (2011).

43. Daviglus, M. L. Favorable Cardiovascular Risk Profile in Young Women and Long-term Risk of Cardiovascular and All-Cause Mortality. *JAMA* **292**, 1588 (2004).

44. Ford, E. S., Greenlund, K. J. & Hong, Y. Ideal cardiovascular health and mortality from all causes and diseases of the circulatory system among adults in the United States. *Circulation* **125**, 987–995 (2012).

45. Brown, J. D., Buscemi, J., Milsom, V., Malcolm, R. & O'Neil, P. M. Effects on cardiovascular risk factors of weight losses limited to 5–10 %. *Behav. Med. Pract. Policy Res.* **6**, 339–346 (2016).

46. Wing, R. R. *et al.* Benefits of Modest Weight Loss in Improving Cardiovascular Risk Factors in Overweight and Obese Individuals With Type 2 Diabetes. *Diabetes Care* **34**, 1481–1486 (2011).

47. Makover, M. E., Shapiro, M. D. & Toth, P. P. There is urgent need to treat atherosclerotic cardiovascular disease risk earlier, more intensively, and with greater precision: A review of current practice and recommendations for improved effectiveness. *Am J Prev Cardiol* **12**, 100371 (2022).

48. Mach, F. *et al.* 2019 ESC/EAS Guidelines for the management of dyslipidaemias: lipid modification to reduce cardiovascular risk. *Eur Heart J* **41**, 111–188 (2020).

49. Cannon, C. P. *et al.* Intensive versus Moderate Lipid Lowering with Statins after Acute Coronary Syndromes. *N Engl J Med* **350**, 1495–1504 (2004).

50. Collins, R. *et al.* Interpretation of the evidence for the efficacy and safety of statin therapy. *Lancet* **388**, 2532–2561 (2016).

51. Silverman, M. G. *et al.* Association Between Lowering LDL-C and Cardiovascular Risk Reduction Among Different Therapeutic Interventions: A Systematic Review and Meta-analysis. *JAMA* **316**, 1289–1297 (2016).

52. Schwartz, G. G. *et al.* Effects of atorvastatin on early recurrent ischemic events in acute coronary syndromes: the MIRACL study: a randomized controlled trial. *JAMA* **285**, 1711–1718 (2001).

53. Gallego-Colon, E., Daum, A. & Yosefy, C. Statins and PCSK9 inhibitors: A new lipid-lowering therapy. *European Journal of Pharmacology* **878**, 173114 (2020).

54. Kersten, S. ANGPTL3 as therapeutic target. *Curr Opin Lipidol* **32**, 335–341 (2021).

55. Ravnskov, U. *et al.* LDL-C does not cause cardiovascular disease: a comprehensive review of the current literature. *Expert Review of Clinical Pharmacology* **11**, 959–970 (2018).

56. Kristensen, M. L., Christensen, P. M. & Hallas, J. The effect of statins on average survival in randomised trials, an analysis of end point postponement. *BMJ Open* **5**, e007118 (2015).

57. Grebe, A., Hoss, F. & Latz, E. NLRP3 Inflammasome and the IL-1 Pathway in Atherosclerosis. *Circ Res* **122**, 1722–1740 (2018).

58. Olsen, M. B. *et al.* Targeting the Inflammasome in Cardiovascular Disease. *JACC: Basic to Translational Science* **7**, 84–98 (2022).

59. Luo, F. *et al.* Metformin in patients with and without diabetes: a paradigm shift in cardiovascular disease management. *Cardiovasc Diabetol* **18**, 54 (2019).

60. Seneviratne, A. *et al.* Metformin directly suppresses atherosclerosis in normoglycaemic mice via haematopoietic adenosine monophosphate-activated protein kinase. *Cardiovascular Research* **117**, 1295–1308 (2021).

61. Pahud de Mortanges, A. *et al.* The Role of SGLT2 Inhibitors in Atherosclerosis: A Narrative Mini-Review. *Front Pharmacol* **12**, 751214 (2021).

62. Liu, Z. *et al.* Impact of sodium glucose cotransporter 2 (SGLT2) inhibitors on atherosclerosis: from pharmacology to pre-clinical and clinical therapeutics. *Theranostics* **11**, 4502–4515 (2021).

63. Koufakis, T., Vas, P., Maltese, G. & Kotsa, K. Antiatherosclerotic Effects of Sodium-Glucose Cotransporter 2 Inhibitors: An Underrecognized Piece of the Big Puzzle? *The Journal of Clinical Endocrinology & Metabolism* **107**, e4244–e4245 (2022).

64. Sabatine, M. S. *et al.* Percutaneous coronary intervention with drug-eluting stents versus coronary artery bypass grafting in left main coronary artery disease: an individual patient data meta-analysis. *The Lancet* **398**, 2247–2257 (2021).

65. Caliskan, E. *et al.* Saphenous vein grafts in contemporary coronary artery bypass graft surgery. *Nat Rev Cardiol* **17**, 155–169 (2020).

66. Thuijs, D. J. F. M. *et al.* Percutaneous coronary intervention versus coronary artery bypass grafting in patients with three-vessel or left main coronary artery disease: 10-year follow-up of the multicentre randomised controlled SYNTAX trial. *The Lancet* **394**, 1325–1334 (2019).

67. Lee, S.-W. *et al.* Randomized Trial Evaluating Percutaneous Coronary Intervention for the Treatment of Chronic Total Occlusion: The DECISION-CTO Trial. *Circulation* **139**, 1674–1683 (2019).

68. Brott, T. G. *et al.* Long-term outcomes of stenting and endarterectomy for symptomatic carotid stenosis: a preplanned pooled analysis of individual patient data. *The Lancet Neurology* **18**, 348–356 (2019).

69. Cole, T. S. *et al.* Nationwide Trends in Carotid Endarterectomy and Carotid Artery Stenting in the Post-CREST Era. *Stroke* **51**, 579–587 (2020).

70. Müller, M. D., Lyrer, P., Brown, M. M. & Bonati, L. H. Carotid artery stenting versus endarterectomy for treatment of carotid artery stenosis. *Cochrane Database of Systematic Reviews* **2020**, (2020).

71. Liakopoulos, V. *et al.* Renal and Cardiovascular Outcomes After Weight Loss From Gastric Bypass Surgery in Type 2 Diabetes: Cardiorenal Risk Reductions Exceed Atherosclerotic Benefits. *Diabetes Care* **43**, 1276–1284 (2020).

72. King, E. A., Davis, J. W. & Degner, J. F. Are drug targets with genetic support twice as likely to be approved? Revised estimates of the impact of genetic support for drug mechanisms on the probability of drug approval. *PLoS Genet* **15**, e1008489 (2019).

73. Hopkins, P. N. *et al.* Characterization of Autosomal Dominant Hypercholesterolemia Caused by PCSK9 Gain of Function Mutations and Its Specific Treatment With Alirocumab, a PCSK9 Monoclonal Antibody. *Circ Cardiovasc Genet* **8**, 823–831 (2015).

74. Nikpay, M. *et al.* A comprehensive 1,000 Genomes-based genome-wide association meta-analysis of coronary artery disease. *Nat Genet* **47**, 1121–1130 (2015).

75. Kent, S. T. *et al.* PCSK9 Loss-of-Function Variants, Low-Density Lipoprotein Cholesterol, and Risk of Coronary Heart Disease and Stroke: Data From 9 Studies of Blacks and Whites. *Circ Cardiovasc Genet* **10**, e001632 (2017).

76. Khera, A. V. & Kathiresan, S. Genetics of coronary artery disease: discovery, biology and clinical translation. *Nat Rev Genet* **18**, 331–344 (2017).

77. Erdmann, J., Kessler, T., Munoz Venegas, L. & Schunkert, H. A decade of genome-wide association studies for coronary artery disease: the challenges ahead. *Cardiovascular Research* (2018) doi:10.1093/cvr/cvy084.

78. Zhou, Z. *et al.* Targeted polyelectrolyte complex micelles treat vascular complications in vivo. *Proc. Natl. Acad. Sci. U.S.A.* **118**, e2114842118 (2021).

79. Claesson-Welsh, L., Dejana, E. & McDonald, D. M. Permeability of the Endothelial Barrier: Identifying and Reconciling Controversies. *Trends in Molecular Medicine* **27**, 314–331 (2021).

80. Stamatovic, S. M., Johnson, A. M., Keep, R. F. & Andjelkovic, A. V. Junctional proteins of the blood-brain barrier: New insights into function and dysfunction. *Tissue Barriers* **4**, e1154641 (2016).

81. Matthay, M. A. & Zimmerman, G. A. Acute lung injury and the acute respiratory distress syndrome: four decades of inquiry into pathogenesis and rational management. *Am J Respir Cell Mol Biol* **33**, 319–327 (2005).

82. Steinberg, D. A critical look at the evidence for the oxidation of LDL in atherogenesis. *Atherosclerosis* **131 Suppl**, S5-7 (1997).

83. Neubauer, K. & Zieger, B. Endothelial cells and coagulation. *Cell Tissue Res* **387**, 391–398 (2022).

84. Michaelis, U. R. Mechanisms of endothelial cell migration. *Cell. Mol. Life Sci.* **71**, 4131–4148 (2014).

85. Pober, J. S. & Sessa, W. C. Evolving functions of endothelial cells in inflammation. *Nat Rev Immunol* **7**, 803–815 (2007).

86. Ingber, D. Mechanobiology and diseases of mechanotransduction. *Annals of Medicine* **35**, 564–577 (2003).

87. Dessalles, C. A., Leclech, C., Castagnino, A. & Barakat, A. I. Integration of substrate- and flow-derived stresses in endothelial cell mechanobiology. *Commun Biol* **4**, 764 (2021).

88. Chien, S., Li, S. & Shyy, J. Y.-J. Effects of Mechanical Forces on Signal Transduction and Gene Expression in Endothelial Cells. *Hypertension* **31**, 162–169 (1998).

89. Santamaría, R., González-Álvarez, M., Delgado, R., Esteban, S. & Arroyo, A. G. Remodeling of the Microvasculature: May the Blood Flow Be With You. *Front. Physiol.* **11**, 586852 (2020).

90. Paszkowiak, J. J. & Dardik, A. Arterial Wall Shear Stress: Observations from the Bench to the Bedside. *Vasc Endovascular Surg* **37**, 47–57 (2003).

91. Davies, P. F. Flow-mediated endothelial mechanotransduction. *Physiological Reviews* **75**, 519–560 (1995).

92. Combs, M. D. & Yutzey, K. E. Heart Valve Development: Regulatory Networks in Development and Disease. *Circulation Research* **105**, 408–421 (2009).

93. O'Donnell, A. & Yutzey, K. E. Mechanisms of heart valve development and disease. *Development* **147**, dev183020 (2020).

94. Vermot, J. *et al.* Reversing Blood Flows Act through klf2a to Ensure Normal Valvulogenesis in the Developing Heart. *PLoS Biol* **7**, e1000246 (2009).

95. Davies, P. F., Civelek, M., Fang, Y. & Fleming, I. The atherosusceptible endothelium: endothelial phenotypes in complex haemodynamic shear stress regions in vivo. *Cardiovascular Research* **99**, 315–327 (2013).

96. Chiu, J.-J., Usami, S. & Chien, S. Vascular endothelial responses to altered shear stress: Pathologic implications for atherosclerosis. *Annals of Medicine* **41**, 19–28 (2009).

97. Ferdian, E. *et al.* 4DFlowNet: Super-Resolution 4D Flow MRI Using Deep Learning and Computational Fluid Dynamics. *Front. Phys.* **8**, 138 (2020).

98. Dai, G. *et al.* Distinct endothelial phenotypes evoked by arterial waveforms derived from atherosclerosis-susceptible and -resistant regions of human vasculature. *Proceedings of the National Academy of Sciences* **101**, 14871–14876 (2004).

99. Krause, M. D. *et al.* Genetic variant at coronary artery disease and ischemic stroke locus 1p32.2 regulates endothelial responses to hemodynamics. *Proc Natl Acad Sci U S A* **115**, E11349–E11358 (2018).

100. Maurya, M. R. *et al.* Longitudinal shear stress response in human endothelial cells to atheroprone and atheroprotective conditions. *Proc Natl Acad Sci U S A* **118**, e2023236118 (2021).

101. Parmar, K. M. Integration of flow-dependent endothelial phenotypes by Kruppel-like factor 2. *Journal of Clinical Investigation* **116**, 49–58 (2005).

102. Wu, C. *et al.* Mechanosensitive PPAP2B Regulates Endothelial Responses to Atherorelevant Hemodynamic Forces. *Circ Res* **117**, (2015).

103. Fang, Y., Wu, D. & Birukov, K. G. Mechanosensing and Mechanoregulation of Endothelial Cell Functions. *Compr Physiol* **9**, 873–904 (2019).

104. Birukov, K. G. Cyclic Stretch, Reactive Oxygen Species, and Vascular Remodeling. *Antioxidants & Redox Signaling* **11**, 1651–1667 (2009).

105. Byfield, F. J., Reen, R. K., Shentu, T.-P., Levitan, I. & Gooch, K. J. Endothelial actin and cell stiffness is modulated by substrate stiffness in 2D and 3D. *Journal of Biomechanics* **42**, 1114–1119 (2009).

106. Stroka, K. M. & Aranda-Espinoza, H. Endothelial cell substrate stiffness influences neutrophil transmigration via myosin light chain kinase-dependent cell contraction. *Blood* **118**, 1632–1640 (2011).

107. Dupont, S. *et al.* Role of YAP/TAZ in mechanotransduction. *Nature* **474**, 179–183 (2011).

108. Bertero, T. *et al.* Vascular stiffness mechanoactivates YAP/TAZ-dependent glutaminolysis to drive pulmonary hypertension. *Journal of Clinical Investigation* **126**, 3313–3335 (2016).

109. Pettersen, K. H., Bugenhagen, S. M., Nauman, J., Beard, D. A. & Omholt, S. W. Arterial Stiffening Provides Sufficient Explanation for Primary Hypertension. *PLoS Comput Biol* **10**, e1003634 (2014).

110. Beltran, A. Arterial compliance abnormalities in isolated systolic hypertension. *American Journal of Hypertension* **14**, 1007–1011 (2001).

111. Benetos, A. *et al.* Mortality and Cardiovascular Events Are Best Predicted by Low Central/Peripheral Pulse Pressure Amplification But Not by High Blood Pressure Levels in Elderly Nursing Home Subjects. *Journal of the American College of Cardiology* **60**, 1503–1511 (2012).

112. Smulyan, H., Lieber, A. & Safar, M. E. Hypertension, Diabetes Type II, and Their Association: Role of Arterial Stiffness. *AJHYPE* **29**, 5–13 (2016).

113. Laurent, S. *et al.* Aortic Stiffness Is an Independent Predictor of All-Cause and Cardiovascular Mortality in Hypertensive Patients. *Hypertension* **37**, 1236–1241 (2001).

114. Cooper, L. L. *et al.* Relations of Microvascular Function, Cardiovascular Disease Risk Factors, and Aortic Stiffness in Blacks: The Jackson Heart Study. *J Am Heart Assoc* **7**, (2018).

115. Cardoso, C. & Salles, G. Aortic Stiffness as a Surrogate Endpoint to Micro- and Macrovascular Complications in Patients with Type 2 Diabetes. *IJMS* **17**, 2044 (2016).

116. Mitchell, G. F. Effects of central arterial aging on the structure and function of the peripheral vasculature: implications for end-organ damage. *Journal of Applied Physiology* **105**, 1652–1660 (2008).

117. Mambetsariev, I. *et al.* Stiffness-Activated GEF-H1 Expression Exacerbates LPS-Induced Lung Inflammation. *PLoS ONE* **9**, e92670 (2014).

118. Birukova, A. A. *et al.* Endothelial barrier disruption and recovery is controlled by substrate stiffness. *Microvascular Research* **87**, 50–57 (2013).

119. Meng, F. *et al.* Attenuation of Lipopolysaccharide-Induced Lung Vascular Stiffening by Lipoxin Reduces Lung Inflammation. *Am J Respir Cell Mol Biol* **52**, 152–161 (2015).

120. Campo, A. *et al.* Hemodynamic Predictors of Survival in Scleroderma-related Pulmonary Arterial Hypertension. *Am J Respir Crit Care Med* **182**, 252–260 (2010).

121. Gan, C. T.-J. *et al.* Noninvasively Assessed Pulmonary Artery Stiffness Predicts Mortality in Pulmonary Arterial Hypertension. *Chest* **132**, 1906–1912 (2007).

122. Hunter, K. S. *et al.* Pulmonary vascular input impedance is a combined measure of pulmonary vascular resistance and stiffness and predicts clinical outcomes better than pulmonary vascular resistance alone in pediatric patients with pulmonary hypertension. *American Heart Journal* **155**, 166–174 (2008).

123. Mahapatra, S., Nishimura, R. A., Sorajja, P., Cha, S. & McGoon, M. D. Relationship of Pulmonary Arterial Capacitance and Mortality in Idiopathic Pulmonary Arterial Hypertension. *Journal of the American College of Cardiology* **47**, 799–803 (2006).

124. Thenappan, T. *et al.* The Critical Role of Pulmonary Arterial Compliance in Pulmonary Hypertension. *Annals ATS* AnnalsATS.201509-599FR (2016) doi:10.1513/AnnalsATS.201509-599FR.

125. Chen, Y., Shen, F., Liu, J. & Yang, G.-Y. Arterial stiffness and stroke: de-stiffening strategy, a therapeutic target for stroke. *Stroke Vasc Neurol* **2**, 65–72 (2017).

126. Brunström, M. & Carlberg, B. Association of Blood Pressure Lowering With Mortality and Cardiovascular Disease Across Blood Pressure Levels: A Systematic Review and Meta-analysis. *JAMA Intern Med* **178**, 28 (2018).

127. Quintero, M., Colombo, S. L., Godfrey, A. & Moncada, S. Mitochondria as signaling organelles in the vascular endothelium. *PNAS* **103**, 5379–5384 (2006).

128. De Bock, K. *et al.* Role of PFKFB3-Driven Glycolysis in Vessel Sprouting. *Cell* **154**, 651–663 (2013).

129. Warburg, O. The Metabolism of Carcinoma Cells. *The Journal of Cancer Research* **9**, 148–163 (1925).

130. Feng, S. *et al.* Mechanical Activation of Hypoxia-Inducible Factor 1α Drives Endothelial Dysfunction at Atheroprone Sites. *ATVB* **37**, 2087–2101 (2017).

131. Wu, D. *et al.* HIF-1α is required for disturbed flow-induced metabolic reprogramming in human and porcine vascular endothelium. *eLife* (2017) doi:10.7554/eLife.25217.

132. Atkins, G. B. & Jain, M. K. Role of Krüppel-Like Transcription Factors in Endothelial Biology. *Circulation Research* **100**, 1686–1695 (2007).

133. Dekker, R. J. *et al.* Prolonged fluid shear stress induces a distinct set of endothelial cell genes, most specifically lung Krüppel-like factor (KLF2). *Blood* **100**, 1689–1698 (2002).

134. Huang, R.-T. *et al.* Experimental Lung Injury Reduces Krüppel-like Factor 2 to Increase Endothelial Permeability via Regulation of RAPGEF3–Rac1 Signaling. *Am J Respir Crit Care Med* **195**, 639–651 (2017).

135. Lin, Z. *et al.* Kruppel-Like Factor 2 (KLF2) Regulates Endothelial Thrombotic Function. *Circulation Research* **96**, (2005).

136. Lin, Z. *et al.* Kruppel-Like Factor 2 Regulates Endothelial Barrier Function. *ATVB* **30**, 1952–1959 (2010).

137. Doddaballapur, A. *et al.* Laminar Shear Stress Inhibits Endothelial Cell Metabolism via KLF2-Mediated Repression of PFKFB3. *Arterioscler Thromb Vasc Biol.* **35**, 137–145 (2015).

138. Yu, P. *et al.* FGF-dependent metabolic control of vascular development. *Nature* **545**, 224–228 (2017).

139. Xu, Y. *et al.* Endothelial PFKFB3 plays a critical role in angiogenesis. *Arterioscler Thromb Vasc Biol* **34**, 1231–1239 (2014).

140. Schoors, S. *et al.* Partial and transient reduction of glycolysis by PFKFB3 blockade reduces pathological angiogenesis. *Cell Metab* **19**, 37–48 (2014).

141. Cao, Y. *et al.* PFKFB3-mediated endothelial glycolysis promotes pulmonary hypertension. *Proc Natl Acad Sci U S A* **116**, 13394–13403 (2019).

142. Poels, K. *et al.* Inhibition of PFKFB3 Hampers the Progression of Atherosclerosis and Promotes Plaque Stability. *Front Cell Dev Biol* **8**, 581641 (2020).

143. Wang, G. *et al.* Shear Stress Regulation of Endothelial Glycocalyx Structure Is Determined by Glucobiosynthesis. *ATVB* **40**, 350–364 (2020).

144. Pries, A. R., Secomb, T. W. & Gaehtgens, P. The endothelial surface layer. *Pflugers Arch - Eur J Physiol* **440**, 653–666 (2000).

145. Tarbell, J. M. & Ebong, E. E. The Endothelial Glycocalyx: A Mechano-Sensor and -Transducer. *Science Signaling* **1**, pt8–pt8 (2008).

146. Fu, B. M. & Tarbell, J. M. Mechano-sensing and transduction by endothelial surface glycocalyx: composition, structure, and function: Mechano-sensing and transduction by endothelial surface glycocalyx. *WIREs Syst Biol Med* **5**, 381–390 (2013).

147. Zeng, Y. & Tarbell, J. M. The Adaptive Remodeling of Endothelial Glycocalyx in Response to Fluid Shear Stress. *PLoS ONE* **9**, e86249 (2014).

148. Curry, F. E. & Adamson, R. H. Endothelial Glycocalyx: Permeability Barrier and Mechanosensor. *Ann Biomed Eng* **40**, 828–839 (2012).

149. Tarbell, J. M. Shear stress and the endothelial transport barrier. *Cardiovascular Research* **87**, 320–330 (2010).

150. Lipowsky, H. H. Protease activity and the role of the endothelial glycocalyx in inflammation. *Drug Discovery Today: Disease Models* **8**, 57–62 (2011).

151. Prabhakar, N. R. & Semenza, G. L. Adaptive and Maladaptive Cardiorespiratory Responses to Continuous and Intermittent Hypoxia Mediated by Hypoxia-Inducible Factors 1 and 2. *Physiological Reviews* **92**, 967–1003 (2012).

152. Semenza, G. L. Hypoxia-Inducible Factors in Physiology and Medicine. *Cell* **148**, 399–408 (2012).

153. Wu, D. *et al.* HIF-1α is required for disturbed flow-induced metabolic reprogramming in human and porcine vascular endothelium. *eLife* **6**, e25217 (2017).

154. Kim, J., Tchernyshyov, I., Semenza, G. L. & Dang, C. V. HIF-1-mediated expression of pyruvate dehydrogenase kinase: A metabolic switch required for cellular adaptation to hypoxia. *Cell Metabolism* **3**, 177–185 (2006).

155. Akhtar, S. *et al.* Endothelial Hypoxia-Inducible Factor-1α Promotes Atherosclerosis and Monocyte Recruitment by Upregulating MicroRNA-19a. *Hypertension* **66**, 1220–1226 (2015).

156. Kawanami, D. *et al.* Kruppel-like Factor 2 Inhibits Hypoxia-inducible Factor 1α Expression and Function in the Endothelium. *Journal of Biological Chemistry* **284**, 20522–20530 (2009).

157. Wang, L. *et al.* Integrin-YAP/TAZ-JNK cascade mediates atheroprotective effect of unidirectional shear flow. *Nature* **540**, 579–582 (2016).

158. Wang, K.-C. *et al.* Flow-dependent YAP/TAZ activities regulate endothelial phenotypes and atherosclerosis. *Proc Natl Acad Sci USA* **113**, 11525–11530 (2016).

159. Koo, J. H. & Guan, K.-L. Interplay between YAP/TAZ and Metabolism. *Cell Metabolism* **28**, 196–206 (2018).

160. Kim, J. *et al.* YAP/TAZ regulates sprouting angiogenesis and vascular barrier maturation. *Journal of Clinical Investigation* **127**, 3441–3461 (2017).

161. Yang, Q. *et al.* PRKAA1/AMPKα1-driven glycolysis in endothelial cells exposed to disturbed flow protects against atherosclerosis. *Nat Commun* **9**, 4667 (2018).

162. Baltazar, F., Afonso, J., Costa, M. & Granja, S. Lactate Beyond a Waste Metabolite: Metabolic Affairs and Signaling in Malignancy. *Front. Oncol.* **10**, 231 (2020).

163. Eelen, G. *et al.* Endothelial Cell Metabolism. *Physiological Reviews* **98**, 3–58 (2018).

164. Lee, H. *et al.* Endothelium-derived lactate is required for pericyte function and blood–brain barrier maintenance. *The EMBO Journal* **41**, (2022).

165. Zhang, J. *et al.* Endothelial Lactate Controls Muscle Regeneration from Ischemia by Inducing M2-like Macrophage Polarization. *Cell Metabolism* **31**, 1136-1153.e7 (2020).

166. Végran, F., Boidot, R., Michiels, C., Sonveaux, P. & Feron, O. Lactate Influx through the Endothelial Cell Monocarboxylate Transporter MCT1 Supports an NF-κB/IL-8 Pathway that Drives Tumor Angiogenesis. *Cancer Research* **71**, 2550–2560 (2011).

167. Sonveaux, P. *et al.* Targeting the Lactate Transporter MCT1 in Endothelial Cells Inhibits Lactate-Induced HIF-1 Activation and Tumor Angiogenesis. *PLoS ONE* **7**, e33418 (2012).

168. Hunt, T. K. *et al.* Aerobically Derived Lactate Stimulates Revascularization and Tissue Repair *via* Redox Mechanisms. *Antioxidants & Redox Signaling* **9**, 1115–1124 (2007).

169. Yang, K. *et al.* Lactate induces vascular permeability via disruption of VE-cadherin in endothelial cells during sepsis. *Sci. Adv.* **8**, eabm8965 (2022).

170. Pucino, V. *et al.* Lactate Buildup at the Site of Chronic Inflammation Promotes Disease by Inducing CD4+ T Cell Metabolic Rewiring. *Cell Metabolism* **30**, 1055-1074.e8 (2019).

171. Feng, T. *et al.* Adipocyte-derived lactate is a signalling metabolite that potentiates adipose macrophage inflammation via targeting PHD2. *Nat Commun* **13**, 5208 (2022).

172. Ekstrand, M. *et al.* Depletion of ATP and glucose in advanced human atherosclerotic plaques. *PLoS ONE* **12**, e0178877 (2017).

173. Wu, D. *et al.* HIF-1α is required for disturbed flow-induced metabolic reprogramming in human and porcine vascular endothelium. *Elife* **6**, e25217 (2017).

174. Quintero, M., Colombo, S. L., Godfrey, A. & Moncada, S. Mitochondria as signaling organelles in the vascular endothelium. *Proceedings of the National Academy of Sciences* **103**, 5379–5384 (2006).

175. Tang, X., Luo, Y.-X., Chen, H.-Z. & Liu, D.-P. Mitochondria, endothelial cell function, and vascular diseases. *Front. Physiol.* **5**, (2014).

176. Kim, B., Lee, H., Kawata, K. & Park, J.-Y. Exercise-Mediated Wall Shear Stress Increases Mitochondrial Biogenesis in Vascular Endothelium. *PLoS ONE* **9**, e111409 (2014).

177. Kim, J.-S. *et al.* Shear stress-induced mitochondrial biogenesis decreases the release of microparticles from endothelial cells. *American Journal of Physiology-Heart and Circulatory Physiology* **309**, H425–H433 (2015).

178. Liao, X. *et al.* Kruppel-like factor 4 is critical for transcriptional control of cardiac mitochondrial homeostasis. *Journal of Clinical Investigation* **125**, 3461–3476 (2015).

179. Chen, Z. *et al.* Shear stress, SIRT1, and vascular homeostasis. *Proceedings of the National Academy of Sciences* **107**, 10268–10273 (2010).

180. Mammoto, A., Muyleart, M., Kadlec, A., Gutterman, D. & Mammoto, T. YAP1-TEAD1 signaling controls angiogenesis and mitochondrial biogenesis through PGC1α. *Microvasc Res* **119**, 73–83 (2018).

181. Yamamoto, K., Nogimori, Y., Imamura, H. & Ando, J. Shear stress activates mitochondrial oxidative phosphorylation by reducing plasma membrane cholesterol in vascular endothelial cells. *Proc Natl Acad Sci USA* **117**, 33660–33667 (2020).

182. Westermann, B. Mitochondrial fusion and fission in cell life and death. *Nat Rev Mol Cell Biol* **11**, 872–884 (2010).

183. Youle, R. J. & van der Bliek, A. M. Mitochondrial fission, fusion, and stress. *Science* **337**, 1062–1065 (2012).

184. Chehaitly, A. *et al.* Role of mitochondrial dynamics in the response of endothelial cells to shear stress during early phase of atherosclerosis. *Archives of Cardiovascular Diseases Supplements* **13**, 181 (2021).

185. Wu, L.-H., Chang, H.-C., Ting, P.-C. & Wang, D. L. Laminar shear stress promotes mitochondrial homeostasis in endothelial cells. *J Cell Physiol* **233**, 5058–5069 (2018).

186. Forrester, S. J. *et al.* Mitochondrial Fission Mediates Endothelial Inflammation. *Hypertension* **76**, 267–276 (2020).

187. Wang, Q. *et al.* Metformin Suppresses Diabetes-Accelerated Atherosclerosis via the Inhibition of Drp1-Mediated Mitochondrial Fission. *Diabetes* **66**, 193–205 (2017).

188. Yamamoto, K., Korenaga, R., Kamiya, A. & Ando, J. Fluid Shear Stress Activates Ca^{2+} Influx Into Human Endothelial Cells via P2X4 Purinoceptors. *Circulation Research* **87**, 385–391 (2000).

189. Wilson, C. *et al.* Mitochondrial ATP production provides long-range control of endothelial inositol trisphosphate–evoked calcium signaling. *Journal of Biological Chemistry* **294**, 737–758 (2019).

190. Antoniotti, S. *et al.* Control of endothelial cell proliferation by calcium influx and arachidonic acid metabolism: A pharmacological approach. *J. Cell. Physiol.* **197**, 370–378 (2003).

191. Dalal, P. J., Muller, W. A. & Sullivan, D. P. Endothelial Cell Calcium Signaling during Barrier Function and Inflammation. *The American Journal of Pathology* **190**, 535–542 (2020).

192. Fiorio Pla, A. *et al.* TRPV4 mediates tumor-derived endothelial cell migration via arachidonic acid-activated actin remodeling. *Oncogene* **31**, 200–212 (2012).

193. Sessa, W. C. Regulation of endothelial derived nitric oxide in health and disease. *Mem. Inst. Oswaldo Cruz* **100**, 15–18 (2005).

194. Tsai, F.-C. *et al.* A polarized Ca2+, diacylglycerol and STIM1 signalling system regulates directed cell migration. *Nat Cell Biol* **16**, 133–144 (2014).

195. Yokota, Y. *et al.* Endothelial Ca2+ oscillations reflect VEGFR signaling-regulated angiogenic capacity in vivo. *eLife* **4**, e08817 (2015).

196. James, N. L., Harrison, D. G. & Nerem, R. M. Effects of shear on endothelial cell calcium in the presence and absence of ATP. *FASEB j.* **9**, 968–973 (1995).

197. Yamamoto, K., Imamura, H. & Ando, J. Shear stress augments mitochondrial ATP generation that triggers ATP release and Ca2+ signaling in vascular endothelial cells. *Am J Physiol Heart Circ Physiol* **315**, H1477–H1485 (2018).

198. Scheitlin, C. G. *et al.* Endothelial mitochondria regulate the intracellular Ca $^{2+}$ response to fluid shear stress. *American Journal of Physiology-Cell Physiology* **310**, C479–C490 (2016).

199. Seeley, E. J., Rosenberg, P. & Matthay, M. A. Calcium flux and endothelial dysfunction during acute lung injury: a STIMulating target for therapy. *J. Clin. Invest.* **123**, 1015–1018 (2013).

200. Ghosh, A., Gao, L., Thakur, A., Siu, P. M. & Lai, C. W. K. Role of free fatty acids in endothelial dysfunction. *J Biomed Sci* **24**, 50 (2017).

201. Wang, X. L. *et al.* Free Fatty Acids Inhibit Insulin Signaling-Stimulated Endothelial Nitric Oxide Synthase Activation Through Upregulating PTEN or Inhibiting Akt Kinase. *Diabetes* **55**, 2301–2310 (2006).

202. Venturini, G. *et al.* Integrated proteomics and metabolomics analysis reveals differential lipid metabolism in human umbilical vein endothelial cells under high and low shear stress. *American Journal of Physiology-Cell Physiology* **317**, C326–C338 (2019).

203. Hirata, T., Yamamoto, K., Ikeda, K. & Arita, M. Functional lipidomics of vascular endothelial cells in response to laminar shear stress. *FASEB j.* **35**, (2021).

204. Kalucka, J. *et al.* Quiescent Endothelial Cells Upregulate Fatty Acid β-Oxidation for Vasculoprotection via Redox Homeostasis. *Cell Metabolism* **28**, 881-894.e13 (2018).

205. Mack, J. J. *et al.* NOTCH1 is a mechanosensor in adult arteries. *Nat Commun* **8**, 1620 (2017).

206. Liu, Y. *et al.* Shear Stress Activation of SREBP1 in Endothelial Cells Is Mediated by Integrins. *ATVB* **22**, 76–81 (2002).

207. Aylon, Y. *et al.* The LATS2 tumor suppressor inhibits SREBP and suppresses hepatic cholesterol accumulation. *Genes Dev.* **30**, 786–797 (2016).

208. Schoors, S. *et al.* Fatty acid carbon is essential for dNTP synthesis in endothelial cells. *Nature* **520**, 192–197 (2015).

209. Patella, F. *et al.* Proteomics-Based Metabolic Modeling Reveals That Fatty Acid Oxidation (FAO) Controls Endothelial Cell (EC) Permeability. *Molecular & Cellular Proteomics* **14**, 621–634 (2015).

210. Xiong, J. *et al.* A Metabolic Basis for Endothelial-to-Mesenchymal Transition. *Molecular Cell* **69**, 689-698.e7 (2018).

211. Dodd, M. S. *et al.* Fatty Acids Prevent Hypoxia-Inducible Factor-1α Signaling Through Decreased Succinate in Diabetes. *JACC Basic Transl Sci* **3**, 485–498 (2018).

212. Noto, A. *et al.* Stearoyl-CoA-desaturase 1 regulates lung cancer stemness via stabilization and nuclear localization of YAP/TAZ. *Oncogene* **36**, 4573–4584 (2017).

213. Williamson, D. H. & Brosnan, J. T. Concentrations of Metabolites in Animal Tissues. in *Methods of Enzymatic Analysis* 2266–2302 (Elsevier, 1974). doi:10.1016/B978-0-12-091304-6.50093-8.

214. Newsholme, P., Procopio, J., Lima, M. M. R., Pithon-Curi, T. C. & Curi, R. Glutamine and glutamate?their central role in cell metabolism and function. *Cell Biochem. Funct.* **21**, 1–9 (2003).

215. Kim, B., Li, J., Jang, C. & Arany, Z. Glutamine fuels proliferation but not migration of endothelial cells. *EMBO J* **36**, 2321–2333 (2017).

216. Huang, H. *et al.* Role of glutamine and interlinked asparagine metabolism in vessel formation. *EMBO J* **36**, 2334–2352 (2017).

217. Pavlova, N. N. *et al.* As Extracellular Glutamine Levels Decline, Asparagine Becomes an Essential Amino Acid. *Cell Metabolism* **27**, 428-438.e5 (2018).

218. DeBerardinis, R. J. & Cheng, T. Q's next: the diverse functions of glutamine in metabolism, cell biology and cancer. *Oncogene* **29**, 313–324 (2010).

219. Kucharzewska, P., Welch, J. E., Svensson, K. J. & Belting, M. Ornithine decarboxylase and extracellular polyamines regulate microvascular sprouting and actin cytoskeleton dynamics in endothelial cells. *Experimental Cell Research* **316**, 2683–2691 (2010).

220. Tousoulis, D., Kampoli, A.-M., Tentolouris Nikolaos Papageorgiou, C. & Stefanadis, C. The Role of Nitric Oxide on Endothelial Function. *CVP* **10**, 4–18 (2012).

221. Palmer, R. M. J., Ashton, D. S. & Moncada, S. Vascular endothelial cells synthesize nitric oxide from L-arginine. *Nature* **333**, 664–666 (1988).

222. Davis, M. E., Grumbach, I. M., Fukai, T., Cutchins, A. & Harrison, D. G. Shear Stress Regulates Endothelial Nitric-oxide Synthase Promoter Activity through Nuclear Factor κB Binding. *Journal of Biological Chemistry* **279**, 163–168 (2004).

223. Tao, J., Yang, Z., Wang, J.-M., Tu, C. & Pan, S.-R. Effects of Fluid Shear Stress on eNOS mRNA Expression and NO Production in Human Endothelial Progenitor Cells. *Cardiology* **106**, 82–88 (2006).

224. Davis, M. E., Cai, H., Drummond, G. R. & Harrison, D. G. Shear Stress Regulates Endothelial Nitric Oxide Synthase Expression Through c-Src by Divergent Signaling Pathways. *Circulation Research* **89**, 1073–1080 (2001).

225. Boo, Y. C. *et al.* Shear stress stimulates phosphorylation of eNOS at Ser ^{635} by a protein kinase A-dependent mechanism. *American Journal of Physiology-Heart and Circulatory Physiology* **283**, H1819–H1828 (2002).

226. Boo, Y. C. *et al.* Shear stress stimulates phosphorylation of endothelial nitric-oxide synthase at Ser1179 by Akt-independent mechanisms: role of protein kinase A. *J Biol Chem* **277**, 3388–3396 (2002).

227. McCormick, S. M. *et al.* DNA microarray reveals changes in gene expression of shear stressed human umbilical vein endothelial cells. *Proceedings of the National Academy of Sciences* **98**, 8955–8960 (2001).

228. Mun, G. I., Lee, S. J., An, S. M., Kim, I. K. & Boo, Y. C. Differential gene expression in young and senescent endothelial cells under static and laminar shear stress conditions. *Free Radical Biology and Medicine* **47**, 291–299 (2009).

229. Goodwin, B. L., Solomonson, L. P. & Eichler, D. C. Argininosuccinate Synthase Expression Is Required to Maintain Nitric Oxide Production and Cell Viability in Aortic Endothelial Cells. *Journal of Biological Chemistry* **279**, 18353–18360 (2004).

230. Dupont, C., Armant, D. R. & Brenner, C. A. Epigenetics: definition, mechanisms and clinical perspective. *Semin Reprod Med* **27**, 351–357 (2009).

231. Portela, A. & Esteller, M. Epigenetic modifications and human disease. *Nat Biotechnol* **28**, 1057–1068 (2010).

232. ENCODE Project Consortium. An integrated encyclopedia of DNA elements in the human genome. *Nature* **489**, 57–74 (2012).

233. ENCODE Project Consortium *et al.* Expanded encyclopaedias of DNA elements in the human and mouse genomes. *Nature* **583**, 699–710 (2020).

234. Kellis, M. *et al.* Defining functional DNA elements in the human genome. *Proc Natl Acad Sci U S A* **111**, 6131–6138 (2014).

235. Heintzman, N. D. *et al.* Histone modifications at human enhancers reflect global cell-type-specific gene expression. *Nature* **459**, 108–112 (2009).

236. Bulger, M. & Groudine, M. Enhancers: the abundance and function of regulatory sequences beyond promoters. *Dev Biol* **339**, 250–257 (2010).

237. Heinz, S., Romanoski, C. E., Benner, C. & Glass, C. K. The selection and function of cell type-specific enhancers. *Nat Rev Mol Cell Biol* **16**, 144–154 (2015).

238. Creyghton, M. P. *et al.* Histone H3K27ac separates active from poised enhancers and predicts developmental state. *Proc Natl Acad Sci U S A* **107**, 21931–21936 (2010).

239. Nord, A. S. *et al.* Rapid and pervasive changes in genome-wide enhancer usage during mammalian development. *Cell* **155**, 1521–1531 (2013).

240. Long, H. K., Prescott, S. L. & Wysocka, J. Ever-Changing Landscapes: Transcriptional Enhancers in Development and Evolution. *Cell* **167**, 1170–1187 (2016).

241. Villar, D. *et al.* Enhancer Evolution across 20 Mammalian Species. *Cell* **160**, 554–566 (2015).

242. Sakabe, N., Savic, D. & Nobrega, M. A. Transcriptional enhancers in development and disease. *Genome Biol* **13**, 238 (2012).

243. Claringbould, A. & Zaugg, J. B. Enhancers in disease: molecular basis and emerging treatment strategies. *Trends in Molecular Medicine* **27**, 1060–1073 (2021).

244. Brown, J. D. *et al.* NF-κB Directs Dynamic Super Enhancer Formation in Inflammation and Atherogenesis. *Molecular Cell* **56**, 219–231 (2014).

245. Hogan, N. T. *et al.* Transcriptional networks specifying homeostatic and inflammatory programs of gene expression in human aortic endothelial cells. *eLife* **6**, e22536 (2017).

246. Örd, T. *et al.* Single-Cell Epigenomics and Functional Fine-Mapping of Atherosclerosis GWAS Loci. *Circ Res* **129**, 240–258 (2021).

247. Guo, Y. *et al.* Integrating Epigenomic Elements and GWASs Identifies BDNF Gene Affecting Bone Mineral Density and Osteoporotic Fracture Risk. *Sci Rep* **6**, 30558 (2016).

248. Hindorff, L. A. *et al.* Potential etiologic and functional implications of genome-wide association loci for human diseases and traits. *Proc. Natl. Acad. Sci. U.S.A.* **106**, 9362–9367 (2009).

249. Won, H.-H. *et al.* Disproportionate Contributions of Select Genomic Compartments and Cell Types to Genetic Risk for Coronary Artery Disease. *PLoS Genet* **11**, e1005622 (2015).

250. Ernst, J. *et al.* Mapping and analysis of chromatin state dynamics in nine human cell types. *Nature* **473**, 43–49 (2011).

251. van der Harst, P. & Verweij, N. Identification of 64 Novel Genetic Loci Provides an Expanded View on the Genetic Architecture of Coronary Artery Disease. *Circ Res* **122**, 433–443 (2018).

252. Wang, Y. & Wang, J.-G. Genome-Wide Association Studies of Hypertension and Several Other Cardiovascular Diseases. *Pulse* **6**, 169–186 (2018).

253. Roselli, C. *et al.* Multi-ethnic genome-wide association study for atrial fibrillation. *Nat Genet* **50**, 1225–1233 (2018).

254. Evangelou, E. *et al.* Genetic analysis of over 1 million people identifies 535 new loci associated with blood pressure traits. *Nat Genet* **50**, 1412–1425 (2018).

255. Stolze, L. K. *et al.* Systems Genetics in Human Endothelial Cells Identifies Non-coding Variants Modifying Enhancers, Expression, and Complex Disease Traits. *The American Journal of Human Genetics* **106**, 748–763 (2020).

256. Gupta, R. M. *et al.* A Genetic Variant Associated with Five Vascular Diseases Is a Distal Regulator of Endothelin-1 Gene Expression. *Cell* **170**, 522-533.e15 (2017).

257. Krause, M. D. *et al.* Genetic variant at coronary artery disease and ischemic stroke locus 1p32.2 regulates endothelial responses to hemodynamics. *Proceedings of the National Academy of Sciences of the United States of America* (2018) doi:10.1073/pnas.1810568115.

258. Wu, C. *et al.* Mechanosensitive PPAP2B Regulates Endothelial Responses to Atherorelevant Hemodynamic Forces. *Circ Res* **117**, e41–e53 (2015).

259. Hnisz, D. *et al.* Super-Enhancers in the Control of Cell Identity and Disease. *Cell* **155**, 934–947 (2013).

260. Whyte, W. A. *et al.* Master transcription factors and mediator establish super-enhancers at key cell identity genes. *Cell* **153**, 307–319 (2013).

261. Pott, S. & Lieb, J. D. What are super-enhancers? *Nat Genet* **47**, 8–12 (2015).

262. Kai, Y. *et al.* Mapping the evolving landscape of super-enhancers during cell differentiation. *Genome Biol* **22**, 269 (2021).

263. Lee, H. K., Willi, M., Shin, H. Y., Liu, C. & Hennighausen, L. Progressing super-enhancer landscape during mammary differentiation controls tissue-specific gene regulation. *Nucleic Acids Research* (2018) doi:10.1093/nar/gky891.

264. Mi, Z. *et al.* Super-enhancer-driven metabolic reprogramming promotes cystogenesis in autosomal dominant polycystic kidney disease. *Nat Metab* **2**, 717–731 (2020).

265. Wilflingseder, J. *et al.* Enhancer and super-enhancer dynamics in repair after ischemic acute kidney injury. *Nat Commun* **11**, 3383 (2020).

266. Huang, H. *et al.* Defining super-enhancer landscape in triple-negative breast cancer by multiomic profiling. *Nat Commun* **12**, 2242 (2021).

267. Miguel-Escalada, I. *et al.* Human pancreatic islet three-dimensional chromatin architecture provides insights into the genetics of type 2 diabetes. *Nat Genet* **51**, 1137–1148 (2019).

268. Lovén, J. *et al.* Selective inhibition of tumor oncogenes by disruption of super-enhancers. *Cell* (2013) doi:10.1016/j.cell.2013.03.036.

269. Kalna, V. *et al.* The Transcription Factor ERG Regulates Super-Enhancers Associated With an Endothelial-Specific Gene Expression Program. *Circ Res* **124**, 1337–1349 (2019).

270. Yan, M. S. & Marsden, P. A. Epigenetics in the Vascular Endothelium: Looking From a Different Perspective in the Epigenomics Era. *ATVB* **35**, 2297–2306 (2015).

271. Wei, X., Yi, X., Zhu, X.-H. & Jiang, D.-S. Histone methylation and vascular biology. *Clin Epigenet* **12**, 30 (2020).

272. Fang, Z., Wang, X., Sun, X., Hu, W. & Miao, Q. R. The Role of Histone Protein Acetylation in Regulating Endothelial Function. *Front. Cell Dev. Biol.* **9**, 672447 (2021).

273. Nakato, R. *et al.* Comprehensive epigenome characterization reveals diverse transcriptional regulation across human vascular endothelial cells. *Epigenetics & Chromatin* **12**, 77 (2019).

274. Alghamdi, T. A. *et al.* Histone H3 Serine 10 Phosphorylation Facilitates Endothelial Activation in Diabetic Kidney Disease. *Diabetes* **67**, 2668–2681 (2018).

275. Sun, L., Zhang, H. & Gao, P. Metabolic reprogramming and epigenetic modifications on the path to cancer. *Protein Cell* **13**, 877–919 (2022).

276. Feron, O. The many metabolic sources of acetyl-CoA to support histone acetylation and influence cancer progression. *Ann Transl Med* **7**, S277–S277 (2019).

277. Zhang, D. *et al.* Metabolic regulation of gene expression by histone lactylation. *Nature* **574**, 575–580 (2019).

278. Sakabe, K., Wang, Z. & Hart, G. W. β- *N* -acetylglucosamine (O-GlcNAc) is part of the histone code. *Proc. Natl. Acad. Sci. U.S.A.* **107**, 19915–19920 (2010).

279. Mentch, S. J. *et al.* Histone Methylation Dynamics and Gene Regulation Occur through the Sensing of One-Carbon Metabolism. *Cell Metabolism* **22**, 861–873 (2015).

280. Sauve, A. A. & Youn, D. Y. Sirtuins: NAD+-dependent deacetylase mechanism and regulation. *Current Opinion in Chemical Biology* **16**, 535–543 (2012).

281. Xiao, M. *et al.* Inhibition of α-KG-dependent histone and DNA demethylases by fumarate and succinate that are accumulated in mutations of FH and SDH tumor suppressors. *Genes Dev* **26**, 1326–1338 (2012).

282. Xu, W. *et al.* Oncometabolite 2-hydroxyglutarate is a competitive inhibitor of α-ketoglutarate-dependent dioxygenases. *Cancer Cell* **19**, 17–30 (2011).

283. Bungard, D. *et al.* Signaling Kinase AMPK Activates Stress-Promoted Transcription via Histone H2B Phosphorylation. *Science* **329**, 1201–1205 (2010).

284. Zhong, L. *et al.* The Histone Deacetylase Sirt6 Regulates Glucose Homeostasis via Hif1α. *Cell* **140**, 280–293 (2010).

285. Sebastián, C. *et al.* The Histone Deacetylase SIRT6 Is a Tumor Suppressor that Controls Cancer Metabolism. *Cell* **151**, 1185–1199 (2012).

286. Lee, D. Y. *et al.* Role of histone deacetylases in transcription factor regulation and cell cycle modulation in endothelial cells in response to disturbed flow. *Proceedings of the National Academy of Sciences of the United States of America* (2012) doi:10.1073/pnas.1121214109.

287. Chen, Z. *et al.* Shear stress, SIRT1, and vascular homeostasis. *Proceedings of the National Academy of Sciences of the United States of America* (2010) doi:10.1073/pnas.1003833107.

288. Maurya, M. R. *et al.* Longitudinal shear stress response in human endothelial cells to atheroprone and atheroprotective conditions. *Proc Natl Acad Sci USA* **118**, e2023236118 (2021).

289. Andueza, A. *et al.* Endothelial Reprogramming by Disturbed Flow Revealed by Single-Cell RNA and Chromatin Accessibility Study. *Cell Reports* **33**, 108491 (2020).

290. Krause, M. D. *et al.* Genetic variant at coronary artery disease and ischemic stroke locus 1p32.2 regulates endothelial responses to hemodynamics. *Proc Natl Acad Sci USA* **115**, E11349–E11358 (2018).

291. Martin, M. Cutadapt removes adapter sequences from high-throughput sequencing reads. *EMBnet.journal* **17**, 10–12 (2011).

292. Langmead, B. & Salzberg, S. L. Fast gapped-read alignment with Bowtie 2. *Nat Methods* **9**, 357–359 (2012).

293. Li, H. *et al.* The Sequence Alignment/Map format and SAMtools. *Bioinformatics* **25**, 2078–2079 (2009).

294. Heinz, S. *et al.* Simple combinations of lineage-determining transcription factors prime cis-regulatory elements required for macrophage and B cell identities. *Mol Cell* **38**, 576–589 (2010).

295. Rao, S. S. P. *et al.* A 3D Map of the Human Genome at Kilobase Resolution Reveals Principles of Chromatin Looping. *Cell* **159**, 1665–1680 (2014).

296. Montefiori, L. E. *et al.* A promoter interaction map for cardiovascular disease genetics. *eLife* **7**, e35788 (2018).

297. Wingett, S. W. *et al.* HiCUP: pipeline for mapping and processing Hi-C data. *F1000Res* **4**, 1310 (2015).

298. Cairns, J. *et al.* CHiCAGO: robust detection of DNA looping interactions in Capture Hi-C data. *Genome Biol* **17**, 127 (2016).

299. Chen, L. & Qin, Z. S. traseR: an R package for performing trait-associated SNP enrichment analysis in genomic intervals. *Bioinformatics* **32**, 1214–1216 (2016).

300. Buniello, A. *et al.* The NHGRI-EBI GWAS Catalog of published genome-wide association studies, targeted arrays and summary statistics 2019. *Nucleic Acids Research* **47**, D1005–D1012 (2019).

301. Kuhn, R. M., Haussler, D. & Kent, W. J. The UCSC genome browser and associated tools. *Briefings in Bioinformatics* **14**, 144–161 (2013).

302. Quinlan, A. R. & Hall, I. M. BEDTools: a flexible suite of utilities for comparing genomic features. *Bioinformatics* **26**, 841–842 (2010).

303. Zhou, Y. *et al.* Metascape provides a biologist-oriented resource for the analysis of systems-level datasets. *Nat Commun* **10**, 1523 (2019).

304. Dai, G. *et al.* Distinct endothelial phenotypes evoked by arterial waveforms derived from atherosclerosis-susceptible and -resistant regions of human vasculature. *Proc Natl Acad Sci U S A* **101**, 14871–14876 (2004).

305. Shah, A. V., Birdsey, G. M. & Randi, A. M. Regulation of endothelial homeostasis, vascular development and angiogenesis by the transcription factor ERG. *Vascul Pharmacol* **86**, 3–13 (2016).

306. Mailman, M. D. *et al.* The NCBI dbGaP database of genotypes and phenotypes. *Nat Genet* **39**, 1181–1186 (2007).

307. Welter, D. *et al.* The NHGRI GWAS Catalog, a curated resource of SNP-trait associations. *Nucleic Acids Res* **42**, D1001-1006 (2014).

308. Schaub, M. A., Boyle, A. P., Kundaje, A., Batzoglou, S. & Snyder, M. Linking disease associations with regulatory information in the human genome. *Genome Res* **22**, 1748–1759 (2012).

309. Schoenfelder, S. & Fraser, P. Long-range enhancer-promoter contacts in gene expression control. *Nat Rev Genet* **20**, 437–455 (2019).

310. Lieberman-Aiden, E. *et al.* Comprehensive mapping of long-range interactions reveals folding principles of the human genome. *Science* **326**, 289–293 (2009).

311. Lalonde, S. *et al.* Integrative analysis of vascular endothelial cell genomic features identifies AIDA as a coronary artery disease candidate gene. *Genome Biol* **20**, 133 (2019).

312. Åkerborg, Ö. *et al.* High-Resolution Regulatory Maps Connect Vascular Risk Variants to Disease-Related Pathways. *Circ: Genomic and Precision Medicine* **12**, (2019).

313. Niskanen, H. *et al.* Endothelial cell differentiation is encompassed by changes in long range interactions between inactive chromatin regions. *Nucleic Acids Research* **46**, 1724–1740 (2018).

314. Mifsud, B. *et al.* Mapping long-range promoter contacts in human cells with high-resolution capture Hi-C. *Nat Genet* **47**, 598–606 (2015).

315. Schoenfelder, S. *et al.* The pluripotent regulatory circuitry connecting promoters to their long-range interacting elements. *Genome Res* **25**, 582–597 (2015).

316. Lovén, J. *et al.* Selective Inhibition of Tumor Oncogenes by Disruption of Super-Enhancers. *Cell* **153**, 320–334 (2013).

317. Huang, J. *et al.* Dissecting super-enhancer hierarchy based on chromatin interactions. *Nat Commun* **9**, 943 (2018).

318. Jia, M. *et al.* Deletion of BACH1 Attenuates Atherosclerosis by Reducing Endothelial Inflammation. *Circ Res* **130**, 1038–1055 (2022).

319. Jiang, L. *et al.* Bach1 Represses Wnt/β-Catenin Signaling and Angiogenesis. *Circ Res* **117**, 364–375 (2015).

320. McSweeney, S. R., Warabi, E. & Siow, R. C. M. Nrf2 as an Endothelial Mechanosensitive Transcription Factor: Going With the Flow. *Hypertension* **67**, 20–29 (2016).

321. Fledderus, J. O. *et al.* KLF2 primes the antioxidant transcription factor Nrf2 for activation in endothelial cells. *Arterioscler Thromb Vasc Biol* **28**, 1339–1346 (2008).

322. Dai, G. *et al.* Biomechanical forces in atherosclerosis-resistant vascular regions regulate endothelial redox balance via phosphoinositol 3-kinase/Akt-dependent activation of Nrf2. *Circ Res* **101**, 723–733 (2007).

323. Zakkar, M. *et al.* Activation of Nrf2 in endothelial cells protects arteries from exhibiting a proinflammatory state. *Arterioscler Thromb Vasc Biol* **29**, 1851–1857 (2009).

324. Milkiewicz, M., Uchida, C., Gee, E., Fudalewski, T. & Haas, T. L. Shear stress-induced Ets-1 modulates protease inhibitor expression in microvascular endothelial cells. *J Cell Physiol* **217**, 502–510 (2008).

325. Meadows, S. M., Salanga, M. C. & Krieg, P. A. Kruppel-like factor 2 cooperates with the ETS family protein ERG to activate Flk1 expression during vascular development. *Development* **136**, 1115–1125 (2009).

326. Fang, Y., Shi, C., Manduchi, E., Civelek, M. & Davies, P. F. MicroRNA-10a regulation of proinflammatory phenotype in athero-susceptible endothelium in vivo and in vitro. *Proc Natl Acad Sci U S A* **107**, 13450–13455 (2010).

327. Hajra, L. *et al.* The NF-kappa B signal transduction pathway in aortic endothelial cells is primed for activation in regions predisposed to atherosclerotic lesion formation. *Proc Natl Acad Sci U S A* **97**, 9052–9057 (2000).

328. Khachigian, L. M., Resnick, N., Gimbrone, M. A. & Collins, T. Nuclear factor-kappa B interacts functionally with the platelet-derived growth factor B-chain shear-stress response element in vascular endothelial cells exposed to fluid shear stress. *J Clin Invest* **96**, 1169–1175 (1995).

329. Siersbæk, R. *et al.* Transcription Factor Cooperativity in Early Adipogenic Hotspots and Super-Enhancers. *Cell Reports* **7**, 1443–1455 (2014).

330. Moorthy, S. D. *et al.* Enhancers and super-enhancers have an equivalent regulatory role in embryonic stem cells through regulation of single or multiple genes. *Genome Res.* **27**, 246–258 (2017).

331. Blobel, G. A., Higgs, D. R., Mitchell, J. A., Notani, D. & Young, R. A. Testing the super-enhancer concept. *Nat Rev Genet* **22**, 749–755 (2021).

332. Kichaev, G. *et al.* Leveraging Polygenic Functional Enrichment to Improve GWAS Power. *The American Journal of Human Genetics* **104**, 65–75 (2019).

333. Neale's Research Group. UK Biobank GWAS data. http://www.nealelab.is/uk-biobank/.

334. Ross, D. & Siegel, D. The diverse functionality of NQO1 and its roles in redox control. *Redox Biology* **41**, 101950 (2021).

335. Chen, X.-L. *et al.* Laminar Flow Induction of Antioxidant Response Element-mediated Genes in Endothelial Cells. *Journal of Biological Chemistry* **278**, 703–711 (2003).

336. Kim, Y.-H. *et al.* Activation of NAD(P)H:quinone oxidoreductase ameliorates spontaneous hypertension in an animal model via modulation of eNOS activity. *Cardiovascular Research* **91**, 519–527 (2011).

337. Siendones, E. *et al.* Membrane-Bound CYB5R3 Is a Common Effector of Nutritional and Oxidative Stress Response Through FOXO3a and Nrf2. *Antioxidants & Redox Signaling* **21**, 1708–1725 (2014).

338. Zhang, N., Zhang, Y., Wu, B., You, S. & Sun, Y. Role of WW domain E3 ubiquitin protein ligase 2 in modulating ubiquitination and Degradation of Septin4 in oxidative stress endothelial injury. *Redox Biology* **30**, 101419 (2020).

339. Gilbert, L. A. *et al.* CRISPR-mediated modular RNA-guided regulation of transcription in eukaryotes. *Cell* **154**, 442–451 (2013).

340. Fulco, C. P. *et al.* Systematic mapping of functional enhancer-promoter connections with CRISPR interference. *Science* **354**, 769–773 (2016).

341. Hinds, D. A. *et al.* Genome-wide association analysis of self-reported events in 6135 individuals and 252 827 controls identifies 8 loci associated with thrombosis. *Hum. Mol. Genet.* **25**, 1867–1874 (2016).

342. Yanagisawa, M. *et al.* A novel potent vasoconstrictor peptide produced by vascular endothelial cells. *Nature* **332**, 411–415 (1988).

343. Wagner, O. F. *et al.* Polar secretion of endothelin-1 by cultured endothelial cells. *Journal of Biological Chemistry* **267**, 16066–16068 (1992).

344. Amiri, F. *et al.* Endothelium-Restricted Overexpression of Human Endothelin-1 Causes Vascular Remodeling and Endothelial Dysfunction. *Circulation* **110**, 2233–2240 (2004).

345. Li, J. S., Larivière, R. & Schiffrin, E. L. Effect of a nonselective endothelin antagonist on vascular remodeling in deoxycorticosterone acetate-salt hypertensive rats. Evidence for a role of endothelin in vascular hypertrophy. *Hypertension* **24**, 183–188 (1994).

346. Ramzy, D. Elevated Endothelin-1 Levels Impair Nitric Oxide Homeostasis Through a PKC-Dependent Pathway. *Circulation* **114**, I-319-I–326 (2006).

347. Wedgwood, S. & Black, S. M. Endothelin-1 decreases endothelial NOS expression and activity through ET A receptor-mediated generation of hydrogen peroxide. *American Journal of Physiology-Lung Cellular and Molecular Physiology* **288**, L480–L487 (2005).

348. Halim, A. *et al.* Endothelin-1 increased immunoreactive von Willebrand factor in endothelial cells and induced micro thrombosis in rats. *Thromb Res* **76**, 71–78 (1994).

349. Baldwin, A. S., LeClair, K. P., Singh, H. & Sharp, P. A. A large protein containing zinc finger domains binds to related sequence elements in the enhancers of the class I major histocompatibility complex and kappa immunoglobulin genes. *Mol Cell Biol* **10**, 1406–1414 (1990).

350. Baar, S. The role of HIVEP1 in endothelial platelet interaction in the context of venous thrombosis. (2019).

351. Morange, P.-E. *et al.* A Follow-Up Study of a Genome-wide Association Scan Identifies a Susceptibility Locus for Venous Thrombosis on Chromosome 6p24.1. *The American Journal of Human Genetics* **86**, 592–595 (2010).

352. Germain, M. *et al.* Genetics of Venous Thrombosis: Insights from a New Genome Wide Association Study. *PLoS ONE* **6**, e25581 (2011).

353. Bruzelius, M. *et al.* PDGFB, a new candidate plasma biomarker for venous thromboembolism: results from the VEREMA affinity proteomics study. *Blood* **128**, e59–e66 (2016).

354. Jaalouk, D. E. & Lammerding, J. Mechanotransduction gone awry. *Nat Rev Mol Cell Biol* **10**, 63–73 (2009).

355. Davies, P. F., Civelek, M., Fang, Y. & Fleming, I. The atherosusceptible endothelium: endothelial phenotypes in complex haemodynamic shear stress regions in vivo. *Cardiovasc Res* **99**, 315–327 (2013).

356. Hahn, C. & Schwartz, M. A. Mechanotransduction in vascular physiology and atherogenesis. *Nat Rev Mol Cell Biol* **10**, 53–62 (2009).

357. Li, J., Fang, Y. & Wu, D. Mechanical forces and metabolic changes cooperate to drive cellular memory and endothelial phenotypes. in *Current Topics in Membranes* vol. 87 199–253 (Elsevier, 2021).

358. Parker, S. C. J. *et al.* Chromatin stretch enhancer states drive cell-specific gene regulation and harbor human disease risk variants. *Proc. Natl. Acad. Sci. U.S.A.* **110**, 17921–17926 (2013).

359. Zhong, H. *et al.* Liver and Adipose Expression Associated SNPs Are Enriched for Association to Type 2 Diabetes. *PLoS Genet* **6**, e1000932 (2010).

360. Musunuru, K. *et al.* From noncoding variant to phenotype via SORT1 at the 1p13 cholesterol locus. *Nature* **466**, 714–719 (2010).

361. Miller, C. L. *et al.* Integrative functional genomics identifies regulatory mechanisms at coronary artery disease loci. *Nat Commun* **7**, 12092 (2016).

362. Howson, J. M. M. *et al.* Fifteen new risk loci for coronary artery disease highlight arterial-wall-specific mechanisms. *Nat Genet* **49**, 1113–1119 (2017).

363. Javierre, B. M. *et al.* Lineage-Specific Genome Architecture Links Enhancers and Non-coding Disease Variants to Target Gene Promoters. *Cell* **167**, 1369-1384.e19 (2016).

364. Rubin, A. J. *et al.* Lineage-specific dynamic and pre-established enhancer–promoter contacts cooperate in terminal differentiation. *Nat Genet* **49**, 1522–1528 (2017).

365. Siersbæk, R. *et al.* Dynamic Rewiring of Promoter-Anchored Chromatin Loops during Adipocyte Differentiation. *Molecular Cell* **66**, 420-435.e5 (2017).

366. Freire-Pritchett, P. *et al.* Global reorganisation of cis-regulatory units upon lineage commitment of human embryonic stem cells. *eLife* **6**, e21926 (2017).

367. Zheng, H. & Xie, W. The role of 3D genome organization in development and cell differentiation. *Nat Rev Mol Cell Biol* **20**, 535–550 (2019).

368. Gosselin, D. *et al.* Environment Drives Selection and Function of Enhancers Controlling Tissue-Specific Macrophage Identities. *Cell* **159**, 1327–1340 (2014).

369. Lan, Q., Mercurius, K. O. & Davies, P. F. Stimulation of transcription factors NF kappa B and AP1 in endothelial cells subjected to shear stress. *Biochem Biophys Res Commun* **201**, 950–956 (1994).

370. Sabari, B. R. *et al.* Coactivator condensation at super-enhancers links phase separation and gene control. *Science* **361**, eaar3958 (2018).

371. Saravanan, B. *et al.* Ligand dependent gene regulation by transient ERα clustered enhancers. *PLoS Genet* **16**, e1008516 (2020).

372. Gasperini, M., Tome, J. M. & Shendure, J. Towards a comprehensive catalogue of validated and target-linked human enhancers. *Nat Rev Genet* **21**, 292–310 (2020).

373. Liang, M. MicroRNA: a new entrance to the broad paradigm of systems molecular medicine. *Physiol Genomics* **38**, 113–115 (2009).

374. Fang, Y. & Davies, P. F. Site-specific microRNA-92a regulation of Kruppel-like factors 4 and 2 in atherosusceptible endothelium. *Arterioscler Thromb Vasc Biol* **32**, 979–987 (2012).

375. Davies, P. F., Civelek, M., Fang, Y. & Fleming, I. The atherosusceptible endothelium: endothelial phenotypes in complex haemodynamic shear stress regions in vivo. *Cardiovasc Res* **99**, 315–327 (2013).

376. Gimbrone, M. A. & García-Cardeña, G. Endothelial Cell Dysfunction and the Pathobiology of Atherosclerosis. *Circ Res* **118**, 620–636 (2016).

377. Hahn, C. & Schwartz, M. A. Mechanotransduction in vascular physiology and atherogenesis. *Nat Rev Mol Cell Biol* **10**, 53–62 (2009).

378. Wu, D. *et al.* HIF-1α is required for disturbed flow-induced metabolic reprogramming in human and porcine vascular endothelium. *eLife* **6**, e25217 (2017).

379. Feng, S. *et al.* Mechanical Activation of Hypoxia-Inducible Factor 1α Drives Endothelial Dysfunction at Atheroprone Sites. *Arterioscler Thromb Vasc Biol* **37**, 2087–2101 (2017).

380. Doddaballapur, A. *et al.* Laminar shear stress inhibits endothelial cell metabolism via KLF2-mediated repression of PFKFB3. *Arterioscler Thromb Vasc Biol* **35**, 137–145 (2015).

381. Yang, Q. *et al.* PRKAA1/AMPKα1-driven glycolysis in endothelial cells exposed to disturbed flow protects against atherosclerosis. *Nat Commun* **9**, 4667 (2018).

382. Wang, Y.-H. *et al.* Cell-state-specific metabolic dependency in hematopoiesis and leukemogenesis. *Cell* **158**, 1309–1323 (2014).

383. Sörensen, I., Adams, R. H. & Gossler, A. DLL1-mediated Notch activation regulates endothelial identity in mouse fetal arteries. *Blood* **113**, 5680–5688 (2009).

384. Yeh, C.-F. *et al.* Targeting mechanosensitive endothelial TXNDC5 to stabilize eNOS and reduce atherosclerosis in vivo. *Sci. Adv.* **8**, eabl8096 (2022).

385. Schneider, C. A., Rasband, W. S. & Eliceiri, K. W. NIH Image to ImageJ: 25 years of image analysis. *Nat Methods* **9**, 671–675 (2012).

386. Wu, D. *et al.* Single-cell metabolic imaging reveals a SLC2A3-dependent glycolytic burst in motile endothelial cells. *Nat Metab* **3**, 714–727 (2021).

387. Harrison, D., Wu, D., Huang, J. & Fang, Y. Single-cell lactate production rate as a measure of glycolysis in endothelial cells. *STAR Protoc* **2**, 100807 (2021).

388. San Martín, A. *et al.* A genetically encoded FRET lactate sensor and its use to detect the Warburg effect in single cancer cells. *PLoS One* **8**, e57712 (2013).

389. Kim, D., Paggi, J. M., Park, C., Bennett, C. & Salzberg, S. L. Graph-based genome alignment and genotyping with HISAT2 and HISAT-genotype. *Nat Biotechnol* **37**, 907–915 (2019).

390. Trapnell, C. *et al.* Differential gene and transcript expression analysis of RNA-seq experiments with TopHat and Cufflinks. *Nat Protoc* **7**, 562–578 (2012).

391. Zhang, Y. *et al.* Model-based Analysis of ChIP-Seq (MACS). *Genome Biol* **9**, R137 (2008).

392. Stark, R. & Brown, G. DiffBind : differential binding analysis of ChIP-Seq peak data.

393. Chen, T.-W. *et al.* ChIPseek, a web-based analysis tool for ChIP data. *BMC Genomics* **15**, 539 (2014).

394. Dai, G. *et al.* DISTINCT ENDOTHELIAL PHENOTYPES EVOKED BY ARTERIAL WAVEFORMS DERIVED FROM ATHEROSCLEROSIS-PRONE AND ATHEROSCLEROSIS-PROTECTED REGIONS OF THE HUMAN VASCULATURE. *Cardiovascular Pathology* **13**, 26 (2004).

395. Wu Congqing *et al.* Mechanosensitive PPAP2B Regulates Endothelial Responses to Atherorelevant Hemodynamic Forces. *Circulation Research* **117**, e41–e53 (2015).

396. Krause, M. D. *et al.* Genetic variant at coronary artery disease and ischemic stroke locus 1p32.2 regulates endothelial responses to hemodynamics. *PNAS* **115**, E11349–E11358 (2018).

397. Dai, M. *et al.* LDHA as a regulator of T cell fate and its mechanisms in disease. *Biomedicine & Pharmacotherapy* **158**, 114164 (2023).

398. Dai, C. *et al.* Lactate Dehydrogenase A Governs Cardiac Hypertrophic Growth in Response to Hemodynamic Stress. *Cell Reports* **32**, 108087 (2020).

399. Claps, G. *et al.* The multiple roles of LDH in cancer. *Nat Rev Clin Oncol* **19**, 749–762 (2022).

400. Cui, H. *et al.* Lung Myofibroblasts Promote Macrophage Profibrotic Activity through Lactate-induced Histone Lactylation. *Am J Respir Cell Mol Biol* **64**, 115–125 (2021).

401. Dichtl, S. *et al.* Lactate and IL6 define separable paths of inflammatory metabolic adaptation. *Sci Adv* **7**, eabg3505 (2021).

402. Galle, E. *et al.* H3K18 lactylation marks tissue-specific active enhancers. *Genome Biol* **23**, 207 (2022).

403. Gao, M., Zhang, N. & Liang, W. Systematic Analysis of Lysine Lactylation in the Plant Fungal Pathogen Botrytis cinerea. *Front Microbiol* **11**, 594743 (2020).

404. Hagihara, H. *et al.* Protein lactylation induced by neural excitation. *Cell Rep* **37**, 109820 (2021).

405. Jiang, J. *et al.* Lactate Modulates Cellular Metabolism Through Histone Lactylation-Mediated Gene Expression in Non-Small Cell Lung Cancer. *Front Oncol* **11**, 647559 (2021).

406. Meng, X., Baine, J. M., Yan, T. & Wang, S. Comprehensive Analysis of Lysine Lactylation in Rice (*Oryza sativa*) Grains. *J. Agric. Food Chem.* **69**, 8287–8297 (2021).

407. Yang, W. *et al.* Hypoxic in vitro culture reduces histone lactylation and impairs pre-implantation embryonic development in mice. *Epigenetics Chromatin* **14**, 57 (2021).

408. Yu, J. *et al.* Histone lactylation drives oncogenesis by facilitating m6A reader protein YTHDF2 expression in ocular melanoma. *Genome Biol* **22**, 85 (2021).

409. Irizarry-Caro, R. A. *et al.* TLR signaling adapter BCAP regulates inflammatory to reparatory macrophage transition by promoting histone lactylation. *Proc. Natl. Acad. Sci. U.S.A.* **117**, 30628–30638 (2020).

410. Kumar, S., Kang, D.-W., Rezvan, A. & Jo, H. Accelerated atherosclerosis development in C57Bl6 mice by overexpressing AAV-mediated PCSK9 and partial carotid ligation. *Laboratory Investigation* **97**, 935–945 (2017).

411. Lagace, T. A. *et al.* Secreted PCSK9 decreases the number of LDL receptors in hepatocytes and inlivers of parabiotic mice. *J. Clin. Invest.* **116**, 2995–3005 (2006).

412. Azzu, V., Vacca, M., Virtue, S., Allison, M. & Vidal-Puig, A. Adipose Tissue-Liver Cross Talk in the Control of Whole-Body Metabolism: Implications in Nonalcoholic Fatty Liver Disease. *Gastroenterology* **158**, 1899–1912 (2020).

413. Lemoine, A. Y. *et al.* Link between Adipose Tissue Angiogenesis and Fat Accumulation in Severely Obese Subjects. *The Journal of Clinical Endocrinology & Metabolism* **97**, E775–E780 (2012).

414. Poisson, J. *et al.* Liver sinusoidal endothelial cells: Physiology and role in liver diseases. *Journal of Hepatology* **66**, 212–227 (2017).

415. Vozenilek, A. E. *et al.* AAV8-mediated overexpression of mPCSK9 in liver differs between male and female mice. *Atherosclerosis* **278**, 66–72 (2018).

416. Oppi, S., Lüscher, T. F. & Stein, S. Mouse Models for Atherosclerosis Research—Which Is My Line? *Front. Cardiovasc. Med.* **6**, 46 (2019).

417. Nakashima, Y., Plump, A. S., Raines, E. W., Breslow, J. L. & Ross, R. ApoE-deficient mice develop lesions of all phases of atherosclerosis throughout the arterial tree. *Arterioscler Thromb* **14**, 133–140 (1994).

418. Akashi, M., Higashi, T., Masuda, S., Komori, T. & Furuse, M. A coronary artery disease-associated gene product, JCAD/KIAA1462, is a novel component of endothelial cell–cell junctions. *Biochemical and Biophysical Research Communications* **413**, 224–229 (2011).

419. Erdmann, J. *et al.* Genome-wide association study identifies a new locus for coronary artery disease on chromosome 10p11.23. *European Heart Journal* **32**, 158–168 (2011).

420. Douglas, G. *et al.* A key role for the novel coronary artery disease gene JCAD in atherosclerosis via shear stress mechanotransduction. *Cardiovascular Research* **116**, 1863–1874 (2020).

421. Xu, S. *et al.* The novel coronary artery disease risk gene JCAD/KIAA1462 promotes endothelial dysfunction and atherosclerosis. *Eur Heart J* **40**, 2398–2408 (2019).

422. Jones, P. D. *et al. JCAD* , a Gene at the 10p11 Coronary Artery Disease Locus, Regulates Hippo Signaling in Endothelial Cells. *ATVB* **38**, 1711–1722 (2018).

423. De Bock, K. *et al.* Role of PFKFB3-Driven Glycolysis in Vessel Sprouting. *Cell* **154**, 651–663 (2013).

424. Doddaballapur, A. *et al.* Laminar shear stress inhibits endothelial cell metabolism via KLF2-mediated repression of PFKFB3. *Arterioscler Thromb Vasc Biol* **35**, 137–145 (2015).

425. Peng, M. *et al.* Aerobic glycolysis promotes T helper 1 cell differentiation through an epigenetic mechanism. *Science* **354**, 481–484 (2016).

426. Castonguay, Z., Auger, C., Thomas, S. C., Chahma, M. & Appanna, V. D. Nuclear lactate dehydrogenase modulates histone modification in human hepatocytes. *Biochemical and Biophysical Research Communications* **454**, 172–177 (2014).

427. Coronary Artery Disease (C4D) Genetics Consortium. A genome-wide association study in Europeans and South Asians identifies five new loci for coronary artery disease. *Nat Genet* **43**, 339–344 (2011).

428. EPIC-CVD Consortium *et al.* Association analyses based on false discovery rate implicate new loci for coronary artery disease. *Nat Genet* **49**, 1385–1391 (2017).

429. Cicha, I. *et al.* Connective Tissue Growth Factor Is Overexpressed in Complicated Atherosclerotic Plaques and Induces Mononuclear Cell Chemotaxis In Vitro. *ATVB* **25**, 1008–1013 (2005).

430. Oemar, B. S. *et al.* Human Connective Tissue Growth Factor Is Expressed in Advanced Atherosclerotic Lesions. *Circulation* **95**, 831–839 (1997).

431. Hilfiker, A. *et al.* Expression of CYR61, an Angiogenic Immediate Early Gene, in Arteriosclerosis and Its Regulation by Angiotensin II. *Circulation* **106**, 254–260 (2002).

432. Klingenberg, R. *et al.* Cysteine-rich angiogenic inducer 61 (Cyr61): a novel soluble biomarker of acute myocardial injury improves risk stratification after acute coronary syndromes. *European Heart Journal* **38**, 3493–3502 (2017).

433. Ramos, C. L. *et al.* Direct demonstration of P-selectin- and VCAM-1-dependent mononuclear cell rolling in early atherosclerotic lesions of apolipoprotein E-deficient mice. *Circ Res* **84**, 1237–1244 (1999).

434. Neumann, F.-J. *et al.* Effect of Human Recombinant Interleukin-6 and Interleukin-8 on Monocyte Procoagulant Activity. *ATVB* **17**, 3399–3405 (1997).

435. Romano, M. *et al.* Role of IL-6 and Its Soluble Receptor in Induction of Chemokines and Leukocyte Recruitment. *Immunity* **6**, 315–325 (1997).

436. Apostolakis, S., Vogiatzi, K., Amanatidou, V. & Spandidos, D. A. Interleukin 8 and cardiovascular disease. *Cardiovascular Research* **84**, 353–360 (2009).

437. Ley, K. & Huo, Y. VCAM-1 is critical in atherosclerosis. *J. Clin. Invest.* **107**, 1209–1210 (2001).

438. Getz, G. S. & Reardon, C. A. Animal Models of Atherosclerosis. *Arterioscler Thromb Vasc Biol* **32**, 1104–1115 (2012).

439. Reardon Catherine A. *et al.* Effect of Immune Deficiency on Lipoproteins and Atherosclerosis in Male Apolipoprotein E–Deficient Mice. *Arteriosclerosis, Thrombosis, and Vascular Biology* **21**, 1011–1016 (2001).

440. Sontag Timothy J. *et al.* Apolipoprotein A-I Protection Against Atherosclerosis Is Dependent on Genetic Background. *Arteriosclerosis, Thrombosis, and Vascular Biology* **34**, 262–269 (2014).

441. Rahman, K. *et al.* Inflammatory Ly6C^{hi} monocytes and their conversion to M2 macrophages drive atherosclerosis regression. *J Clin Invest* **127**, 2904–2915 (2017).

442. Nam, D. *et al.* Partial carotid ligation is a model of acutely induced disturbed flow, leading to rapid endothelial dysfunction and atherosclerosis. *American Journal of Physiology-Heart and Circulatory Physiology* **297**, H1535–H1543 (2009).

443. Kaya-Okur, H. S. *et al.* CUT&Tag for efficient epigenomic profiling of small samples and single cells. *Nat Commun* **10**, 1930 (2019).

444. Andueza, A. *et al.* Endothelial Reprogramming by Disturbed Flow Revealed by Single-Cell RNA and Chromatin Accessibility Study. *Cell Reports* **33**, 108491 (2020).

445. Schoenfelder, S., Javierre, B.-M., Furlan-Magaril, M., Wingett, S. W. & Fraser, P. Promoter Capture Hi-C: High-resolution, Genome-wide Profiling of Promoter Interactions. *J Vis Exp* 57320 (2018) doi:10.3791/57320.

446. Dai, Z., Ramesh, V. & Locasale, J. W. The evolving metabolic landscape of chromatin biology and epigenetics. *Nat Rev Genet* **21**, 737–753 (2020).

447. Sassone-Corsi, P. When Metabolism and Epigenetics Converge. *Science* **339**, 148–150 (2013).

448. Zhu, C. *et al.* Joint profiling of histone modifications and transcriptome in single cells from mouse brain. *Nat Methods* **18**, 283–292 (2021).

449. Wang, J., Niu, N., Xu, S. & Jin, Z. G. A simple protocol for isolating mouse lung endothelial cells. *Sci Rep* **9**, 1458 (2019).

450. Wang, J.-M., Chen, A. F. & Zhang, K. Isolation and Primary Culture of Mouse Aortic Endothelial Cells. *JoVE* 52965 (2016) doi:10.3791/52965.

451. Su, C. *et al.* A novel human arterial wall-on-a-chip to study endothelial inflammation and vascular smooth muscle cell migration in early atherosclerosis. *Lab Chip* **21**, 2359–2371 (2021).

452. Drent, M., Cobben, N., Henderson, R., Wouters, E. & van Dieijen-Visser, M. Usefulness of lactate dehydrogenase and its isoenzymes as indicators of lung damage or inflammation. *Eur Respir J* **9**, 1736–1742 (1996).

453. Ždralević, M. *et al.* Double genetic disruption of lactate dehydrogenases A and B is required to ablate the "Warburg effect" restricting tumor growth to oxidative metabolism. *Journal of Biological Chemistry* **293**, 15947–15961 (2018).

454. Oberleithner, H. *et al.* Plasma sodium stiffens vascular endothelium and reduces nitric oxide release. *Proc. Natl. Acad. Sci. U.S.A.* **104**, 16281–16286 (2007).